Power Management in Wireless Sensor Networks (WSNs)

A thesis submitted for the Degree of Master of Philosophy

By

Thanisara Kamsuvan

Department of Electronic and Computer Engineering

Brunel University London

June 2016

ABSTRACT

The wireless sensor network (WSN) is increasingly used in many areas nowadays. It can be applied to provide the solutions to environmental problems, help increasing security and safety systems, and make the detection of the problems more efficient, e.g. the earthquake or tidal wave, which will harmful to humans. The WNS is durable and resistant to all types of terrain and climate, but while the WSN system is more and more widespread, one of the obstacles hindering the growth of this technology and the demand for WSN applications is the limited battery lifespan.

Consequently, there is a significant requirement for techniques for prolonging the battery's lifespan. Therefore, one potential solution is to use alternative energy sources combined with the sensor nodes in WSN, specifically energy harvesting from existing environmental sources. This research project reviews the characteristics of each kind of energy harvesting, understanding the various energy sources (solar energy, vibration energy and wind power), including wireless power transfer (WPT) by using electromagnetic (EM) radiation energy transfer or RF radio-frequency emission and magnetic coupled energy transfer. They are adopted for extending node's life in the WSN, based on published information. Then it compares these diverse alternative energy methods and identifies for the most suitable energy harvesting method for application to wireless sensor nodes in order to prolong the lifespan of the battery.

The major findings from the researcher include that wireless power transfer energy harvesting (WPT) using the magnetic field is the most appropriate tool for extending the lifespan of the WSN system. In addition, the author also designed an experiment to test this alternative energy, achieving by modelling the wireless power transfer with four coils. From the experimental results, it can be seen that the WPT technique using energy harvesting with magnetic inductive source can be applied to prolong the lifespan of the WSN system.

ACKNOWLEDGEMENTS

This dissertation would never have been possible without the kindness of my supervisor, Dr. Qing Ping Yang. Therefore I would like to convey my profound appreciation to my supervisor for encouraging me, offering me guidance and supporting my topic throughout my course at Brunel University, including rectifying my mistakes. I am sincerely grateful for his assistance and patience.

I would also like to express my sincere gratitude to all the technicians and staff members in the engineering and design school at Brunel University. I have greatly appreciated their patience and advice during my period of study.

I am exceedingly thankful to all the professors who taught and educated me at Kasetsart University. This successful thesis is the result of the application of the knowledge that I gained from all my instructors.

Finally, I deeply appreciate my parent steady encouragement during my research and who have supported me in everything. I would like to thank them for their endurance and their understanding. Without my parents, it would have been difficult opportunity to complete this research project. Moreover, I would like to thank all my friends, who have willingly assisted me and helped me overcome difficult periods of tension

TABLE OF CONTENTS

Chapter 1 – Introduction 1

1.1 Introduction 1

1.2 Problem statement 2

1.3 Aims and objectives 3

1.4 Significance of the study 3

1.5 Organisation of the study 4

Chapter 2 – Literature review 6

2.1 Introduction 6

2.2 Characteristic of WSN 6

2.2.1 WSN Structure 8

2.2.2 WSN deployment and operation system 9

2.2.3 WSN architecture 10

2.3 Power consumption in WSN 14

2.3.1 Power consumption in sensing 14

2.3.2 Power consumption in processing 15

2.3.3 Power consumption in communications 15

2.4 Lifespan of WSN 18

2.5 Energy supply for WSN 19

2.5.1 Batteries 19

2.5.2 Energy harvesting 21

Chapter 3 – Design for prolonging the lifespan of the WSN 42

3.1 Introduction 42

3.2 The design for WSN 42

3.3 The design principle to prolong WSN lifespan by using coupling magnetic resonant WPT 44

3.3.1 Consideration of the model....44
3.3.2 The equivalent circuit of the design....46
3.4 Setting the parameters of the experiment....49
Chapter 4 – Methodology and implementation....53
4.1 Introduction....53
4.2 Research strategy....53
4.3 Data collection....54
4.4 Experimental design....54
4.5 Experimental equipment....54
4.6 Implementation and experimental process....57
4.7 Measurement methodology and process....60
4.7.1 Oscilloscope....60
4.7.2 Measurement of the voltage source....63
4.7.3 Measurement of the current in coil 1 and the current in coil 4....63
4.7.4 Measuring the mutual inductances....65
4.7.5 Measuring and finding the relative power transfer efficiency....67
Chapter 5 – Results and analysis....68
5.1 Introduction....68
5.2 The results....68
5.3 Discussion....85
Chapter 6 – Conclusions, limitations and recommendations....87
6.1 Conclusions....87
6.2 Limitations....89
6.3 Recommendations and future work....89
Bibliography....91
APPENDIX ……...……..…..……104

LIST OF TABLES

Table 2.1: The required power consumption of MCU……15
Table 2.2: The example battery power consumption of IRIS sensor node operating at 100% and 1% duty cycles using two AA batteries with the output between 2.7 to 3.6 VDC……17
Table 2.4: The example of the maximum estimated lifespan of IRIS mote using two AA batteries with the output between 2.7 to 3.6 VDC……...18
Table 3.1: The summary of particulars of the coil physical……..50
Table 5.1: The summary of all parameter values for this experiment……..69
Table 5.2: Summary the voltage of load resistance (V_L) and voltage across R_0 (V_0) vary at the distances d_{23} between the transmitter coil and the receiver coil in voltage peak-to-peak (V_{pk-pk}) and in the peak voltage (V_{pk}) by measurement……....…….....77
Table 5.3: The current in coil 1 (I_1) varies at the distances d_{23} between the transmitter coil and the receiver coil by measurement…….……....78
Table 5.4: The relative power transfer efficiency at the distances d_{23} between coil 2 and coil 3 by measurement……79
Table 5.5: The voltage across R_{sense_1} (V_{sense_1}) and voltage across inductance in coil 3 V_{L3} vary at the distances d_{23} when coil 3 is an open circuit……....82
Table 5.6: The mutual inductance M_{23} between coil 2 and coil 3 vary at the distances d_{23}…..83
Table 5.7: The relative power transfer efficiency at the distances d_{23} between coil 2 and coil 3 by calculation…….....84

LIST OF FIGURES

Figure 2.1: Berkeley mote (MICAz MPR 2400) 6
Figure 2.2: Generic sketch of a wireless sensor network 7
Figure 2.3: The components of WSN 9
Figure 2.4: Single hop and multi hop wireless sensor network architecture 11
Figure 2.5: Network architecture 12
Figure 2.6: The hierarchical ad hoc architecture or Cluster architecture 13
Figure 2.7: The distribution of power consumption in WSN 14
Figure 2.8: A comparison the lifespan from various batteries powers. 21
Figure 2.9: The ordinary wireless sensor network node with energy harvesting device 22
Figure 2.10: The various example of the supercapacitor; 23
(a) Supercapacitor 10F/2.5V with 13mm x 33.5mm.
(b) Supercapacitor Low ESR - 1F/2.5V with 8.5mm x 13.5mm.
Figure 2.11: 25
(a) The small polycrystalline silicon solar panel 0.5V with diameter of 6.6mm x 9.4mm x 0.51mm (2.6" x 3.7" x 0.2")
(b) The wireless sensor node collaborating with solar panel energy harvesting
Figure 2.12: Typical of piezoelectric energy harvesting system 27
Figure 2.13: A piezoelectric material is squeezed or stretched from the vibration sources providing the electric. 27
Figure 2.14: The prototype of bimorph piezoelectric generator 28
Figure 2.15: Types of WPT technology 29
Figure 2.16: A comparison of WPT methods between distance of transferred power and transmission power 30
Figure 2.17: The wireless identification and sensing platform (WISP) 32
Figure 2.18: The stop positions of RFID reader in the WSN 33
Figure 2.19: The basic block diagram of magnetic coupled resonance WPT system 36
Figure 2.20: Coil lumped model 36
Figure 2.21: The simplified schematic of the WPT system 37
Figure 2.22: (a) The equivalent circuit model of system architecture with three coils 37
Figure 2.23: A mobile WCV in WSN 39

Figure 2.24:
A travelling path of WCV visits each sensor node for charging battery via WPT 39
Figure 2.25: 41
(a) A mobile WCV in WSN
(b) Showing a cellular structure that partitioned the two dimensional plan into several adjacent hexagonal cells in WSN and a travelling path of WCV visits cell in order to charge battery for multiple nodes via WPT
Figure 3.1: The model structure of magnetic coupled resonant wireless power transfer 45
Figure 3.2: Equivalent circuit of the model structure of the experiment 46
Figure 4.1: Tektronix TDS2002C digital oscilloscope 55
Figure 4.2: 56
(a) Digital programmable multimeter HM8012
(b) Multimeter with inductance measurement
Figure 4.3: Function generator HM8030-6 57
Figure 4.4: Function generator setting the frequency at 10.5 MHz 57
Figure 4.5: The loop coil 1, loop coil 2, loop coil 3 and loop coil 4 58
Figure 4.6: Load coil with load resistance R_L and LED's 59
Figure 4.7: Transmitter part and receiver part 59
Figure 4.8: The over all of the experiment 60
Figure 4.9: Oscilloscope 61
Figure 4.10: Common voltage sine wave parameters 62
Figure 4.11: the circuit for measurement voltage source 63
Figure 4.12: (a) The measure current for coil 1; (b) The measurement current for coil 4 64
Figure 4.13: The measurement I_1 and I_4 in this experiment 64
Figure 4.14: Circuit for measurement the mutual inductance M_{12} 65
Figure 4.15: Circuit for measurement the mutual inductance M_{34} 66
Figure 4.16: Circuit for measurement the mutual inductance M_{23} 67
Figure 5.1: The voltage input source 68
Figure 5.2: The example of the experiment with LED's light at 3.5 cm between the transmitter coil and the receiver coil 70
Figure 5.3: The voltage V_0 across R_0 is shown in yellow graph, whereas blue graph presents as the voltage V_L at the distance d_{23} of 0.5 cm 71
Figure 5.4: The voltage V_0 across R_0 is shown in yellow graph, whereas blue graph presents as the voltage V_L at the distance d_{23} of 1 cm 71

Figure 5.5: The voltage V_0 across R_0 is shown in yellow graph, whereas blue graph presents as the voltage V_L at the distance d_{23} of 1.5 cm 72
Figure 5.6: The voltage V_0 across R_0 is shown in yellow graph, whereas blue graph presents as the voltage V_L at the distance d_{23} of 2 cm 72
Figure 5.7: The voltage V_0 across R_0 is shown in yellow graph, whereas blue graph presents as the voltage V_L at the distance d_{23} of 2.5 cm 73
Figure 5.8: The voltage V_0 across R_0 is shown in yellow graph, whereas blue graph presents as the voltage V_L at the distance d_{23} of 3 cm 73
Figure 5.9: The voltage V_0 across R_0 is shown in yellow graph, whereas blue graph presents as the voltage V_L at the distance d_{23} of 3.5 cm 74
Figure 5.10: The voltage V_0 across R_0 is shown in yellow graph, whereas blue graph presents as the voltage V_L at the distance d_{23} of 4 cm 74
Figure 5.11: The voltage V_0 across R_0 is shown in yellow graph, whereas blue graph presents as the voltage V_L at the distance d_{23} of 4.5 cm 75
Figure 5.12: The voltage V_0 across R_0 is shown in yellow graph, whereas blue graph presents as the voltage V_L at the distance d_{23} of 5 cm 75
Figure 5.13: The voltage V_0 across R_0 is shown in yellow graph, whereas blue graph presents as the voltage V_L at the distance d_{23} of 5.5 cm 76
Figure 5.14: The voltage V_0 across R_0 is shown in yellow graph, whereas blue graph presents as the voltage V_L at the distance d_{23} of 6 cm 76
Figure 5.15: (a) Voltage across loop coil 1 V_{L1}; (b) Voltage across loop coil 2 V_{L2}.....80
Figure 5.16: (a) Voltage across loop coil 3 V_{L3}; (b) Voltage across loop coil 4 V_{L4}.....81
Figure 5.17: The relative power transfer efficiency as a function of the distances d_{23} between coil 2 and coil 3. The circle point is the relative power transfer efficiency by measurement, whereas the + point represents the efficiency by calculation 85

Chapter 1 – Introduction

1.1 Introduction

The advanced technologies of sensors, processors and wireless communications have the advantages of high quality, energy efficiency and small size. Both the academic and the industrial worlds provide a way to measure and collect the data by using many small sensor units spread over and embedded in the environment or in the interested objects in order to store information, and to combine this with wireless communication. Each sensor node serves as a part of the network which creates and transmits data by using a wireless network for communication. This becomes the wireless sensor network (WSN), which can then work by itself.

A WSN comprises numerous distributed small sensors which are used to measure various properties of physical or the environmental conditions in order to process and store data. The accumulated data is utilised for collecting and searching for new knowledge, or for responding to a change in the environment automatically.

The WSN is easy to install because the sensor nodes have a small size and can be set up without fixed infrastructure. It can put into unreachable areas such as the sea, mountains, rural places, or deep forests; or it can be applied underground or underwater. Moreover, the cost of sensor nodes and their implementation is low (Bhattacharyya et al., 2010). In consequence, the WSN has been quite well-known in the past few years. Many companies and researchers have focused attention on this network and developed it to be more useful.

In recent years, given its ease of installation, the WSN has been applied in various arenas, such as: buildings, utilities, industry, the home, shipboard, moving systems automation, aircraft, health, industrial, transport, environment, medical, military, entertainment, crisis management, homeland defence, agriculture and smart spaces, and even warfare (Jain, 2011; Stankovic, 2006). The Examples include WSN for traffic on highways or in parts of town (Knaian, 2000), WSN to monitor environmental changes (Corke et al., 2010; Oliveira and Rodrigues, 2011), WSN to manage parking areas (Reve and Choudhri, 2012), WSN to monitor the effects of the earthquakes on structures (Tomicek et al., 2013), and so on.

Regrettably, the WSN also has explicit problems, like the battery power supply, which can limit the life of the device. For this reason, the network life of the WSN is the primary concern. This work will therefore propose a novel solution to improve energy efficiency and increase the lifespan of the battery in the sensor devices.

There have been many different ways to improve and extend battery life. However, this study investigates the methods which may extend the lifespan of this sensor network by energy harvesting by using alternative energy, which transforms the ambient energy sources (mechanical energy) into electrical energy, for example by converting solar energy into power energy through photovoltaic cells, or by transforming the mechanical vibrations from the environment into electrical energy through the piezoelectric effect (Nechibvute et al., 2012). Moreover, the wireless power transfer to power the WSN is also included in the one of the technique to prolong the WSN.

This research begins with a brief description of the WSN. Subsequently, this research presents and explains the solution methods, which aim to develop the ability to enhance the efficiency and life expectancy of the WSN by the alternative energy technique. This work also identifies the most suitable method to prolong network lifespan of the WSN. Furthermore, the experiment supporting the most appropriate design will be shown.

1.2 Problem statement

Currently, the world of WSN becomes well-known and is developing because the WSN can be applied in extensive and various areas, as mentioned above. Nevertheless, the limited lifespan of WSN is an important barrier for using WSN. The lifespan of this network depends on the battery inside each sensor node. Due to the compact size of the wireless sensor nodes, the battery in the node is constrained. Generally, an AA battery is used for the nodes, which can operate for months or even years. As indicated in work by Tan (2012), Jackson (2010), and Vasanthi et al. (2010), the typically battery life for WSN sensor nodes is approximately 1–3 years. Given this limited lifespan, many researchers invented various methods, including using low duty-cycle applications and/or managing the network protocols, to enhance the battery's lifespan. These customised methods can extend the lifespan of the battery by almost 300% for some cases, making the lifespan 5–10 years (Silva et al., 2012).

Evidently from the above method, extending the lifespan, however, does not mean that there is no need to replace the battery. This can be very difficult if the WSN is in a place that is arduous to access, or if the WSN has thousands of nodes. Hence, energy harvesting becomes the key challenge for the potential of extension of the battery's lifespan.

1.3 Aims and objectives

This study aims to analyse and recognise each type of the alternative energy combined with sensor node for the extension of the WSN's lifespan. This involves applying energy harvesting, including solar energy, vibration energy, wind power, and a wireless power transfer (WPT) which comprising the electromagnetic (EM) radiation energy transfer and magnetic coupled energy transfer, in order to identify the most suitable method to adopt to prolong lifespan.

This research aims to answer interrelated research questions.

1. How many types of alternative energy method applying for extending the WSN lifespan work?

In this research, the technology of harvesting energy such as solar power, vibration energy, wind energy (by piezoelectric) and WPT covering EM radiation energy transfer by RF radio-frequency emission and the magnetic coupled resonance energy transfer method will be explained and analysed, in terms of prolonging the battery lifespan in sensor nodes.

2. Which type of the alternative energy technology is the most suitable to prolong battery energy for the WSN?

This work will study, identify and conclude the most appropriate method for applying in the WSN in order to enhance the battery's lifespan in each sensor node by gathering and exploring information from other researchers and from professionals.

1.4 Significance of the study

In this study, the findings of this research are significant for the following reasons. This paper shows various methods which can be applied at the sensor node to increase the lifespan for the WSN. The energy harvesting technologies for the expansion of battery's life

are represented in this report. In addition, this investigation illustrates the most suitable method in order to enhance lifespan for the WSN.

However, as already stated, the WSN can be applied in various areas, even though the places may be difficult to reach. Therefore, the consideration to prolong the lifespan of the battery sensor in the WSN is very useful in order to eliminate the cost of replacing the battery in each sensor node and for ease of maintenance.

This information may encourage and help investors, inventors, manufacturers, government policy makers and planners to select the best techniques for obtaining the most efficient and worthy way to prolong the WSN lifespan.

1.5 Organisation of the study

This research consists of six main chapters:

Chapter 1: Introduction

This chapter illustrates and explains the background and the objectives of this study, including the problem statement. In addition, the answer to the research question aims and the significance of this research are indicated.

Chapter 2: Literature review

This chapter presents and explains the state of the research, as gathered from journal articles and textbooks which relate to answer the research question. This chapter can be divided into two parts: firstly, the general explanation about WSN and the battery used in the wireless sensor node, which includes the understanding of how the wireless sensor works and recognising the problem of limited battery life; secondly, the descriptions of the solution to prolonging energy in the sensor node by using alternative energy, indicating many types of alternative energy and also illustrating the theory of each type.

Chapter 3: Design for prolonging the lifespan of the WSN

Firstly, this chapter discusses each type of alternative energy that could be used for WSN, and explains why the most suitable choice of alternative energy is the wireless power transfer. Moreover, this chapter shows and explains about the method for design and how to

set up and evaluate the parameter values of the experiment used in this study. The theories of the wireless power transfer have been presented in this part.

Chapter4: Methodology and implementation

This chapter interprets the research method that used to carry out this study. This part explains the process put in place to set up the experiment and test the model. Moreover, this chapter establishes the measurement methods used to achieve and collect the data.

Chapter 5: Results and analysis

This chapter displays all the data that comes from the results of the experiment, then calculates and clarifies the data for ease of understanding. Moreover, this part also presents the analysis and discusses the results from the experiment to support the objective and show how the data is related to the literature.

Chapter 6: Conclusions, limitations and recommendations

This chapter is the final chapter of this thesis; it contains the summaries all of the research, and also lays out the limitations and theoretical implications. In addition, recommendations are offered in this part.

Chapter 2 – Literature review

2.1 Introduction

This chapter focuses on the significance of the literature related to the topic of this study. This review has two main purposes:

- To understand the basics of the wireless sensor network (WSN); and
- To synthesise the research findings from multiple journals, books and texts related to various alternative energy sources which can be used to prolong sensor node life.

2.2 Characteristic of WSN

Wireless sensor network (WSN) consists of a combination of the technology of embedded systems and wireless communication systems that use a group of very tiny sensor nodes known as ‘motes’. One example was developed by the Intel Company and the University of California (UC) at Berkeley (Stankovic, 2006), as shown in Figure 2.1 (Crossbow Technology Inc., 2004).

Figure 2.1: Berkeley mote (MICAz MPR 2400)

(Crossbow Technology Inc., 2004)

The mote is the basic device in the WSN that performs collaboratively in the network in order to collect data about physical or environmental conditions. The mote refers to a small computer used for measuring temperature, humidity, pressure, pollution levels, wind speed and direction, sound, and light intensity from the environment in which it is deployed (Jawarkar et al., 2013). This device can communicate with other imminent motes by using ad hoc wireless network to transfer data to the destination.

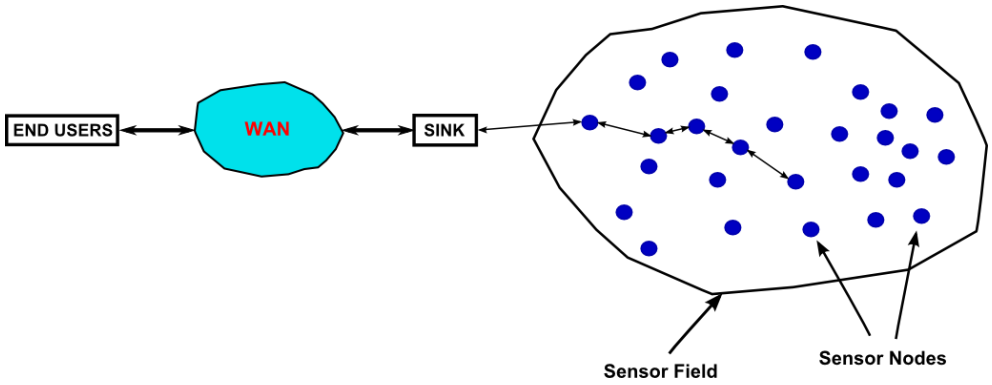

Figure 2.2: Generic sketch of a wireless sensor network

(Galán et al., 2010)

The advantages of WSN are the ease of use and the fact that it is a self-organizing independent communication system that uses ad hoc connectivity system in order to eliminate installation by humans. Moreover, another legible advantage of WSN is their cost because microcontrollers and transceivers are inexpensive. The total cost used in a network is less than 100 US dollars (Guibas and Zhao, 2004). For this reason, it is possible to use the WSN in various areas, such as health, industry, transportation, environment, medical, military, entertainment, crisis management, homeland defence, agriculture and smart spaces (Stankovic, 2006).

In the recent years, installation and use of WSN has been attempted in various places, such as using WSN to study and investigate the behaviour of seabirds on a small island off the coast of Maine streaming, Great Duck Island (Mainwaring et al., 2002), WSN in smart homes for the elderly and those suffering from Alzheimer's (Intel, 2004; Centre for technology and aging, 2009), etc.

2.2.1 WSN Structure

A WSN consists of a large number of motes, between ten and several thousand depending on the users (Moschitta and Neri, 2014). Nowadays, the storage of motes stores approximately ten of kilobytes and has a 1-MIPS processor. Current mote size is measured about five square centimetres (Levis et al., 2004).

Each typical sensor node device normally contains four basic components, as follows;

- **Sensing unit**

  The sensing unit comprises the sensors and analogue-to-digital converters (ADCs). The sensors are the devices for sensing and measuring a physical condition from the environment such as humidity, temperature, pressure, vehicular movement, noise level, lighting condition, mechanical stress, or the presence or absence of the objects, etc. The sensors provide an analogue signal, raw data, which is transferred to digital signals by using ADCs in order to produce understandable information. Then the data is sent to a processor unit for further processing (Gungor and Hancke, 2009).

- **Processing unit**

  The processing unit is the part for controlling all the sensor nodes and WSN. The main element of this unit is a digital microcontroller (MCU) to translate captured or sensed data from sensor nodes for the users to understand. It has multiple types of memory/storage to hold sensor data (Krishnamachari, 2005; Kochláň and Ševčík, 2012).

- **Communication unit**

  A radio transceiver or a wireless interface is used to exchange data with other nodes within its radio range by using a low-rate, short-range wireless radio (10–100kbps, <100m) (Krishnamachari, 2005).

- **Power unit**

  A portable power source provides the power unit for the sensor node; normally the device receives power from small batteries, e.g. LiMH AA batteries (Krishnamachari, 2005).

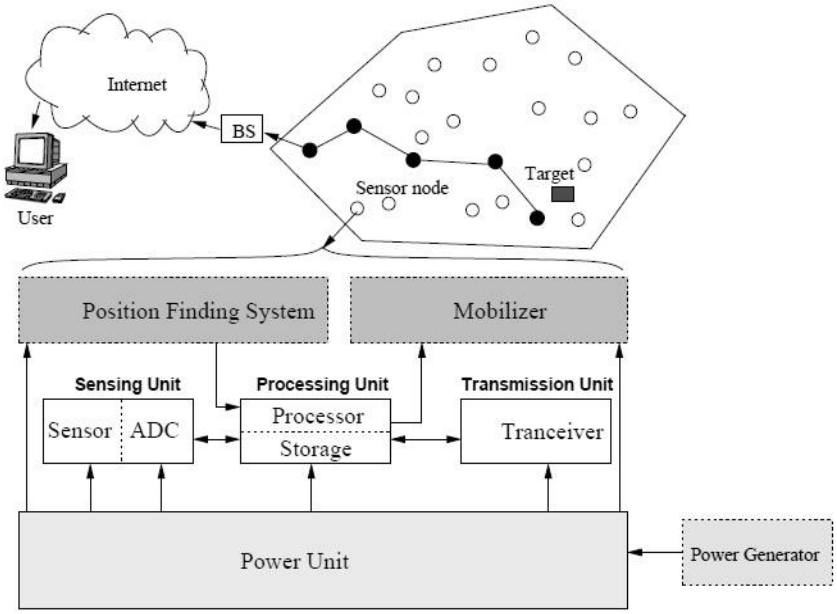

Figure 2.3: The components of WSN

(Matin and Islam, 2012)

2.2.2 WSN deployment and operation system

To control the motes in the WSN, the researchers from the University of California at Berkeley have developed an operating system (OS) called TinyOS or Tiny Micro threading OSs, which is an open source software and can be downloaded from the website of the TinyOS (http://www.tinyos.net). Currently, TinyOS is regarded as the standard for WSN operating system. This software system is running on every mote by handling its power and operations (Gay et al., 2003).

TinyOS manages the data transfer between motes in multi-hops, by which the data is sent to a nearby mote. Then, the mote that has received the data forwards it in the same manner, and circulates until it reaches the destination. This communication method uses less energy and is more effective (Levis et al., 2004).

The features of the TinyOS are as follows:

- TinyOS compiles each component to work together in what is called an Event Driven Model. TinyOS works in response to the incident (a Component-Based Model), which makes the programmed concurrent data aggregation easier (Levis et al., 2004). The

benefit of data aggregation is that it saves energy for WSN because this application helps to reduce the number of data transfers.

- TinyOS only uses the microcontroller (MCU) sparingly, thus the power consumption in terms of memory and processing unit in the system decreases.
- TinyOS has a sleep mode function for power saving; this uses extremely low power consumption in microwatts when entering such a status.
- TinyOS has TinyDB, which is a tool for users to browse query data from the sensor nodes via network by using the Structure Query Language (SQL).
- TinyOS is an open source programme which it is expanded in various models.

Many researchers have improved the application for TinyOS by using the NesC language. The NesC language has been developed and amended from the C language (Levis and Gay, 2009). This language can be supported and adjusted for the WSN application and thus it is very useful. Moreover, the reason for using the NesC language for programming is its low power operation because of its low memory requirements (Gay et al., 2003).

2.2.3 WSN architecture

The network architecture indicates how sensors report to the access points called sink nodes. Sink nodes act as the gateway where the end-user can access the data. The role of the sink nodes is usually for collecting and processing the required information from the sensor to the users. Likewise, it also receives orders from the users to operate in the network (Moschitta and Neri, 2014). Nevertheless, since sink nodes are high processing and have large storage capacities, they have a high energy capacity, more processing power and more memory, compared with general sensor nodes (Camilo et al., 2006).

The ways that nodes can communicate the data to sink nodes are in a single hop or in a multiple hop, as shown in Figure 2.4 (Intanagonwiwat et al., 2013). Basically, the single hop communicates directly to the sink while the multi-hop is communication by transferring the data to its neighbour. Furthermore, a single hop is normally set in small areas whereas a multiple hop is used typically for larger areas and networks, as reported by Krishnamachari (2005). Nevertheless, most WSNs use a multiple hop communication type to pass the information on its neighbour because a single hop has a long distance transmission, and as a result this single hop type of communication leads to high energy consumption. The communication in a multiple hop type has shorter transmission distance than a single hop

type, thus it can save more energy and increase the network lifespan (Moschitta and Neri, 2014).

Single hop

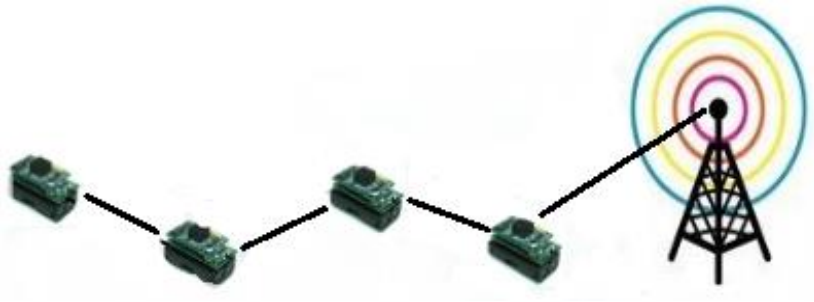

Multiple hop

Figure 2.4: Single hop and multi hop wireless sensor network architecture

(Intanagonwiwat et al., 2013)

However, there are two main kinds of multi-hop network architecture for data communication in the sensor network, which have been considered in the literature and are shown in Figure 2.5 (Moschitta and Neri, 2014) and Figure 2.6 (Khan and Sampalli, 2012). The first is the flat ad hoc architecture. The data is transferred to other sensors by multiple hops until it reaches the access points. The advantage of this network architecture is that it is easy to form the paths for communication between nodes (Agrawal et al., 2006). The second, the hierarchical ad hoc architecture or cluster architecture, that it sends the data to the access points by using cluster heads which are responsible for collecting and reporting the aggregated information. The cluster heads are formed and randomly chosen by various criteria, for instance available energy, other cluster heads, and the distance of the

transmission between cluster members (Moschitta and Neri, 2014). In addition, the hierarchical network architecture is typically energy efficient for collecting and aggregating the information within a large target area, as has been reported by Agrawal et al. (2006).

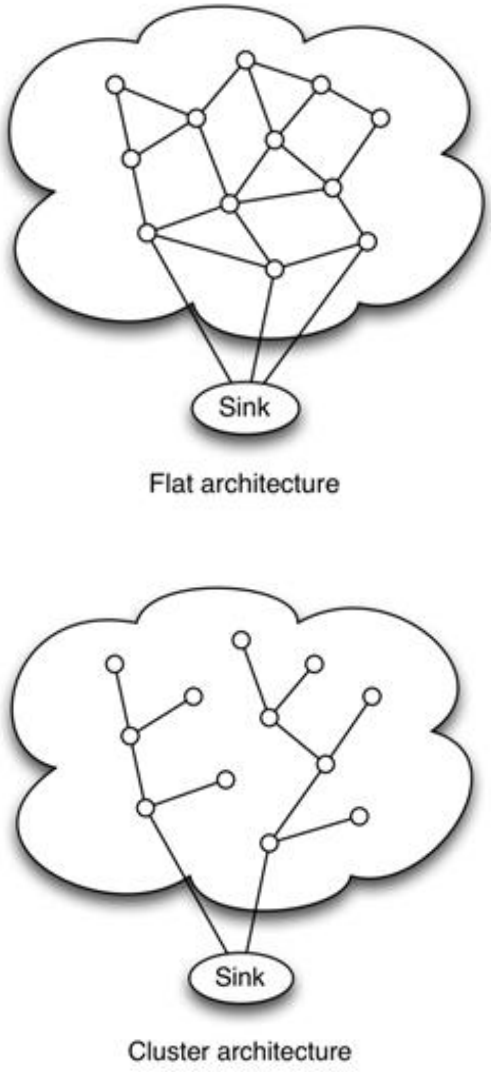

Figure 2.5: Network architecture

(Moschitta and Neri, 2014)

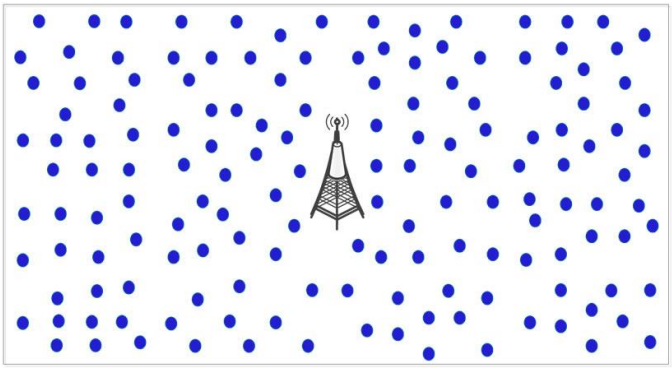

(a) Basic WSNs architecture

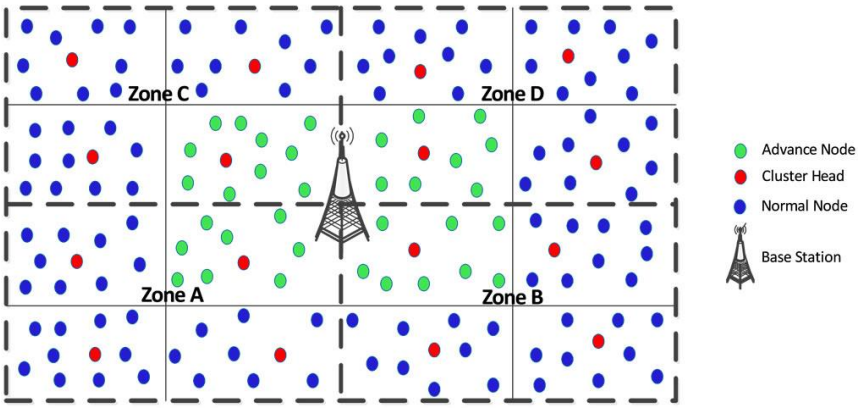

(b) Cluster head selection

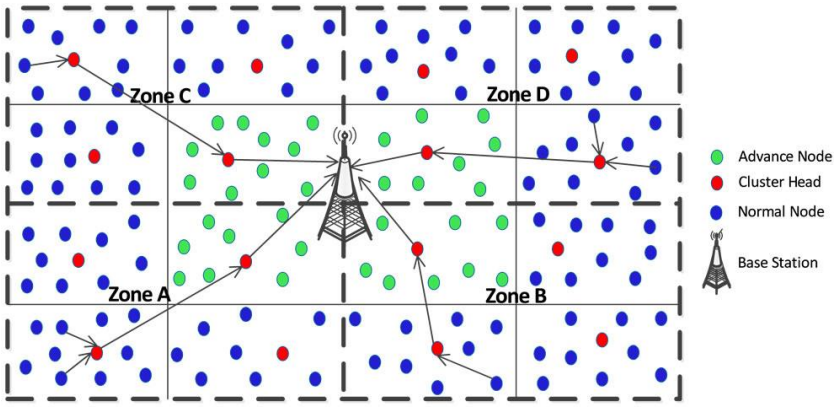

(C) Communication paradigm

Figure 2.6: The hierarchical ad hoc architecture or Cluster architecture

(Khan and Sampalli, 2012)

2.3 Power consumption in WSN

The power of WSNs is consumed by three parts of the wireless sensor nodes: sensing, data communication, and data processing activities (Akyildiz et al., 2002). However, each node is separately distributed and operated as individual device.

Hill (2003) has shown that the power consumption of data processing and sensing uses less energy compared to data communication. Therefore, the vast majority of power energy use for the WSN comes from the data communication subsystem. Figure 2.7 demonstrates the portion of power consumption distribution in the wireless sensor node (Nechibvute et al., 2012).

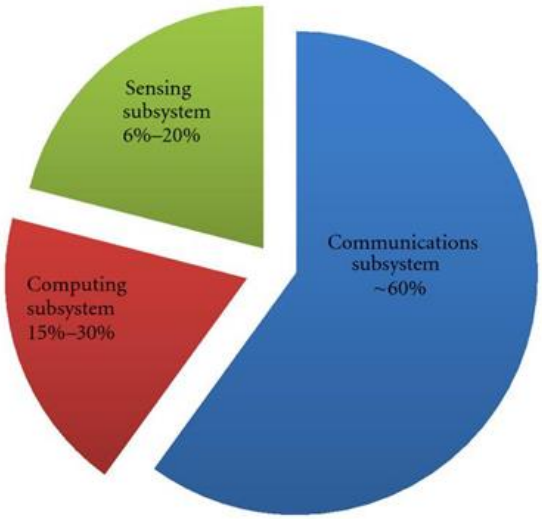

Figure 2.7: The distribution of power consumption in WSN

(Nechibvute et al., 2012)

2.3.1 Power consumption in sensing

In the sensors unit, the source of power consumption can be divided into three sections: signal sampling and the conversion of physical signals to electrical ones, signal conditioning, and analogue-to-digital conversions (ADCs) (Gungor and Hancke, 2009). Moreover, the power consumption depends upon the wake-up time, the stabilisation time, and the off time (offline) of the sensing devices. When the sensor is completely off, meaning no perform operation and no power consumption. Therefore, the sensing subsystem has the lowest energy requirement (Nechibvute et al., 2012). However, if some specific higher ADC

or energy-hungry sensors are used, the power requirement will be nearly equivalent to the communication power consumption (Alippi et al., 2009).

2.3.2 Power consumption in processing

The power consumption of the computing subsystem depends on the various different types of MCUs and the processing, such as the size of the programs, the data memory/storage, the set of integrated peripherals, the development tools availability and so on (Kochláň and Ševčík, 2012), as presented in Table 2.1. This section has a low power requirement because it can be on sleep mode when the system operations are not controlled and processed (Nechibvut et al., 2012).

MCU Name	MCU Family	Power Consumption
Strong ARM (CPU)	32-bit	300mW, 1.5 V/ 200 MHz
Atmel ARM7	32-bit	90mW, 3.3 V/ 48 MHz
TI MSP 430F5437	16-bit	1mW, 3.0 V/ 8MHz
Atmel ATmega 644	8-bit	0.72mW, 1.8 V/ 1 MHz

Table 2.1: The required power consumption of MCU

(Kochláň and Ševčík, 2012)

2.3.3 Power consumption in communications

It can be seen from Figure 2.7 that the highest power requirements come from the communication subsystem. The reason is that every sensor node has to communicate with its neighbour nodes or send the data to the base station wirelessly. Hence, in this project, power energy expenditure in data communication is considered in more detail than others.

In every circuit, the computation of the power consumption for the communication subsystem is divided into two types: active power and start-up power. The start-up power is significant and non-negligible, although the start-up time is approximately hundreds of micro-seconds. Moreover, due to the transmission has a small size, the power consumption when the start-up time is comprehensive the active power consumption. Therefore, a large amount of power energy is used when the transceiver turns on and off on each time (Akyildiz et al., 2002).

In addition, the communication includes both the data transmission and the data reception (Akyildiz et al., 2002). Shih et al. (2001) presents a formulation for the communication power consumption (P_c) as:

$$P_c = N_T [P_T (T_{ON} + T_{ST}) + P_{OUT} (T_{ON})] + N_R [P_R (R_{ON} + R_{ST})] \quad (2.1)$$

Where N_T is the average number of times per second that the transmitter is used, N_R is the average number of times per second that the receiver is used, P_T is the power consumption of the transmitter, P_R is the power consumption of the receiver, T_{ON} is the transmitter on time, T_{ST} is the start-up time of the transceiver, P_{OUT} is the output transmitting power, R_{ON} is the receiver on time, and R_{ST} is the receiver start-up time.

Since the communication in WSN consumes the most power, Callaway (2003) and Hill (2003) identifie that the way to get low average power consumption is for the operation of the transceiver in a WSN node to have a low duty cycle. Low power expenditure leads higher battery capacity and network lifespan. However, the power consumption is hard to generalise for the power requirement for each element, depending on the application and the operation mode of the device, for instance sleep mode, transmitting mode, and receiving data mode (Gilbert and Balouchi, 2008).

System Specifications	Current Value	Duty Cycles Model 1 (%)	Duty Cycles Model 2 (%)
Microprocessor (Atmega 128L)			
Full operation	8 mA	100	1
Sleep	8 µa	0	99
Radio			
Receiving	16 mA	75	0.75
Transmitting (3dB)	17 mA	25	0.25
Sleep	1 µa	0	99
Logger			
Write	15 mA	0	0
Read	4 mA	0	0
Sleep	2 µa	100	100
Sensor board			
Full operation	5 mA	100	1
Sleep	5 µa	0	99
Computed average current consumed		**Model 1 (mA)**	**Model 2 (mA)**
µP		8.0000	0.0879
Radio		16.2500	0.1635
Flash memory		0.0020	0.0020
Sensor board		5.0000	0.0550
Total current (mA) used		**29.2520**	**0.3084**

Table 2.2: The example battery power consumption of IRIS sensor node operating at 100% and 1% duty cycles using two AA batteries with the output between 2.7 to 3.6 VDC

(Crossbow Technology, Inc., 2007)

The research of Jackson in 2010 considers the scenario of the power requirement in sensor nodes, and active mode operation (real time mode: RTC) consumes hundreds of milliwatts while the consumption of power during sleep mode or idle mode drops to a few microwatts. As tabulated in Table 2.2, the findings from Crossbow Technology in 2007 compares and shows the power consumption of each working component between full duty cycle (100% operation) and 99% of sleep mode in sensor nodes, by using an IRIS mote for the test. Therefore, from this sample test, the highest current consumption of a sensor node is approximately 30 mA, with a supply voltage of 3 V.

2.4 Lifespan of WSN

A WSN has a limited lifespan. The analysis of network lifespan relies on various factors which are difficult to distinguish and diagnose, including network architecture and protocols, data collection method, channel characteristics, and the energy consumption model. Overall, the primary limiting factor on lifespan is the power supply; the WSN lifespan strongly depends on the self-powered battery power efficiency of its individual sensor nodes (Hill, 2003).

Each WSN has a different limited lifespan depending on type of sensor, the type of batteries, or the requirement of specific application styles. From work by Tan in 2012, the normative lifespan of WSN sensor nodes by typical batteries is approximately one to two years. An example of the power consumption from Table 2.2, it can be calculated the lifespan of the battery for the sensor node which is based on two AA alkaline batteries of 250 mA-h (milliamp-hours) (coin battery type), 1000 mA-h, and 3000 mA-h; their operation time is approximately at most 1.13, 4.5 and 13.51 months, respectively (Crossbow Technology, Inc., 2007), as shown in Table 2.3.

Battery Capacity (mA-h)	Battery Life (months)
250	1.13
1000	4.5
3000	13.51

Table 2.3: The example of the maximum estimated lifespan of IRIS mote using two AA batteries with the output between 2.7 to 3.6 VDC

Nevertheless, each node contains enough stored energy to use for months or years thus it is critical to design and manage energy power to enhance total network lifespan to the maximum. Therefore, many researchers have encountered the method of extending lifespan in the WSN by using new technologies. For example, design and set the WSN to have the average power consumption of itself as low as possible. Vasanthi et al.'s study (2010) shows it was possible to extend node life to reach three years' operation by using a low-power circuit and networking technologies, based on two AA batteries with a 1% low duty cycle working mode. Moreover, the research of Jackson in 2010 reaches a three-year lifespan of the

sensor nodes, based on four AA batteries by using the new low-power WSN system like National Instruments' WSN platform.

However, using scavenged energy from the environment (energy harvesting) instead of batteries can also be deployed for the WSN to reach an expected time. The nodes are charged by using the environmental energy converted into electrical energy, such as solar energy, thermal energy, wind energy, electromagnetic energy, and mechanical vibration sources (Kumar and Kashwan, 2013). Nevertheless, the external power may be suitable in some situations, and it may face some restrictions in others.

2.5 Energy supply for WSN

The power supply for WSN has various different technology options for storage power – batteries or energy harvesting. Howsoever, Jackson (2010) describes that the most portable and popular energy supply method used for the power all nodes in WSN is the alkaline and the rechargeable battery, respectively.

2.5.1 Batteries

WSN uses an AA battery which converts the chemical energy inside itself into electrical energy. The batteries for use in WSN have two types: primary cells and secondary cells. Primary cells cannot be recharged. They are cheap and widely available, while secondary cells are rechargeable batteries. However, the secondary cells have low energy density when compared to primary cells. Moreover, the secondary cells have higher rates of self-discharge than primary cells (Callaway, 2003).

Starting from the primary battery, there are two types of batteries which are normally used in the WSN: alkaline and lithium. Following the description by Hill (2003), an AA alkaline has a voltage range from 0.8V to 1.65V. It is rated at 2850 mA-h and it has an energy density of about 1500 joules/cm^3 with a volume of 8.5 cm^3. This kind of battery is cheap and has a high capacity for power energy but it has a wide voltage range and large physical size. An AA alkaline minimum discharge rate is 25 mA (Hill, 2003).

The lithium battery has a small physical size, about a few millimetres. This kind of battery does not have to be tolerant to voltage change because it supplies a constant voltage. Moreover, it can operate in a wide temperature range, such as at temperatures to -40 C. It

provides 3 V and 255 mA-h. The energy density is approximately 2400 J/cm^3, with a volume of 1 cm^3. However, this battery has very low discharge current, compared to an AA Alkaline: the minimum current is 3 mA (Hill, 2003).

The secondary battery type is a rechargeable battery, of which there are ordinarily four types: nickel cadmium (NiCd), nickel metal hydride (NiMH), lithium based (Li+), and sealed lead acid (SLA) (Bhuvaneswari et al., 2009). However, Bhuvaneswari et al. (2009) report that SLA and NiCd batteries are rarely applied for the WSN since they have low energy density and suffer from temporary capacity loss. For the Li+ batteries type, they have long lifespan, a low rate of self-discharge and more efficiency than NiMH batteries type. Nevertheless, their cost is high and their circuit is significantly complicated. Hence, the secondary battery type used for the WSN is normally an AA NiMH battery.

However, one problem of the rechargeable battery is a notable decrease in energy density. It provides only 1.2 V. An AA NiMH battery has around half of the energy density and about five times the cost compared to an AA alkaline battery (Hill, 2003). In addition, Callaway (2003) indicates that NiMH batteries have low internal resistance hence this kind of battery is suitable for high peak current applications, such as for cellular telephones and land mobile radios. Nevertheless, some designers have replaced cadmium due to concern about environmental impact, which is NiCd. In addition, these rechargeable batteries can also receive and store energy power from the ambient environment, such as solar energy by using solar cell during sunlight, through which the energy is slowly transferred back into battery.

Figure 2.8 shows the lifespan of various battery powers (Roundy et al., 2003). AA alkaline and lithium batteries have about five years of lifespan whilst the rechargeable batteries have less than a year to a few years. Nevertheless, the typically, the estimated life of Lithium rechargeable battery is approximately two to three years, or 300 to 500 charge cycles, even they are unused (Tektronix, N.D.; M. Brain, 2006).

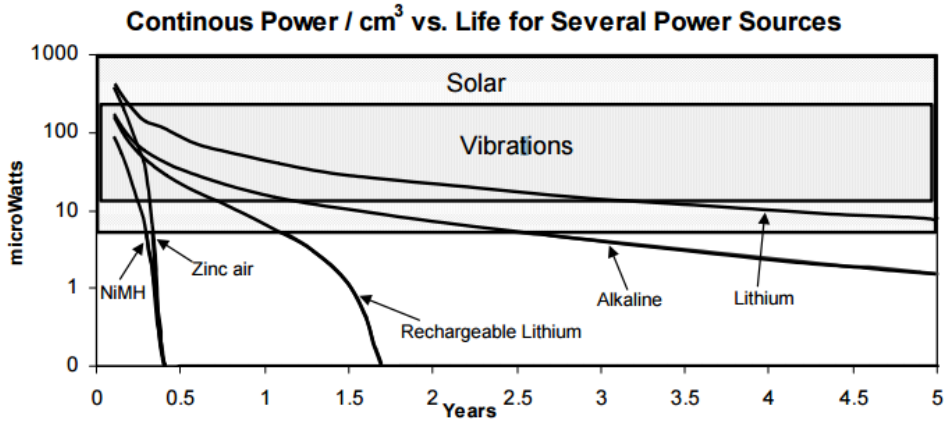

Figure 2.8: A comparison the lifespan from various batteries powers.

(Roundy et al., 2003)

2.5.2 Energy harvesting

Energy harvesting or energy scavenging is a renewable power source for the WSN by extracting energy from an existing source within their environment, as reported by Callaway (2003). This kind of energy offers an infinite lifespan, as long as the ambient source persists. Power energy from the surroundings energy source is transformed by transducer into electrical energy for powering the WSN (Chandrakasan et al., 1999; Zahid et al., 2014).

Numerous researchers have searched for ways to obtain long-term sustainability and performance of batteries by using ambient energy sources for wireless networks. The scavenge energy includes solar energy (photovoltaic or solar cell), thermoelectric energy; thermal of solar and thermal of combustion, kinetic energy; wind energy, waves energy, mechanical vibration, and body motion, wireless power transmission, RF radiation energy, and electromagnetic ambient energy; inductive coupling. However, to select the energy harvesting for nodes should depend on the application of WSN (Lee, 2012). The ordinary elements of energy harvesting devices for WSN are shown in Figure 2.9 (Gilbert and Balouchi, 2008).

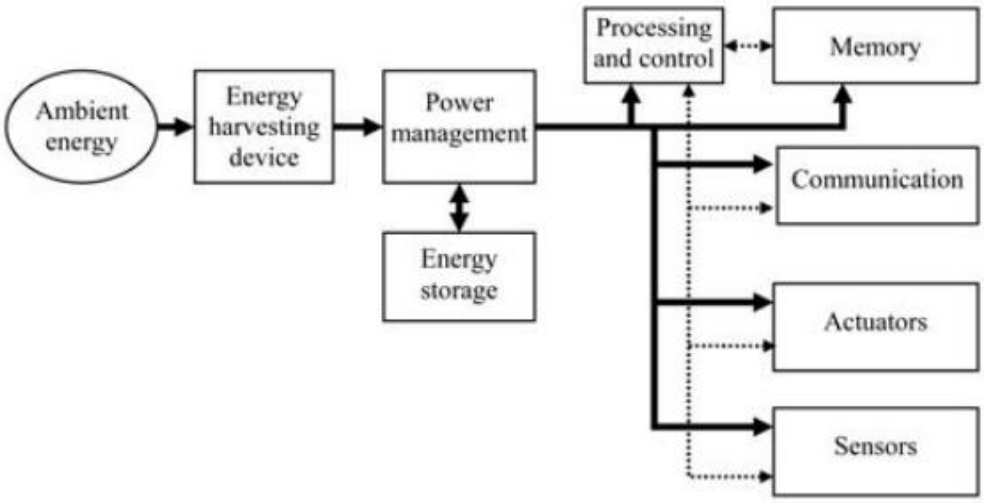

Figure 2.9: The ordinary wireless sensor network node with energy harvesting device (Gilbert and Balouchi, 2008)

The energy harvesting devices embedded in sensor nodes collaborate with the energy storage element for collecting the power and transferring it to the WSN. While the power management is for controlling the energy harvesting devices, and the processing and control part is for generating a stable voltage supply and then providing it to the wireless sensor nodes, as shown in Figure 2.9 (Gilbert and Balouchi, 2008).

From many researchers, rechargeable batteries and supercapacitors are used as the energy reservoir. Nowadays, the supercapacitor or ultra-capacitor is outstanding and is selected to store and deliver the power (Kochláň and Ševčík, 2012). The supercapacitor has very high capacitance, higher than the commonly electrolytic capacitor by thousands of times. Therefore, the self-discharge of this capacitor is higher than others, higher especially than that of electrochemical batteries. The work of Akbari (2014) shows the percentage of self-discharge of a supercapacitor is 100% per month. It has a steady voltage that it has a linear graph of the discharge voltage, reducing from the full voltage to zero voltage. The supercapacitor can perfectly support with short and frequent cycles of charging and discharging at high currents, which means that it can be charged and discharged multiple of times. Hence, the supercapacitor is suitable for coordinating with energy harvesting devices. The operation of this type is around 2.5 - 2.7V. However, several supercapacitors can be linked in a series for higher voltage operation. Moreover, this type can be set in high or low temperature conditions as in the hot or cold weather. The capacity of the supercapacitor

gradually decreases from 100 percent to 80 percent within 10 years (Buchmann, 2003). The supercapacitor has numerous types to select, and is produced in many sizes; the Figure 2.10 displays examples of the supercapacitor type (SparkFun Electronics, 2014).

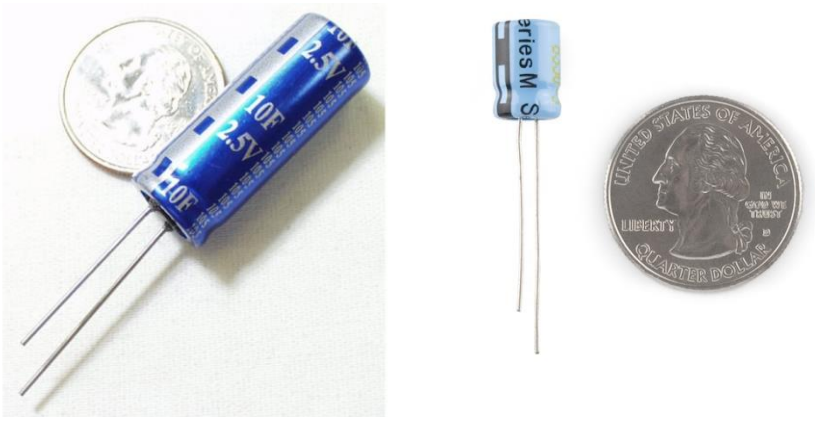

(a) (b)

Figure 2.10: The various example of the supercapacitor; (a) Supercapacitor 10F/2.5V with 13mm x 33.5mm. (b) Supercapacitor Low ESR - 1F/2.5V with 8.5mm x 13.5mm.

(SparkFun Electronics, 2014)

This research will propose energy harvesting from solar energy (Photovoltaic cells), vibration source (Mechanical vibration), and by wireless power transfer (WPT) for installed and applied for WSN. Since these three energy sources are existing in everywhere and never run out. Additionally, these energy harvesting are ease to installation and high efficiency.

2.5.2.1 Photovoltaic cells

The photovoltaic or solar cell is the most familiar and popular type of typical energy harvesting, as described by Callaway (2003). Power electrical energy is converted from the ambient light source, which includes the sun's rays and indoor illumination by solar panel cells or photovoltaic cells. This solar energy harvesting technique can provide the highest power density: 15 mW/cm^3. Hence, it is easy to use to power to sensor nodes which consume several mW of energy (Voigt et al., 2003; Bhuvaneswari et al., 2009; Jackson, 2010).

Photovoltaic cells come in many different kinds. The most widely used is the silicon-based cell type because of the suitable cost and sensitive light detection with a wavelength of

about 800 nm. Furthermore, the silicon cells can divide into three groups: monocrystalline, polycrystalline and amorphous. The monocrystalline type has the highest price and efficiency (about 15 percent), whereas the amorphous silicon cell type has the lowest cost and efficiency (near 6 percent). The polycrystalline silicon cell type offers the efficiency of approximately 14 percent (Callaway, 2003).

- **Photovoltaic cells for WSN**

The energy from the solar energy harvesting is transferred straight from the solar panel. Then the energy is delivered and collected in the energy storage element to provide a stable voltage to the sensor nodes. Therefore, the energy output for WSN is relative to the light intensity during the time of day and the area of the cell. Moreover, the prevailing atmospheric conditions and the angle of installation the photovoltaic cell device also result in the efficiency of energy harvesting from solar energy (Gilbert and Balouchi, 2008).

The fully illuminated solar power detected from the direct sunlight is approximately 100 mW/cm^2, which means the electrical energy is harvested at 100 mW with a volume of 1 cm^2 of the solar panel, whereas the indoor light density is detected at a lower power density than outdoor, roughly 100 $\mu W/cm^2$ or less depending on the type of lighting (Callaway, 2003). Furthermore, from the research of Dondi et al. (2008), the testing 1000 W/m^2 light intensity with temperature of 25 Celsius for charging energy low power application as WSN nodes, represents that it can achieve the efficiency approximately 80 to 90 percent, by providing a stable power supply voltage about 3.3 V. However, they mentioned that the efficiency of this energy harvesting would also depend on the storage element, which means the type of supercapacitor voltage.

Figure 2.11 illustrates a small polycrystalline silicon solar panel 0.5V with a diameter of 6.6mm x 9.4mm x 0.51mm (2.6" x 3.7" x 0.2") and also presents the example of installation solar energy harvesting with wireless sensor nodes for WSN (ApogeeKits Electronic Kits and Tools, 2015; Libelium Comunicaciones Distribuidas S. L., N.D).

(a)

(b)

Figure 2.11: (a) The small polycrystalline silicon solar panel 0.5V with diameter of 6.6mm x 9.4mm x 0.51mm (2.6" x 3.7" x 0.2") (ApogeeKits Electronic Kits and Tools, 2015); (b) The wireless sensor node collaborating with solar panel energy harvesting (Libelium Comunicaciones Distribuidas S. L., N.D)

The expediency of applying solar panel to sensor nodes is low cost and low voltage level, matching with a requirement of sensor devices. However, the solar energy harvesting method can only provide energy in day time. Therefore, it requires an energy storage element, which is battery. For day-time, the energy comes from the solar panels. Conversely, throughout the night, the energy is delivered from the power stored in the batteries to the sensor nodes. In accordance with the above, the stored energy that is collected from solar ray during the day must be enough energy to drain for night operation (Callaway, 2003).

2.5.2.2 Mechanical vibration

The electrical energy supply of the mechanical vibration is converted from mechanical energy in the form of random movement and vibrations. This kind of vibration source is installed in the vibrating areas including the intermittent motion. Examples of an environment in vibration areas are automotive, buildings, structures (bridges, highways, railways and pedestrian lanes), industrial machines, household appliances, and so on (Mathúna et al., 2008). The energy from intermittent movement source includes human or animal activities such as footfall and typing, or from the vehicles passing over the energy

harvesting device (Gilbert and Balouchi, 2008). For example, Starner (1996) and Kymissis et al. (1998) have produced and demonstrated energy harvesting from the energy of footsteps, converting this to energy power by inserting a piezoelectric transducer in the heel of the shoes. The available power during human footfall is approximately 67 W with 68 kg of human weight and for the finger typing is about 7 mW. A paper by Leland et al. in 2004 indicates that they used vibration energy from foot traffic to power a sensor from the wooden staircase by putting a piezoelectric generator under stairway. In addition, a study of Taufik et al. in 2012 presents this kind of alternative energy can apply for wind energy by using piezoelectric material which will be described later.

The transformation of energy from mechanical vibrational sources to electrical energy involves using a suitable mechanical-to-electrical energy converter or generator. There are three main ways varying with the sources, namely, electromagnetic, electrostatic, and piezoelectric (Nechibvute et al., 2012). The electrostatic converter needs to separate the voltage source for the initial processing, so the scale of this converter will be large. In contrast, the piezoelectric converter does not require any voltage source, similar as electromagnetic converters. The piezoelectric gives voltage output about 3-8 V, while electromagnetic gives 0.1-0.2 V (Roundy et al., 2003). Therefore, the piezoelectric generator is one well-known method that has been used for many years (Cook-Chennault et al., 2008). However, the first essential examination for selection of the generator type is up to the vibration source and the application.

The piezoelectric generator is found by Jacques and Pierre Curie in 1880. They discover that the certain crystals are subjected to mechanical strain, and then becoming to electrically polarize when performing in the electric field. Therefore, the electric is produced when force or stress is applied to the piezoelectric material. These generators have various types of materials, for example piezoceramic (e.g. lead zirconate titanate or PZT), single crystal (e.g. quartz), thin film (e.g. sputtered zinc oxide) and polymeric materials such as polyvinylidenefluoride (PVDF) (White and Turner, 1997). PZT is the most widespread because it has a high electromechanical coupling ability. Nevertheless, PZT is not durable forasmuch it is a friable material. Hence, PVDF can be used instead of PZT because it is more flexible (Sodan et al., 2005).

The most well-known design for the vibration source generator uses the bimorph piezoelectric, as can be seen from Figure 2.12. The bimorph piezoelectric has good potential

in power density and it is easy to devise (Leland et al., 2004). This device has generally two layers, which are piezoelectric layer and the metal layer. The energy electric is alternative voltage (AC). AC voltage is provided between electrodes generated from the oscillating mass. Afterward, the piezoelectric material causes tension and compression in the piezoelectric patch, which is mechanically deformed to the beam, as shown in Figure 2.13. (Cook-Chennault et al., 2008; Nechibvute et al., 2012).

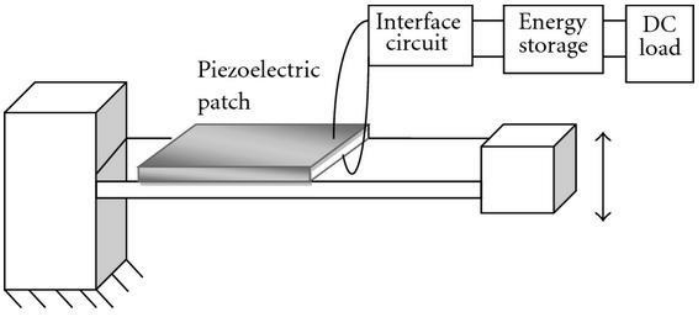

Figure 2.12: Typical of piezoelectric energy harvesting system

(Cook-Chennault et al., 2008)

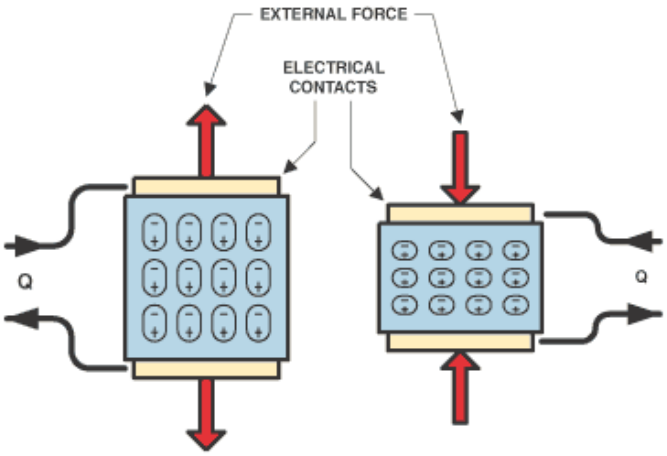

Figure 2.13: A piezoelectric material is squeezed or stretched from the vibration sources providing the electric.

(Ramsden and Dix, 2003)

- **Mechanical vibration for WSN**

The output energy of vibration energy harvesting method is obtained directly from the energy harvesting element, as mentioned before, and this energy will be stored in the energy reservoir for powering the sensor nodes in WSN. The advantage of this energy harvesting is that it can provide a high amount of voltage compared to the other sources (Erturk and Inman, 2011).

The source of vibration ambient provides the electrical energy power for sensors, approximately 4 $\mu W/cm^2$ to 800 $\mu W/cm^2$ (Nechibvute et al., 2012), for which the average power density is about 300 $\mu W/cm^3$ (Roundy et al., 2003; Bhuvaneswari et al., 2009). Nevertheless, the energy extracted from the source of a vibration ambient depends on many situations, for instance it can vary considerably in the frequency and the amplitude of the vibration sources, the extent of the energy vibration detecting device, and the mass of the harvesting device (Gilbert and Balouchi, 2008). As Leland et al. (2004) mention, the power will be optimal when the resonant frequency of the generator accurately matches the frequency of the vibration source. However, the energy charge produces higher energy by using multi-layer stacks or increasing the piezoelectric element's thickness (Beeby et al., 2006). Besides, the efficiency and properties of the piezoelectric device also depends on the age, stress and temperature. Figure 2.14 shows the example of bimorph piezoelectric generator used for WSN which has 31.5mm x 12.7mm x 5.1mm (1.25" x 0.50" x 0.02") with 52g tungsten (Leland et al., 2004).

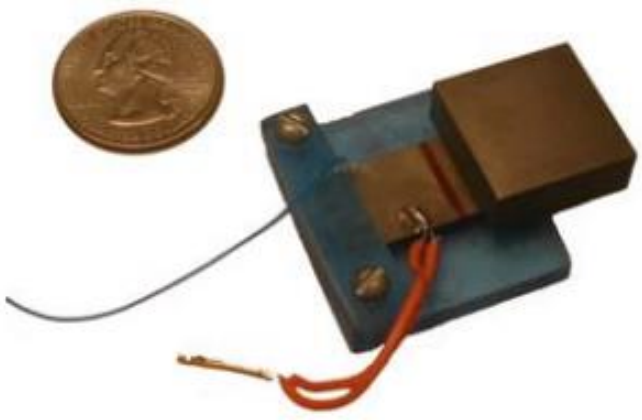

Figure 2.14: The prototype of bimorph piezoelectric generator

(Leland et al., 2004)

2.5.2.3 Wireless power transmission

It is clear from the discussion of using energy harvesting techniques above requires power to be extracted from sources in the environment. In practice, the energy scavenging approach still remains a limitation because it is highly dependent on the places where the WSN is embedded. Additionally, one of the problems about the energy harvesting is the scale of the devices, which sometimes have a larger size than the sensor nodes (Shi et al., 2011). Hence, during the past decade, many researchers have investigated and developed a new enabling energy transfer technology for extending the energy power in WSN. As a consequence, the transmitting of electrical energy wirelessly – first discovered by Nikola Tesla in 1914 – has re-emerged. Nikola Tesla is pioneer of electrical engineering. He sent the electrical signal across the Atlantic in Long Island, New York. However, his invention was not successful and could not be used in practice due to its huge electric fields and the cause of low power transfer efficiency (Tesla, 1914).

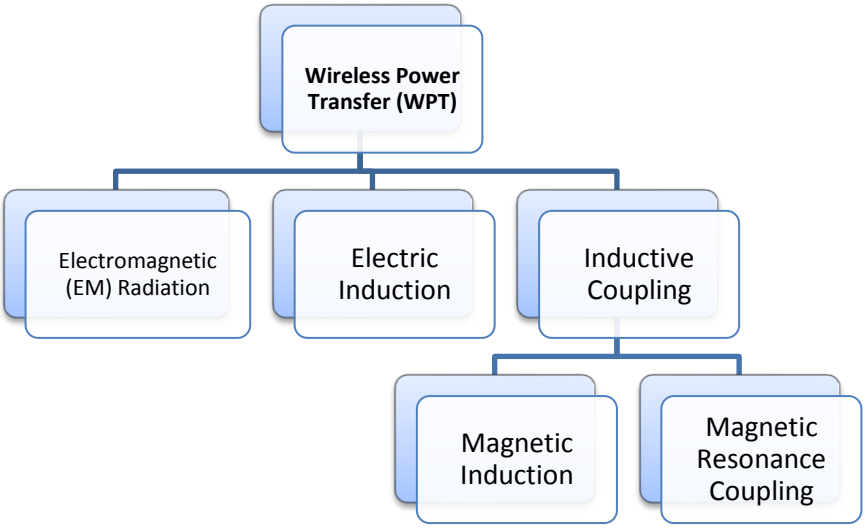

Figure 2.15: Types of WPT technology

The transmitting of electrical energy wirelessly or wireless power transfer (WPT) at wireless sensor nodes has the ability to take clean energy from elsewhere to generate electric power energy for the sensor node periodically without any plugs or wires between the energy charging devices and the receiving nodes (Shi et al, 2011). There are three types of WPT technologies: electromagnetic (EM) radiation, electric induction and magnetic induction, which are divided by the source. The magnetic induction can be divided into inductive coupling and magnetic resonant coupling (Sah and Pant, 2014), as shown in Figure 2.15.

However, in the article by Xie et al. in 2013, they identify that omnidirectional emitting EM radiation and magnetic resonant coupling are suitable for WSN. The inductive coupling is not suitable for wireless sensor networks because it has a limited short charging distance between the transmitters and receivers, from a few millimetres to a few centimetres, while the distance for using in WSN is around ten centimetres to several tens of metres (Lee et al., 2012). The Figure 2.16 illustrates that EM radiation (RF radio-frequency emission) and magnetic resonant coupling can transfer power across longer ranges than electromagnetic induction, which is the one reason for choosing two kinds of WPT technologies used in the WSN (Akimoto and Iizuka, 2013; Sample et al., 2011). In addition, as can be seen from Figure 2.16, the electric field resonance technique has similar efficiency and distance of transfer power as the magnetic resonance method. However, Kim and Bien in 2013 stated that the electric field resonance technique has many conditions to consider for using in WSN such as the weather conditions and especially in safety problems because this technique uses metal plate which needs insulator coated; the effect of material coated is mainly considered. Thus, Kim and Biem recommended that the electric field resonance method is not suitable for using in WSN. Therefore, this research paper will show and explain only two kinds of WPT; magnetic resonant coupling and omnidirectional emitting EM radiation (RF radio emission).

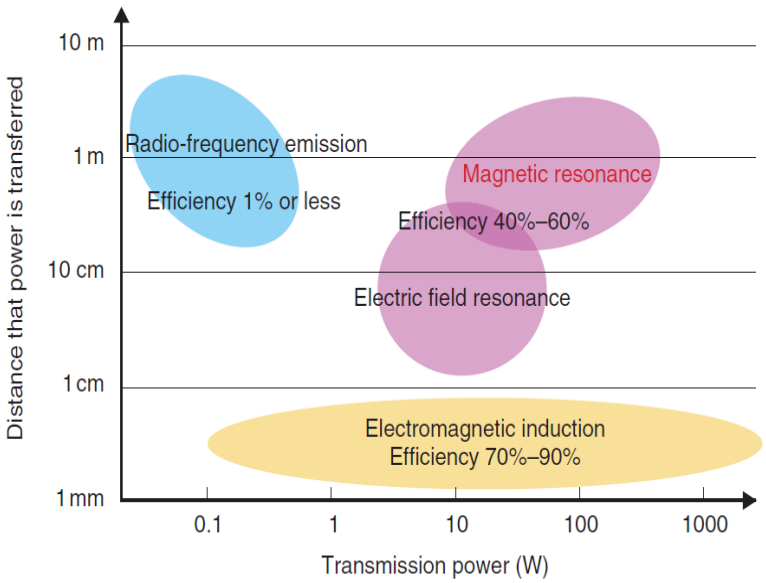

Figure 2.16: A comparison of WPT methods between distance of transferred power and transmission power

(Akimoto and Iizuka, 2013)

2.5.2.3.1 EM radiation

EM radiation method uses the radio frequency (RF) signal. EM radiation can be divided into two types by the energy-emitting direction: omnidirectional radiation and unidirectional radiation. From the paper of Xie et al. in 2013, omnidirectional radiation is suitable for the WSN since this kind of direction is applied in unknown or uncontrollable applications. Moreover, the radiation provided in omnidirectional waves is also necessary for ultra-low power applications such as using for very low sensing (e.g. temperature, moisture, and light) in the milliwatt and microwatt range, depending on the distance from the sources or based on the limited of transmitters, which is approximately not more than 10 mW. Consequently, omnidirectional EM radiation is suitable for the WSN while unidirectional radiation is not suitable because of the undesirable requirements.

The EM radiation energy is emitted by the transmitting antenna of the power source to the receiving antenna; which the RF transmitter broadcasts radio waves in an assigned ISM (Industrial-Scientific-Medical) band is from 902 MHz to 928 MHz with an average centre frequency of 915 MHz (Sample et al., 2008). Then the RF receiver adjusts the frequency to the same band to the radio power harvesting.

The RF energy harvesting distributes the power from one source to many wireless sensor nodes even over distances (Ostaffe, 2009). The omnidirectional EM radiation has some serious efficiency problems in energy transfer for the WSN since EM waves decay quickly over distance; they have only 1.5 % of energy transfer efficiency when the distance of transmitting and receiving antenna is 30 cm away (He et al., 2013). Furthermore, this radiative technology is sensitive to obstruction when sending the energy between transmitters to receivers (Xie et al., 2013). Therefore, this EM radiation method has some limitations for applying to the WSN. Nevertheless, the omnidirectional EM radiation is still applied for providing energy to WSN such as a wireless identification and sensing platform (WISP) device.

- **The EM radiation for WSN**

The wireless identification and sensing platform (WISP) was applied for RF energy harvesting for WSN by Intel in 2010. The WISP has the advantages of the radio frequency identification (RFID) technology at ultra-high frequency (UHF) EM wave band with the

range between 860 to 960 MHz, and it can distribute metres away from itself (Buettner et al., 2008; Lee et al., 2012). The RFID comprises tags which are small size, low cost and battery-free device. They can be attached with any object for identifying. The typical RFID tag device is fixed function, non-programmable, no general purpose computation, and no sensing capabilities (Buettner et al., 2008). The RFID tags can be divided into two types, which are active and passive (Want, 2006). The active RFID tag is powered by the battery itself while the passive RFID tag receives the RF signals by an RFID reader rather than requiring an on-board battery to power the communication circuitry, sensors, and MCU autonomously. However, the passive RFID also can remotely transfer energy, and interrogate for identifiers and other information at the range of approximately 9.144 metres (Weinstein, 2005). Therefore, the passive UHF RFID is used to be assembled as a part of the WISP, with an operating distance of several meters (Sample et al., 2008). In addition, the advantages of passive UHF RFID are inexpensive tags and small size. Moreover, it can reliable and face no limits on battery life (Buettner et al., 2008).

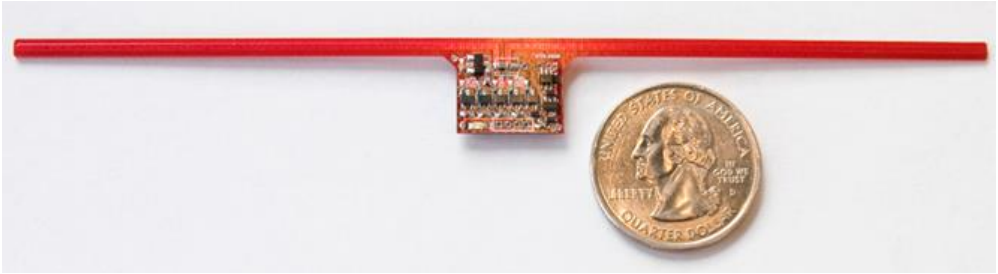

Figure 2.17: The wireless identification and sensing platform (WISP)

(Smith et al., 2011)

The RFID WSN consists of the WISP (RFID sensor nodes) and UHF RFID reader, which may have multiple of WISPs and one or more readers. The attraction of using WISP is its very small size, about 147 mm x 12.7 mm x 2.54 mm (15.24 mm^3) (5.5" x 0.5" x 0.10" (0.60 in^3)) (Buettner et al., 2008), and the long-lived power source. Additionally, it has unpowered functionality for up to 24 hours even though there is a lack of internal or long-lived battery since it uses a storage capacitor to store RF energy when in range of a reader (Buettner et al., 2008).

The WISP is a device that is powered by the RF energy: the energy is transferred from the UHF RFID reader in the manner of standard RFID tags because it has no batteries. It is implemented as a printed circuit board (PCB), as can be seen from Figure 2.17. The WISP

features a wireless power supply, bidirectional UHF communication, and an open source. The WISP has a fully programmable, ultra-low-power, 16-bit general purpose MCU with analogue to digital converter (ADC) for performing the sensing and computation while operating from RF harvested energy (Lee et al., 2012). Moreover, the WISR has 32K bytes of program space, 8K bytes of flash, an accelerometer, temperature sensors, and 8K bytes of serial flash. It can transfer 64 bits of the data per query. The communication and power harvesting of WISP use the Electronic Product Code (EPC) global Class-1 Generation-2 (EPC Class 1 Gen 2) protocol with a range of approximately 3 metres (EPCglobal, 2005).

A recent experiment by Fu et al. in 2013 shows that the WISP charging time of 155 seconds can reach 1.8 volts with 100 µF capacitor when the RFID reader is 10 metres away.

As known that the WSN has a big size; sometimes the area of WSN is larger than the signal of RFID reader can reach the WISP, and to prevent irregular signals by the reason of some the obstruction between transmitters and receivers. Besides, the RFID reader is much more expensive than WISPs, by a factor of approximately 100 times. So, for the practical, robots are applied to carry the RFID reader and drive around network for charging to nodes, as Fu et al. (2013), and Lin et al. (2008) have presented. Figure 2.18 illustrates the three stop positions of the RFID reader robot for charging the WISP sensor nodes in the network.

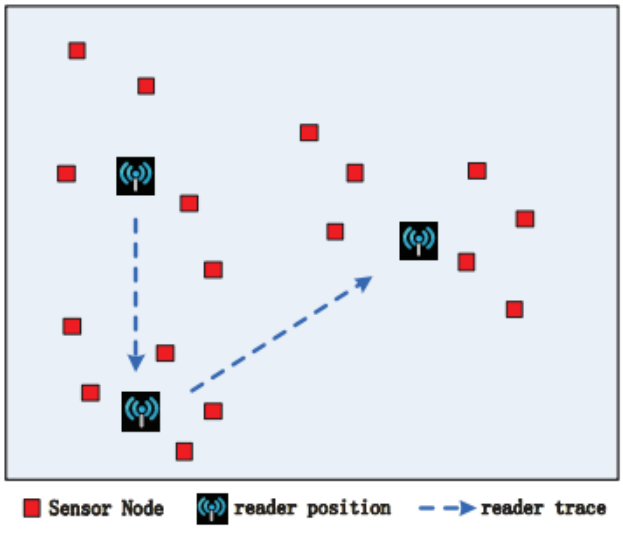

Figure 2.18: The stop positions of RFID reader in the WSN

(Fu et al., 2013)

2.5.2.3.2 Magnetic resonant coupling

Even though the EM radiation method is used for the transfer of power, the energy is quite low efficiency because of the omnidirectional radiation which means it wastes the energy through the free space (Karalis et al., 2008). For this reason, another method of WPT technology is magnetic resonant coupling. The theoretical and experiment paper by Kurs et al. (2007) presents the principle of resonant coupling, which using two magnetic resonant coils operating at the same resonance frequency in order to exchange energy efficiently for a mid-range power transfer. This method of WPT is non-radiative wireless power transfer. The distance for transfer energy by magnetic resonant coupling is approximately 10–300 cm (Jonah and Georgakopoulos, 2012), with power level spans from less than one watt to multiple kilowatts (Kesler and McCarthy, 2013).

In this way, the power transfer is high efficiency because the dissipating energy while in an extraneous off-resonant objects loses little energy power. Moreover, the magnetic resonant coupling is omnidirectional irrespective of the geometry of the surrounding area (Karali et al., 2008). In addition, the distance is very flexible between the source and the receiver coil, which it can be vary from a very close range to long distance. For instance, the range may be less than the diameter of the coil to several times the coil diameter. Furthermore, since the magnetic fields do not interact with most of the ordinary materials, magnetic resonance would barely suitable for every application. Besides, the magnetic resonant coupling WPT technology is also waterproof, which means it can be set in humid areas or underwater, as the work of Kesler and McCarthy in 2013 involving transfer energy by using an unmanned underwater vehicle. Hence, the magnetic resonant coupling is the most appropriate WPT technology for the WSNs, as reported by Xie et al. in 2013.

The experiment paper by Kurs et al. (2007) notes that the distance between the energy source storage and energy receiving devices for fully powering a 60 W of light bulb is about two metres for several tens of watts of the energy transfer with 0.5 m of the diameter of transmitter and receiver coils. Therefore, the distance of sending electric energy could be four times that of the coil diameter. However, the power transfer efficiency from the transmitter coil to the receiver coil under the resonance coupling decreases with the distance (Kurs et al., 2007). In addition, Yao et al. (2011) have done an experiment that this method can charge a NOKIA cell phone wirelessly over 40 cm with power input less than four watts, and 52% of efficiency over a 32 cm distance.

The principle of the magnetic resonant coupling power transfer is the matching resonance frequency between the two couple resonant coils, the transmitting coil and receiving coil, and the transmission of the energy with electromagnetic coupling from the transmitter coil to the receiver coil by oscillating, even though there is a long range between two coils. The power can transfer much more amount of the energy efficiency and sent in longer distance if the coils are driven at their resonant frequency, which this frequency is generated when an object naturally vibrates or rings.

The magnetic resonance coupling WPT technology includes the power amplifier, the transmitting and receiving coils, and the receiver, as can be seen from the block diagram of this WPT system from the Figure 2.19, which illustrates the power transmission from the transmitter coil to the receiver coil by an oscillating magnetic coupled resonator. The first step is the direct current (DC) coming from the power supply and then converting the DC to alternating current (AC) by rectifier. Then the oscillator generates a signal of the required frequency. Next the signal is amplified by the power amplifier and then through to the power coil and transmitter coil respectively. Then the transmitter coil (Tx coil) receives the signal frequency and stores the energy. Afterwards, it begins to resonate and produces the evanescent resonated waves that the receiver coil (Rx coil) will pick up. Finally, it transfers to the load coil, rectifier and load devices, respectively. These are the keys to send the power by wirelessly and the interaction between two coils (Nair, 2012). Furthermore, as Sah and Pant (2014) have documented, the power amplifier in this system acts as the control mechanism because it can determine the performance of the system; it is not just only for a power converter, and thus they elucidates that the power amplifier is the one of the most important components.

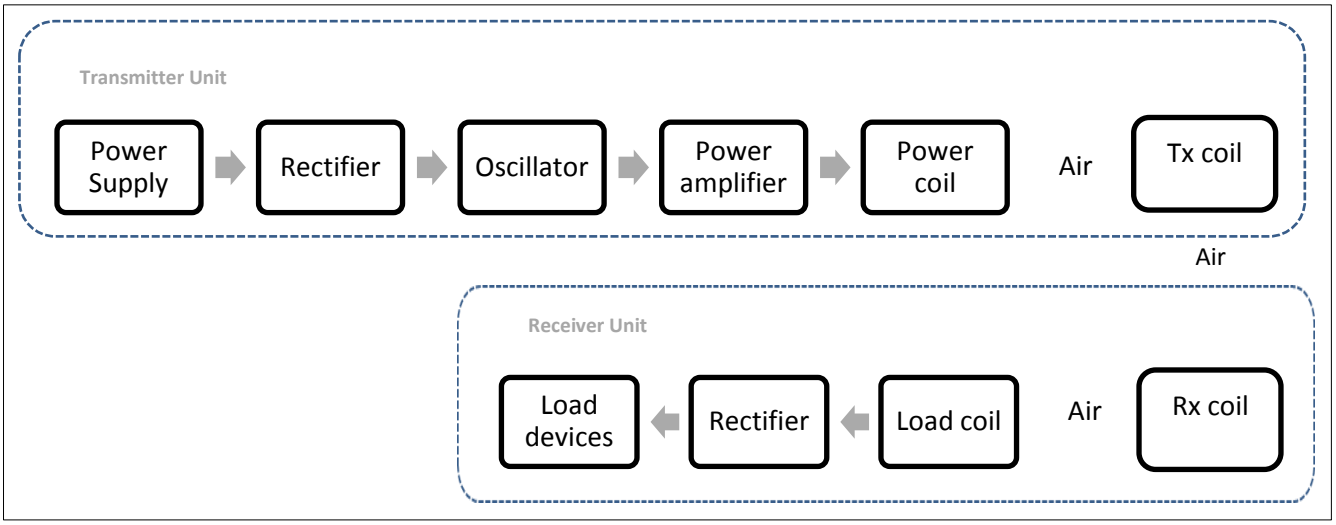

Figure 2.19: The basic block diagram of magnetic coupled resonance WPT system

The magnetic resonance coupling transfers the energy with the electromagnetic coupling in term of lumped circuit elements, i.e. resistor R, inductor L and capacitor C, as illustrated in Figure 2.20 (RamRakhyani et al., 2011), which the key of magnetic coupled WPT is add the capacitor in series in order to create the resonant frequency of the network (Wei et al., 2014).

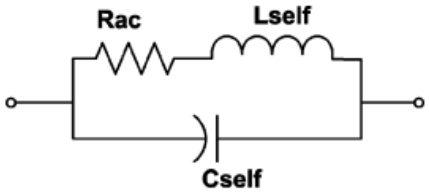

Figure 2.20: Coil lumped model

(RamRakhyani et al., 2011)

In Figure 2.21, the simplified schematic of the magnetic resonance coupling WPT system is shown. The basic circuit structures of magnetically coupled resonator WPT technology have parallel-parallel and series-series compensations (Wei et al., 2014). However, for the simplicity, the series-series compensation is presented in this research.

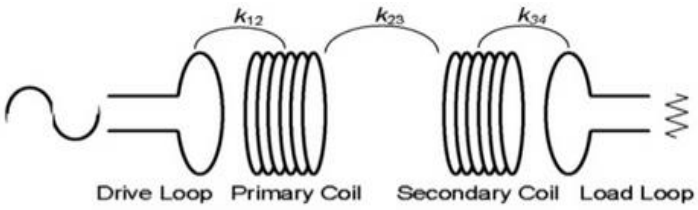

Figure 2.21: The simplified schematic of the WPT system

(Sah and Pant, 2014)

The equivalent circuit model of the WPT via magnetic resonant coupling system architecture has three or four coils. A recent paper by Wei et al. (2014) reports that the system architecture with four coils is low transfer power despite the high transfer efficiency whereas three coils architecture can adjust to more power transfer and simultaneously keep the efficiency invariable. However, the system architecture with four coils is easier to understand and more obtainable, and thus this paper will focus on this system. Figure 2.22(a) and Figure 2.22(b) indicate the equivalent circuit model of the WPT system architecture of three coils and four coils respectively as a series resonator (Wei et al., 2014).

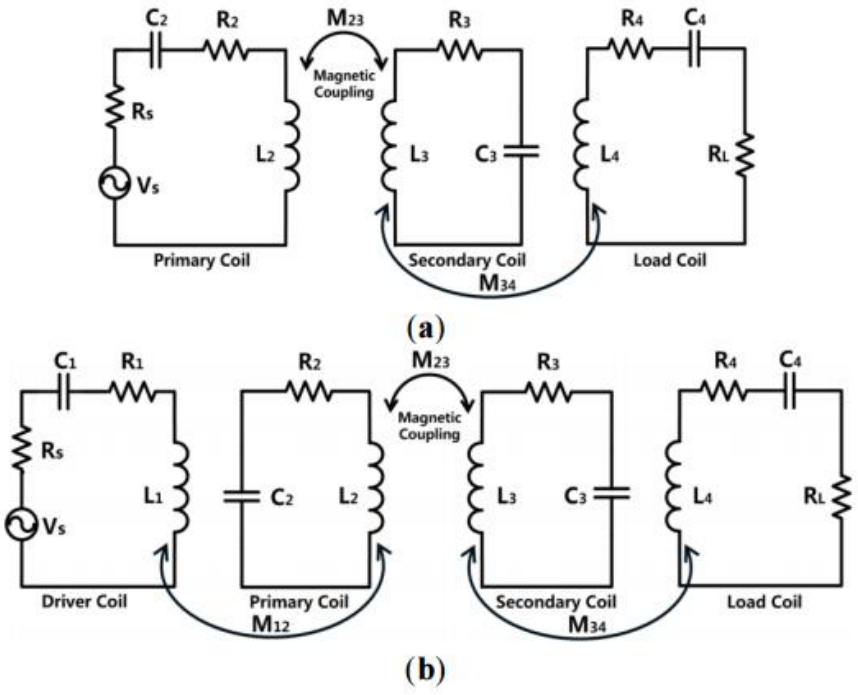

Figure 2.22: (a) The equivalent circuit model of system architecture with three coils

(b) The equivalent circuit model of system architecture with four coils

(Wei et al., 2014)

The four-coil architecture system consists of the driver (power) coil, transmitting coil, receiving coil and load coil which the three mutual magnetically by coupling coefficients between adjacent coil; M_{12}, M_{23} and $M_{34,}$ as indicated in Figure 2.22(b). From Figure 2.22(b), following the study of Wei et al. (2014), firstly, the drive loop is modelled by a simple one turn or a few turns inductor L_1 with parasitic resistance R_1 and capacitor C_1. Secondly, the transmitter coil (primary coil) is a multi-turn of spiral inductor L_2 with parasitic resistance R_2 and self-capacitance C_2. The receiver coil (secondary coil) and load coil are the same schematic as the drive coil and transmitter coil respectively. The inductors coil L_1 and resonant helix L_2 are linked by the mutual inductance M_{12} for the transmit unit. Likewise, M_{34} connects both inductors L_3 and L_4 of the receiver unit. For M_{23}, it is a coupling coefficient relating between the transmitter coil and the receiver coil. Normally, the drive coil and the transmitting coil are built in the same device like the receiver coil and load coil. M_{12} and M_{34} would be fixed, whereas M_{23} varies by the distance between the transmitter and receiver coil, which it is the uncontrolled value. In this system analysis, it is assumed that the cross-coupling terms can be neglected because they are very weak. The cross-coupling terms are the coupling efficient between the driver coil and the transmitter coil (M_{13} or M_{31}), the transmitter coil and the load coil (M_{24} or M_{42}), and the driver coil and the load coil (M_{14} or M_{41}) (Sample et al. 2011; Sanghoon et al., 2011).

- **Magnetic resonance coupling for WSN**

For the WSNs, as Xie et al. (2012a) have documented, they applied a mobile wireless charging vehicle (WCV) using a robot or helicopter for carrying power-charger from the service station to each sensor node wirelessly, based on magnetic resonant coupling, as can be seen from Figure 2.23 and Figure 2.24, which illustrate a mobile WCV in the wireless sensor network and the travelling path of a WCV in the network respectively. This WCV can also be controlled by a human or be autonomous depending on the setting and application. Upon completing the visit to all sensor nodes in the network, a WCV returns to the service station for resting and recharging battery, called ‘vacation time’, and gets ready for starting the next trip.

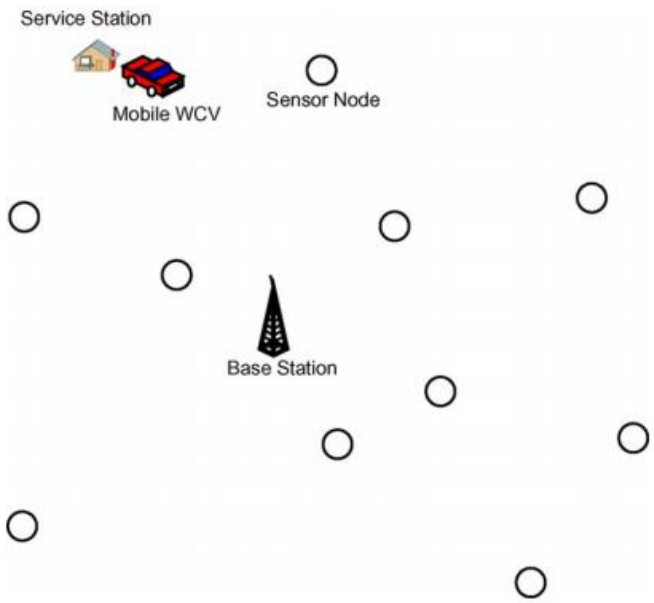

Figure 2.23: A mobile WCV in WSN

(Xie et al, 2012a)

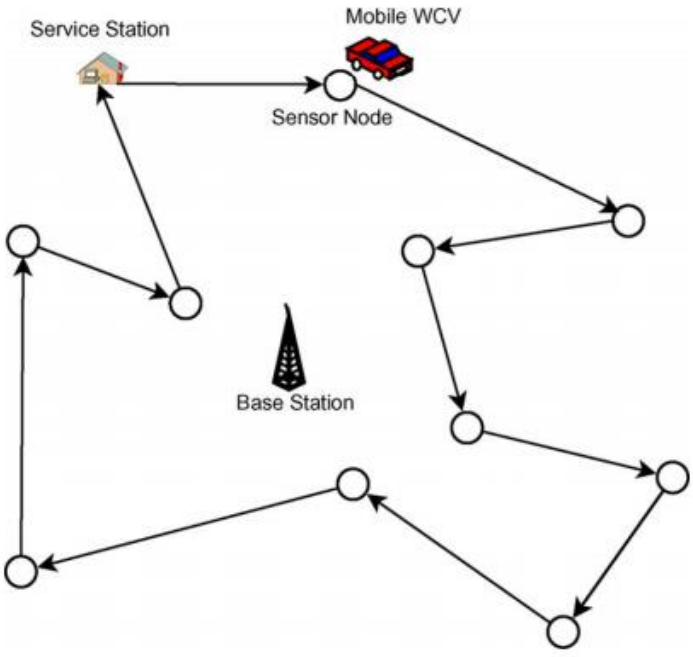

Figure 2.24: A travelling path of WCV visits each sensor node for charging battery via WPT

(Xie et al., 2012a)

Furthermore, Xie et al. (2012b) develop and improve the WCV for applying in WSN based on the paper of Kurs et al. (2010); and Cannon et al. (2009), according to which a WCV can charge multiple sensor nodes simultaneously when within the charging range. The charging range of the WCV is modelled on a cellular structure that partitions the two dimensional plan into several adjacent hexagonal cells. Then, a WCV travels to the centre of each cell for charging all nodes in a hexagonal cell, as can be shown in the Figure 2.25. In this figure, the solid dots indicate cell centres and the empty circles mention the sensor nodes. Nevertheless, the researchers assumes that the power transfer from a mobile WCV has sufficient energy for charging all sensor nodes within one completed travelling path before returning to recharge the battery at a service station (Xie et al., 2012a; Xie et al., 2012b).

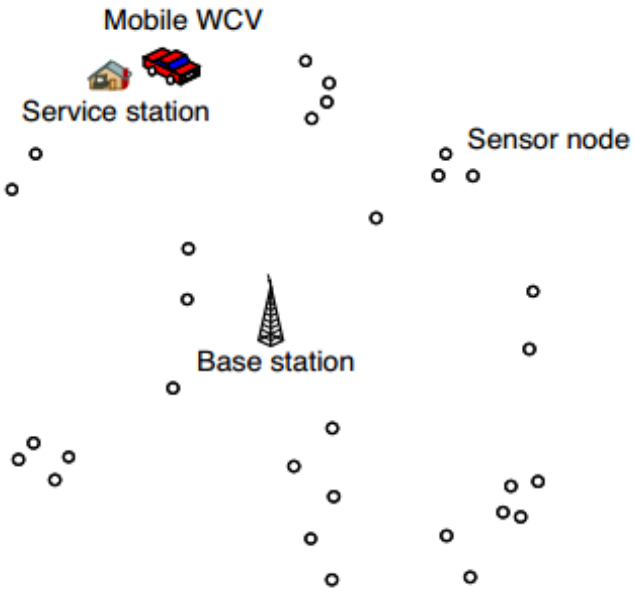

(a)

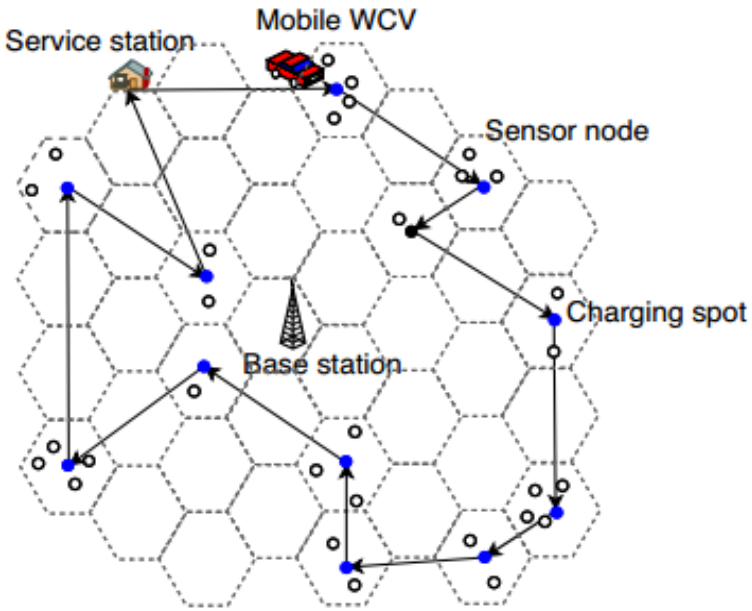

(b)

Figure 2.25: (a) A mobile WCV in WSN; (b) Showing a cellular structure that partitioned the two dimensional plan into several adjacent hexagonal cells in WSN and a travelling path of WCV visits cell in order to charge battery for multiple nodes via WPT

(Xie et al., 2012b)

Chapter 3 – Design for prolonging the lifespan of the WSN

3.1 Introduction

As mentioned in Chapter 2, using energy harvesting device embedded with sensor nodes may increase to prolong the lifespan of WSN systems by collecting energy from the surrounding environment. There have been many techniques of energy harvesting, as presented in Chapter 2, such as solar energy, vibration source, and wireless power transfer (WPT). However, the WPT by coupled resonance magnetic is selected here. Therefore, this study will direct to apply the magnetic resonance coupling WPT in order to increase the life time of WSN.

This chapter represents the method for the design of the experiment. In addition, this section gives the specific information and the theories about the WPT of this study model, and also evaluates the parameter values for demonstration in the experiment.

3.2 The design for WSN

Recently, the WSN has become well-known because this network can be applied in various areas, such as utilities, industry, home, shipboard, aircraft, medical, military, etc. However, this system has a limited lifespan due to the batteries used in nodes. Some researchers have attempted to extend the life power energy of the nodes by developing the operating systems which explore different routing protocols, for instance LEACH (Low Energy Adaptive Clustering Hierarchy), CB-DHRP (Cluster Based Directed Hierarchical Routing Protocol), BCBE (Balanced Cluster and Balanced Energy) (Jain, 2011).

Nevertheless, to improve the protocol or operating system also cannot prolong the lifetime of the sensor nodes as contented. Therefore, the techniques of using energy harvesting instead of the batteries applying in all nodes become to the one of the appropriate solution to expand the lifespan WSN, because the energy harvesting methods may produce energy from the environment which cannot run out. The energy harvesting have many types, for the main energy harvesting using for wireless sensor network have been described in Chapter 2, such as solar energy (photovoltaic), mechanical vibration energy, electromagnetic sources, and magnetic inductive field. Notwithstanding this, many researchers have stated that solar power is the most available and suitable for energy harvesting nowadays, as the

Solar Foundation and SEIA in 2014 and the poll from Ipsos MORI in 2011 have mentioned. Therefore, normally, the power scavenged taken from solar energy should be the most efficient and ubiquitously used in WSN. However, the solar energy has a constraint: its optimisation relies on the light conditions; heavy light or low light. A photovoltaic cell may not an excellent provider of power energy if it is embedded in dim or inadequate light areas where sunlight is not available, such as in indoors or in forest terrains. Hence, other technologies of energy harvesting, such as mechanical vibration, wind power (by piezoelectric) or WPT become an attractive alternative solution choices which may potentially outperform solar energy for some applications, while being similarly easily accessible (Roundy et al., 2003), as mentioned in Chapter 2. However, the vibration energy or wind energy also depend on the environmental conditions, unless the WPT technique can be applied to all situations. Balouchia and Gohn in 2012 from the Pike research acknowledge that the coupling magnetic resonant WPT will be up to more than 70 percent in 2020.

However, there have two ways of WPT to apply for WSN: EM radiation energy harvesting and magnetic inductive. EM radiation energy harvesting method has low efficiency compared to the coupled magnetic resonant induction WPT (Karalis et al., 2008). Furthermore, the transmission power between transmitter and nodes by EM radiation energy harvesting method can be easily disturbed by the obstructions. Accordingly, the WPT energy harvesting has been selected as the most suitable for powering the energy to all nodes in the WSN by using magnetic coupling resonance WPT. Due to the magnetic coupling resonance, the WPT method is easy to design. The electronic system of this energy harvesting is reliable. The cost is low and it can be watertight (Kesler, 2103).

In addition, this kind of energy harvesting uses the magnetic fields to transfer the energy, as in cell phones, wireless routers, Bluetooth headphones, radio transmitters, etc. (Kesler, 2103). It is a matter of human safety which is related to Institute of electrical and electronics engineers (IEEE) (2006) and International commission on non-ionizing radiation protection (ICNIRP) (1998); they indicated that humans cannot get cancer from exposure to radio frequency electromagnetic fields.

3.3 The design principle to prolong WSN lifespan by using coupling magnetic resonant WPT

To prolong lifespan for WSN by the coupling magnetic resonant WPT method, this system is using a magnetic field to charge a battery which can send power across a distance.

This system can be divided into two parts: the transmitter part and the receiver part. The transmitter part is embedded in the mobile wireless charging vehicle (WCV)–here, a robot is chosen to carry this part for powering energy to the receiver part. Whereas the receiver part is placed into all nodes in order to receive and collect the power when the transmitter part coming in the same axis with the node. The energy will be transferred for charging to the supercapacitor which is embedded and applied to all sensor nodes of the system in order to collect the power by the coupling magnetic resonant WPT technique.

This study focuses on the WPT by magnetic coupling resonance for powering all nodes on the WSN. Moreover, the researcher designs an experiment suitable for this network.

3.3.1 Consideration of the model

The model of the experiment shown in Figure 3.1 has four coils following from the paper by Wei et al. (2014) which they report that the system architecture with four coils has high transfer efficiency, easy to understand and more obtainable. The model can be divided into two parts: a transmitter part and a receiver part. The transmitter part includes loop coil 1 (input coil) and loop coil 2 (transmitting coil; Tx), whereas the receiver part consists of loop coil 3 (receiving coil; Rx) and loop coil 4 (output coil). The power source is connected to loop coil 1 and the load is connected to loop coil 4. Loop coil 1 and coil 4 have N_1-turn coil and N_4-turn coil, respectively, called the feeding coil. Loop coil 2 and coil 3 have N_2-turn coil and N_3-turn coil, respectively, called the resonant coil. The power is transported between two resonant coils by the magnetic coupled resonance, whilst the power is transferred from the feeding coil to the resonant coil and from the feeding coil to the load coil by magnetic inductance (Hirayama, 2012).

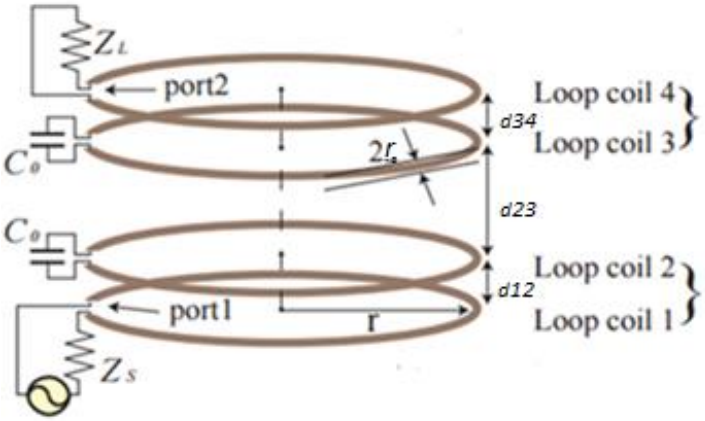

Figure 3.1: The model structure of magnetic coupled resonant wireless power transfer (Hirayama, 2012)

Figure 3.1 illustrates the loop radius of the loop coil; r and radius of wire copper; r_c. The distance between loop coil 1 and 2, loop coil 2 and 3, and loop coil 3 and 4 are replaced in d_{12}, d_{23}, and d_{34}, respectively. Moreover, C_0 is presented the resonant capacitors which are placed for modulation to be the same resonant frequency in order to be the magnetic resonant coupling between loop coil 2 and loop coil 3. Finally, Z_S and Z_L are indicated to the impedance of the source and the impedance of load, respectively (Hirayama, 2012).

However, for simplicity of the model and calculation, the researcher designs all loop coils to have the same diameter. In addition, the researcher presumes that the system is symmetrical, which means the input loop and transmitting coil identical to the output loop and the receiving coil, respectively. The number of turns of loop coil 1 and loop coil 4 are equal ($N_1 = N_4$). Likewise, the number of turns of loop coil 2 is same as the number of turns of loop coil 3 ($N_2 = N_3$). Therefore, this design means the inductance of loop coil 1 equals the inductance of loop coil 4 ($L_1 = L_4$). The resistance of loop coil 1 equals the resistance of loop coil 4 ($R_1 = R_4$). In the similar way, inductance from loop coil 2 has the same inductance from loop coil 3 ($L_2 = L_3$), and resistance from loop coil 2 is the same as resistance from loop coil 3 ($R_2 = R_3$). Furthermore, the distance between loop coil 1 and loop coil 2, and loop coil 3 and loop coil 4 are fixed range; this means the distance between loop coil 1 and loop coil 2, and loop coil 3 and loop coil 4, is fixed, which means d_{12} equals d_{34}.

3.3.2 The equivalent circuit of the design

The equivalent circuit of this experiment model structure by magnetic resonant coupling from Figure 3.1 is presented in Figure 3.2.

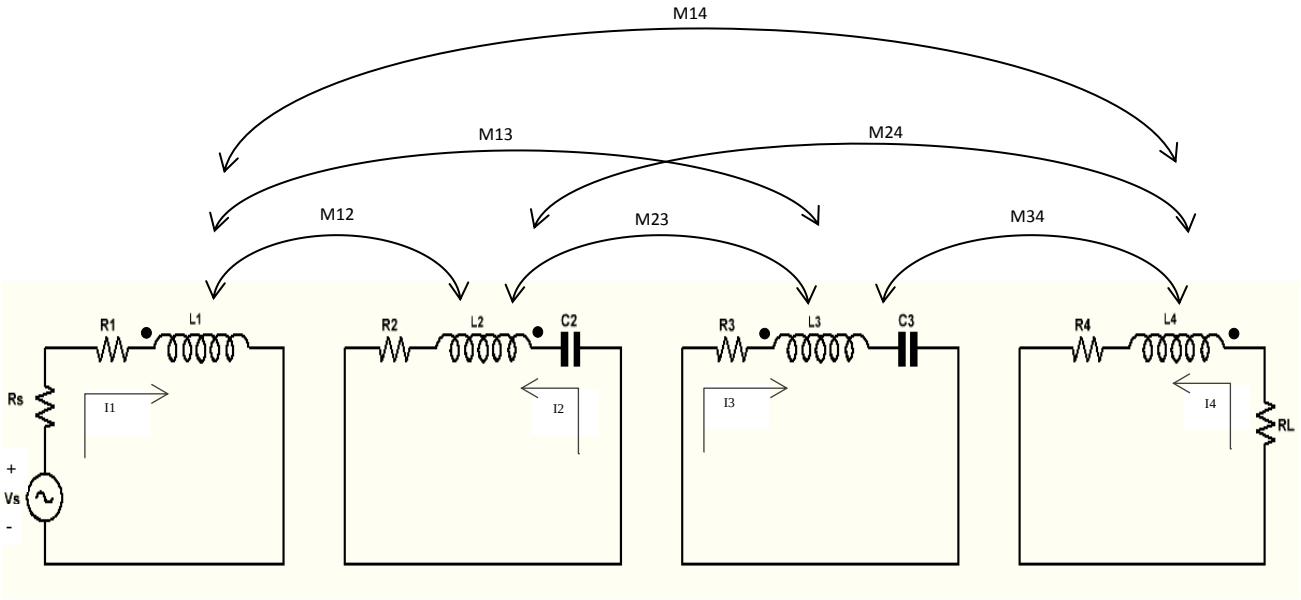

Figure 3.2: Equivalent circuit of the model structure of the experiment

As can be seen from this Figure 3.2, L_1, L_2, L_3 and L_4 are self-inductance of loop coil 1, coil 2, coil 3 and coil 4, respectively. Likewise, parasitic resistance R_1, R_2, R_3 and R_4 indicate the ohm loss resistance (the loss of copper) of loop coil 1, coil 2, coil 3 and coil 4. However, there also has been a radiation loss resistance of loop coil R_r; loss resistance is insignificant because the value is very small compared with the ohm resistance (Cannon et al., 2009). Hence, in this study, the resistance R_r of all loop coils are considered to be 0Ω for uncomplicated calculation. In addition, as mentioned above, the capacitors are added in order to be the coupling resonance. C_2 and C_3 substitute as capacitance of loop coil 2 and loop coil 3, respectively. Nevertheless, C_2 and C_3 are assumed to be same parameter C_0 since the experiment is assumed to be symmetrical.

Moreover, from Figure 3.2, M_{23} is represented as the mutual inductance of the magnetic coupling coefficient between transmitting and receiving helix coils, while M_{12} and M_{34} are demonstrated as the mutual inductance between loop coil 1 to loop coil 2 and loop coil 3 to loop coil 4, respectively (Hirayama, 2012). Notwithstanding this, the mutual inductances of the cross coupling between non-adjacent inductors can be neglected. Hence, the mutual inductance M_{13}, M_{14} and M_{24} is zero ($k_{13} = k_{14} = k_{24} = 0$) (Kim et al., 2013). For

this experiment, M_{12} and M_{34} are fixed values by reason of the researcher setting the distance d_{12} and d_{34} to be same and constant. Hence, M_{12} and M_{34} are same values. The value of M_{23} varies according to the range between loop coil 2 and loop coil 3.

The equivalent circuit of this WPT system can be calculated based on the theory of Kirchhoff's voltage law (KVL), which has four equations regarding to the currents from loop coil 1 to loop coil 4 and source voltage (V_S), at frequency ω in rad/sec as follows:

$$(R_S + R_1 + j\omega L_1)\, I_1 + j\omega M_{12} I_2 = V_s \tag{3.1}$$

$$(R_2 + j\omega L_2 + \frac{1}{j\omega C_2})\, I_2 + j\omega\, (M_{12} I_1 + M_{23} I_3) = 0 \tag{3.2}$$

$$(R_3 + j\omega L_3 + \frac{1}{j\omega C_3})\, I_3 + j\omega\, (M_{34} I_4 + M_{23} I_2) = 0 \tag{3.3}$$

$$(R_L + R_4 + j\omega L_4)\, I_4 + j\omega M_{34} I_3 = 0 \tag{3.4}$$

From the equations (3.1)–(3.4), it is possible to calculate the current of each coil in the matrix formula following Kumar et al. (2009); Kim et al. (2013); and Duong and Lee (2011).

$$\begin{bmatrix} I_1 \\ I_2 \\ I_3 \\ I_4 \end{bmatrix} = \begin{bmatrix} Z_{11} & Z_{12} & Z_{13} & Z_{14} \\ Z_{21} & Z_{22} & Z_{23} & Z_{24} \\ Z_{31} & Z_{32} & Z_{33} & Z_{34} \\ Z_{41} & Z_{42} & Z_{43} & Z_{44} \end{bmatrix}^{-1} \begin{bmatrix} V_S \\ 0 \\ 0 \\ 0 \end{bmatrix} \tag{3.5}$$

Where:

For $m = n;\ Z_{mn} = Z_{nm} = R_n + j\omega L_n + \frac{1}{j\omega C_n}$

For $m \neq n;\ Z_{mn} = j\omega M_{mn}$

Where R_n, L_n and C_n are the series resistance, the inductance and capacitance of coil n, respectively. At the frequency (ω_0):

$$\omega_0 = 2\pi f_0 = \frac{1}{\sqrt{L_i C_i}} \text{ (rad/sec.)} \tag{3.6}$$

M_{mn} is the mutual inductance between coil m and coil n as:

$$M_{mn} = k_{mn}\sqrt{L_m L_n} \tag{3.7}$$

Therefore, for this experiment, for the equations (3.5), (3.6) and (3.7) can be obtained the following expressions:

$$\begin{bmatrix} I_1 \\ I_2 \\ I_3 \\ I_4 \end{bmatrix} = \begin{bmatrix} Z_{11} & j\omega M_{12} & 0 & 0 \\ j\omega M_{12} & R_2 & j\omega M_{23} & 0 \\ 0 & j\omega M_{23} & R_3 & j\omega M_{34} \\ 0 & 0 & j\omega M_{34} & Z_{44} \end{bmatrix}^{-1} \begin{bmatrix} V_S \\ 0 \\ 0 \\ 0 \end{bmatrix} \tag{3.8}$$

Where: $Z_{11} = R_S + R_1 + \mathrm{j}\omega L_1$

$Z_{44} = R_4 + R_L + \mathrm{j}\omega L_4$

The quality factor (the Q-factor) of this RLC circuit in each coil at the resonance frequency operation is given by Jonah and Georgakopoulos (2012); and Kesler (2103):

$$Q = \frac{\omega \mathrm{L}}{\mathrm{R}} = \frac{2\pi f_0 \mathrm{L}}{\mathrm{R}} = \frac{\omega}{2\Gamma} = \frac{1}{R}\sqrt{\frac{L}{C}} \tag{3.9}$$

Manipulating the equation (3.8), the current coil 1 to coil 4 can be calculated. The current of coil 4 (I_4) and current of coil 1(I_1) at the resonance frequency are shown as:

$$I_1 = \frac{(R_2R_3Z_{44} + R_2\omega^2M_{34}^2 + Z_{44}\omega^2M_{23}^2)}{[Z_{11}R_2R_3Z_{44} + Z_{11}R_2\omega^2M_{34}^2 + Z_{11}Z_{44}\omega^2M_{23}^2 + R_2R_3\omega^2M_{12}^2 + \omega^4M_{12}^2M_{34}^2]} \cdot V_S \tag{3.10}$$

$$I_4 = -\frac{\omega^3M_{12}M_{23}M_{34}}{[Z_{11}R_2R_3Z_{44}+Z_{11}R_2\omega^2M_{34}^2+Z_{11}Z_{44}\omega^2M_{23}^2+R_2R_3\omega^2M_{12}^2+\omega^4M_{12}^2M_{34}^2]} \cdot jV_S \tag{3.11}$$

However, to simplify the calculation the current I_4, it may be derived as:

$$I_4 = -\frac{\omega^3M_{12}M_{23}M_{34}j}{(R_2R_3Z_{44} + R_2\omega^2M_{34}^2 + Z_{44}\omega^2M_{23}^2)} \cdot I_1 \tag{3.12}$$

The efficiency is related to the power of coil 1 (power of V_S) and power of R_L. Nevertheless, Abatti et al. (2015) consider that all the power which is delivered by the generator P_{IN}, is dissipated by ohmic losses. Therefore, for ease of calculation, the efficiency can be measured by P_L divided by P_{IN} (P_L/ P_{IN}), where $P_{IN} = V_SI_1\cos\theta$.

The calculation of the power transfer efficiency of the system (η) is yielding in the equation (3.14), from the equations (3.10), (3.11), (3.12) and (3.13).

$$|\eta| = \frac{P_{OUT}}{P_{IN}} = \frac{P_L}{P_{IN}} = \frac{I_4^2 R_L}{I_1 V_S cos\theta} \times 100\ \% \tag{3.13}$$

$$|\eta| = \frac{(\omega^6 M_{12}^2 M_{23}^2 M_{34}^2)(R_2 R_3 Z_{44} + R_2 \omega^2 M_{34}^2 + Z_{44} \omega^2 M_{23}^2) \times 100\ \%}{[Z_{11} R_2 R_3 Z_{44} + Z_{11} R_2 \omega^2 M_{34}^2 + Z_{11} Z_{44} \omega^2 M_{23}^2 + R_2 R_3 \omega^2 M_{12}^2 + \omega^4 M_{12}^2 M_{34}^2] \times cos\theta} \tag{3.14}$$

While θ is the angle of the current in coil 1 (I_1) from the equation (3.10).

The mutual inductance (M) can be calculated by using Neumann's formula (Russell, 1906):

$$\mathrm{M} = \mu_0 N_1 N_2 \sqrt{r_1 r_2} \left[\left(\frac{2}{m} - m \right) K(m) - \frac{2}{m} E(m) \right] \tag{3.15a}$$

$$m = \sqrt{\frac{4 r_1 r_2}{d^2 + (r_1 + r_2)^2}} \tag{3.15b}$$

Where r_1 and r_2 are the radius of coil 1 and coil 2 with distance d. N_1 and N_2 are the number of turns of coil 1 and coil 2, respectively. μ_0 is the magnetic permeability of free space, which is $4\pi \times 10^{-7}$ H/m, N/A^2, T·m/A or Wb/(A·m). For K(m) and E(m) are the elliptic integrals of first and second kind with modulus m, respectively; m is defined as the equation (3.15b), where the values of m are between 0 and 1 ($0 \ll m \ll 1$).

3.4 Setting the parameters of the experiment

The parameters values of the experiment are defined following the procedures. Firstly, the frequency of the whole system is determined. Following the paper of Beh et al. in 2010 presents the WPT should be fixed at a usable range and applied within the ISM (Industrial-Scientific-Medical) band in the MHz range in order to achieve the maximum power efficiency of the transmission. Hence, this study will use the frequency of 10.5 MHz at about ten volts amplitude in a sinusoidal signal wave (sine wave) AC signal waveform to drive the source coil. Afterwards, the researcher needs to define the number of all the coils. The source coil and load coil have three turns, whereas the primary coil and secondary coil have seven turns. For all the coils in this experiment, the researcher chooses a single copper 24 AWG (American wire gauge) wire, wound to be a circular with diameter of 4.5 cm, as

shown in Table 3.1, which shows the number of each coil (N) in turns, the diameter of the each coil (D) in cm, the wire diameter of each coil (r_c) in mm, the length of each coil (l) in cm, and the frequency of the system (f) that is the same identity resonant frequency at 10.5 in MHz.

Coil (Antenna)	**N (turns)**	**D (cm)**	**r_c (mm)**	***l* (cm)**	***f* (MHz)**
Power coil (Loop coil 1)	3	4.5	0.53	0.172	10.5
Transmitter coil (Loop coil 2)	7	4.5	0.53	0.393	10.5
Receiver coil (Loop coil 3)	7	4.5	0.53	0.393	10.5
Load coil (Loop coil 4)	3	4.5	0.53	0.172	10.5

Table 3.1: The summary of particulars of the coil physical

Coil 1 and coil 2 are wrapped together with 2 mm of the distance between them, following the study and findings of Kürschner et al. in 2013 that for the inductive coupling of WPT, the power efficiency of transmission is affected by the coil diameter and air gap between two coils by lower coil diameter and larger air gap caused to decrease the coupling. In this manner, the efficiency of WPT has the correlation with the ratio between the air gap (a) and the coil diameter (d). Assuming a constant Q factor values of about 100, the efficiency of transmission is greater than 80%, if the air gap (a) is smaller than the half of coil diameter (d); $a/d < 0.5$. In addition, an efficiency of 90% is reached when the air gap is smaller than a quarter of the coil diameter; $a/d < 0.25$. As similar as coil 3 and coil 4, they are also wrapped together, in order to create the most efficient transfer power.

The self-inductances of all loop coils, the parasitic resistances of all loop coils, and the lumped capacitances for coil 2 and coil 3 are calculated by the following formulas.

The parameter value of self-inductance of each coil can be calculated by Wheeler's formula which is for the single-layer air core solenoid (Wheeler, 1928) as shown in the equation (3.16) below.

$$L = \frac{N^2R^2}{2.54(9R+10H)} \text{ (μH)} \quad (3.16)$$

Where, L supersedes the inductance of the coil (Micro-Henry; μH)

N supersedes the number of turns of wire

R supersedes the radius of coil (cm)

H supersedes the height of the coil (cm)

The resistance of each coil in this circuit can be divided into two types of parasitic resistance as the ohm loss resistance or the loss of copper in wire (R_{ohm}) and the radiation resistance (R_{rad}). The formula equations of these two resistances can be calculated as Balanis (2005) and Cannon et al. in 2009.

$$R_{ohm} = \frac{2\pi rN}{\sigma 2\pi r_c \delta} = \frac{rN}{\sigma r_c \delta} (\Omega) \quad (3.17)$$

As, r means the radius of the coil (cm)

r_c means the cross-sectional radius of wire (mm)

N means the number of turns

σ means copper conductivity, which is equal to 5.8×10^7 S/m

δ means skin depth, which $\delta = \frac{1}{\sqrt{\pi f \mu_0 \sigma}}$ (m)

f means source frequency (Hz)

μ_0 means permeability, which replaces $4\pi \times 10^{-7}$ H/m

$$R_{rad} = 20\left(\frac{2\pi}{\lambda}\right)^4 (\pi r^2 N)^2 \quad (3.18)$$

λ is the corresponding free space wavelength; $\lambda = c/f$ where c = 3.0 x 10^8 m/s.

The radiation resistance of each coil can be neglected because the correspondence between the radiation values is too small in comparison with the ohm loss resistance. Therefore, the resistance of each coil depends on the loss resistance ($R = R_{ohm}$).

However, the self-inductance and parasitic resistances can be computed by using the equations (3.16) and (3.17). Moreover, both of the parameters can also be measured with a multimeter. Nevertheless, the measured parameters are applied and focused more than calculated parameters for this experiment, in order to get the accurate values.

For the lumped capacitances in this experiment, these are applied to yield identical resonant frequency. Hence, the calculation of the lumped capacitances depends on the self-inductance of the coil, from the equation (3.6), so the lumped capacitance is described by

$$C_i = \frac{1}{(2\pi f)^2 L_i} \text{ (F)} \tag{3.19}$$

Where, ω_0 is angular frequency (rad/sec.)

L is self-inductance (H)

C is lumped capacitance (F)

For the value of the internal source resistance (R_S), this value depends on the function generator; HM8030-6 function generator has specified R_S at 50 Ω. In addition, the load resistance R_L for this experiment is set at 10 Ω.

Chapter 4 – Methodology and implementation

4.1 Introduction

This chapter relates to the process of setting up and testing the experiment of this study. The materials for use in this study are shown and all of the equipment is explained.

The implementation of the experiment in this part can be divided into two parts: the contrivance method and the process of the experiment, and the methodology and technique for the measurement of all data – all are described in this part in order to provide the correct information.

4.2 Research strategy

The research process can be broken down into two methods. There is a quantitative research approach and a qualitative research approach, applied according to the data required. The quantitative research approach usually concentrates on measuring, counting, collecting and analysing the quantifiable numerical data, including in terms of the application to statistics, such as questionnaires or experiments. In contrast, the qualitative research approach is to answer by words or text. With this approach, the researcher will get information from a direct, specific group to gain an understanding about the topic and peoples' attitudes (Wilson and Natale, 2001; Creswell, 2008).

However, this research uses only quantitative research approach in the experiment since this study is to evaluate the most suitable alternative method for charging sensor motes instead of using a battery in order to prolong the life cycle for WSN by selecting the coupled magnetic resonant WPT method to be the most appropriate for all applications. Therefore, the idea of a combination between magnetic resonant coupling WPT technique and sensor motes in WSN is shown. The experiment aims to prove that the magnetic resonant coupling WPT technique can deliver energy power to sensor motes.

4.3 Data collection

The data collection method can be divided into two mains, based on the sources: the primary source and the secondary source. Firstly, the primary source of data is collected by the researchers themselves, e.g. a questionnaire or interviews with the specialists, or observation from the experiments (Driscoll, 2011). Secondly, the secondary source of data is the information that has already been produced, which may be contemporary or historical, for example, journal articles, textbooks, previous research, conference proceedings, reports, government publications, diaries and web information (Burton, 2007).

This study uses both of the data collection sources, which the data from primary source from the experiment and the secondary source of data from researching or investigating the documents mentioned above.

4.4 Experimental design

In this research demonstrates the WPT in the WSN system by using the magnetic resonant coupling mechanism in order to charge the power from the source coil to the receiver sensors, which is the most suitable power management method for the WSN, as explained in Chapter 3. This experiment is modelled for the basic understanding of the WPT method in the WSN system focused on the coupling resonant frequency from the signal source coil to the load receiver. It is designed by applying one signal generator (source) supplying power wirelessly to the illuminated LED (load) through the magnetic resonant coupling.

For this experiment, the researcher intends that the signal generator is an energy source for powering the sensor motes; the LED is used instead of a sensor mote, illustrating that this alternative technique may transfer the energy to sensor nodes in order to long-lived sensor motes in WSN.

4.5 Experimental equipment

The essential equipment used in the experiment is illustrated and explained below:

1. Wire (Insulated single copper wire 24 AWG)

2. Capacitors (2 x *59pF)*

3. Resistances (1 x *10* Ω and *1* x *5* Ω*)*

4. Light Emitting Diodes (LED's)

5. Oscilloscope

An oscilloscope is an electronic measurement tool which illustrates the visual display of the signal waveform and also indicates the changeable signal voltage over time. An oscilloscope has a two-dimensional plot which can show one or more signals as a function of time (Tektronix, Inc., 2009). For this experiment, the Tektronix TDS2002C digital oscilloscope is utilised, as shown in Figure 4.1.

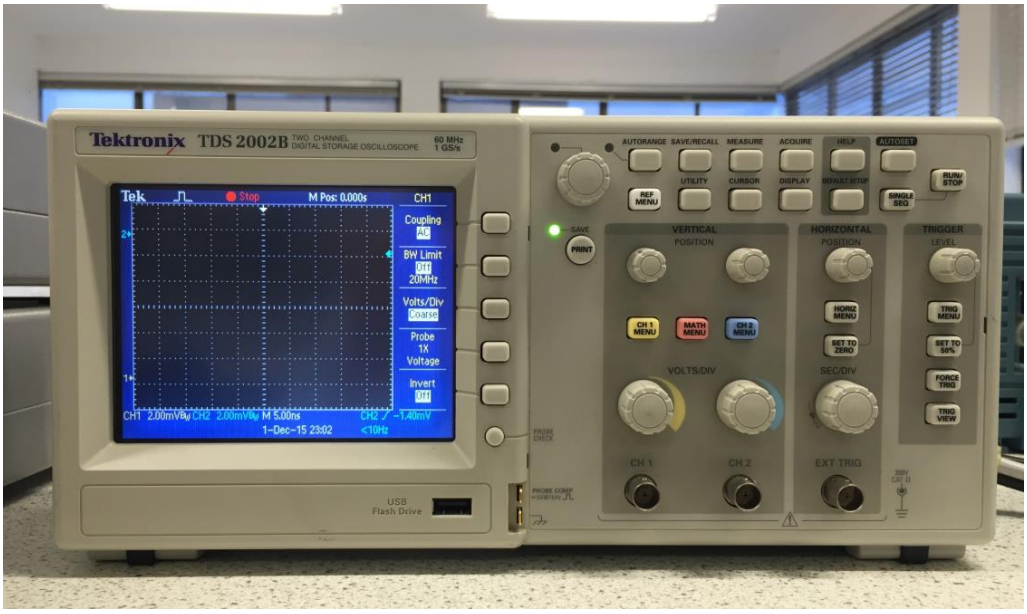

Figure 4.1: Tektronix TDS2002C digital oscilloscope

6. Multimeter

A multimeter is the basic measuring instrument in electronics and electrical equipment, and comes in two types: analogue and digital. The typical multimeter gauges voltage, current and resistance (Elliott, 2010). Nevertheless, there have multimeters for measurement inductance and capacitance. In this study, the digital programmable multimeter HM8012 is applied. Moreover, the researcher will also use the multimeter with inductance measurement for establishing the inductance value of each loop coil, presented in Figure 4.2.

(a)

(b)

Figure 4.2: (a) Digital programmable multimeter HM8012; (b) Multimeter with inductance measurement

7. Function generator

The function generator is an electronic device that can produce a signal waveform in various types, such as a sine wave, a triangular wave, a saw tooth wave, a square wave and a pulse wave, with the signal frequency. However, the frequency of signal can be adjusted over a wide range (Bakshi et al., 2008). For this model, the function generator HM8030-6 is used, as shown in Figure 4.3.

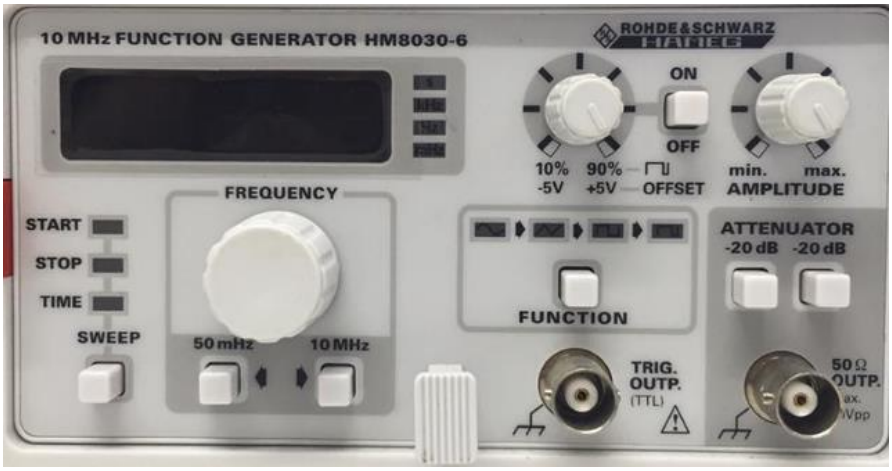

Figure 4.3: Function generator HM8030-6

4.6 Implementation and experimental process

Following the design and the theories presented in Chapter 3, the implementation of the experiment will be clarified step by step here.

***Step 1*:** Starting with the function generator by adjusting and setting the input signal to drive the source coil in AC sine wave waveform with the 10.5 MHz frequency, as presented in Figure 4.4.

Figure 4.4: Function generator setting the frequency at 10.5 MHz

***Step 2*:** Creating a source coil, a primary coil, a secondary coil, and a load coil. The researcher defines the source coil and load coil as having three turns, whereas the primary coil and secondary coil have seven turns. For all the coils, the researcher chooses to twine the

coil to be circular with diameter of 4.5 cm, following the Table 3.1. Then each coil should be wrapped with tape to prevent unwinding. For the edge of each coil's end of every coil, it should be scraped off the insulation, as shown in Figure 4.5.

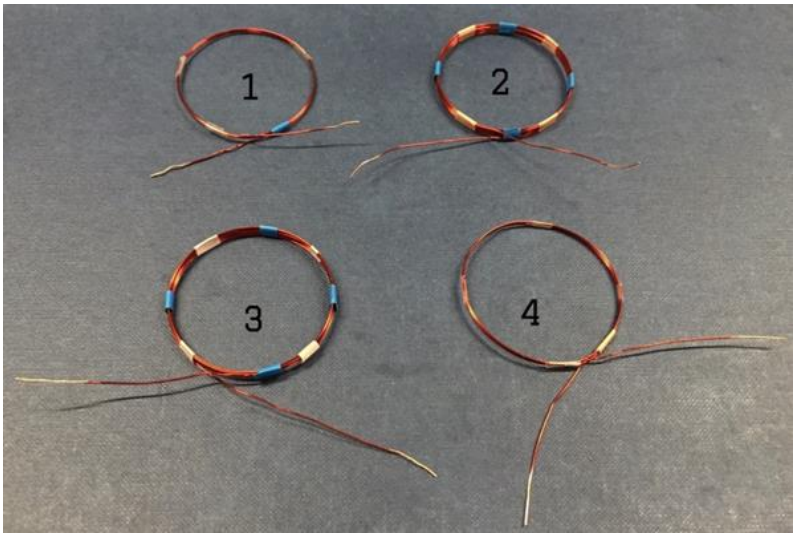

Figure 4.5: The loop coil 1(source coil), loop coil 2 (primary coil or transmitter coil), loop coil 3 (secondary coil or receiver coil), and loop coil 4 (load coil)

***Step 3*:** Measurement of the self-inductances and parasitic resistances of all coils, especially the self-inductance of transmitter coil (coil 2) and the receiver coil (coil 3) in order to calculate the values of the lumped capacitors, applying the same resonant frequency for coil 2 and coil 3 by the equation (3.19).

The researcher measures the parameters of all coils using the multimeter. The researcher utilises the digital multimeter to determine the parameters of the ohm resistance, while the parameters of self-inductances are gauged by a multimeter with an inductance measurement.

For this experiment, the values of the capacitors for soldering with coil 2 and coil 3 are the same values, which are 59 pF following by Equation (3.19), because the self-inductances of coil 2 and coil 3 are the same (3.9 μH by measurement as mentioned in Chapter 3).

Step4: Soldering the 10 Ω load resistance and LED's in series with load coil, as shown in Figure 4.6.

Figure 4.6: Load coil with load resistance R_L and LED's

***Step 5*:** Wrapping the source coil and transmitter coil, and the receiver coil and the load coil together, respectively, with the distance between source coil and transmitter, and receiver coil and load coil are 2 mm, as presented in Figure 4.7.

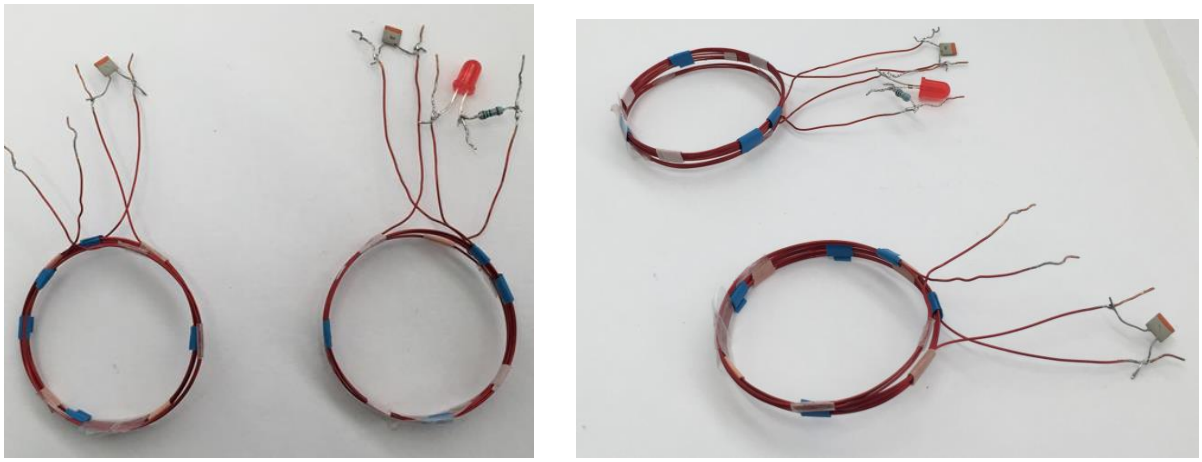

Figure 4.7: Transmitter part and receiver part

Step 6: Testing the model by setting the receiver part and transmitter part away from each other 5 mm; then, sliding every 5 mm and observing the light of the LED. As shown in Figure 4.8, the transmitter part was approximately 3.5 cm from the receiver part.

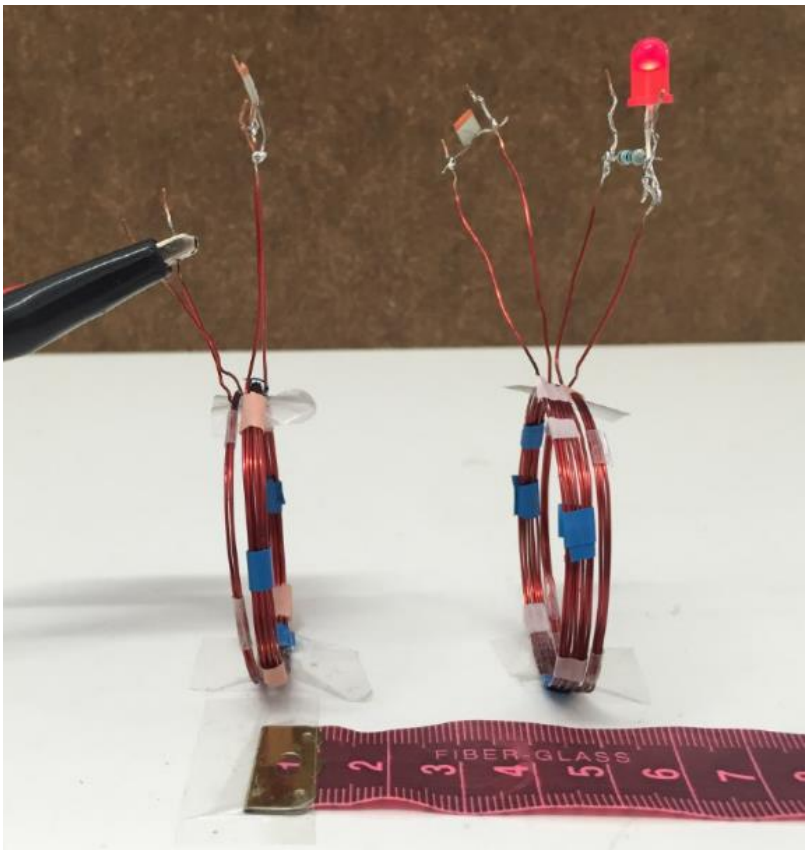

Figure 4.8: The over all of the experiment

4.7 Measurement methodology and process

After the model of the experiment is complete, the testing and measurement of this system is illustrated below. However, the researcher takes the LEDs off for ease of measuring and collecting the data.

4.7.1 Oscilloscope

The oscilloscope is a tool for measuring the voltage and time by observing the signal which can be displayed the signal in the figure of a waveform on the screen. Moreover, it can measure and show the signal frequency of the model. For this experiment, the data is

collected from the oscilloscope. This section will briefly describe the operation of the oscilloscope, the use of the oscilloscope, and reading the values from the oscilloscope.

4.7.1.1 Feature and function of knobs on oscilloscope

The knobs on an oscilloscope which have mainly been used for this experiment are illustrated. Additionally, the functions and applications of each knob are explained in Figure 4.9.

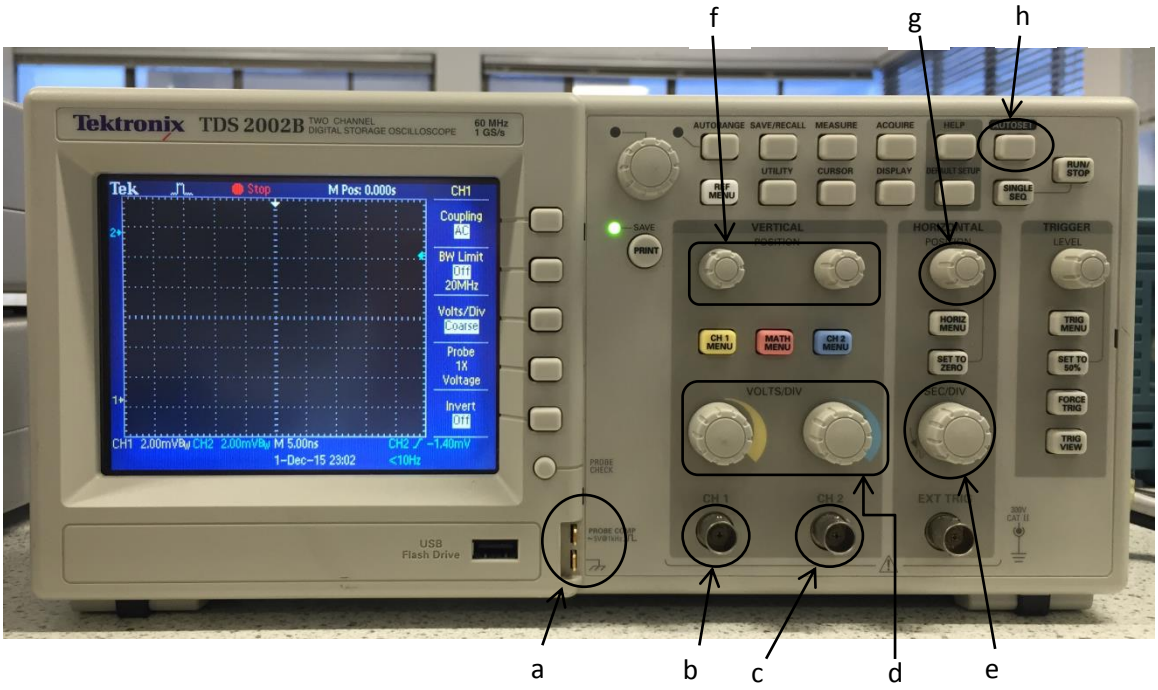

Figure 4.9: Oscilloscope

a. PROBE COMP: For test the oscilloscope probe
b. CH 1: Input signal channel 1
c. CH 2: Input signal channel 2
d. VOLTS/DIV: Switch to select attenuation of the input signal of CH1 and CH2
e. SEC/DIV: Switch to select the time of the input signal
f. POSITION for VERTICAL: Control of the graph along the vertical axis for CH1 and CH2, which is normally adjusted to be the centre of the screen
g. POSITION for HORIZONTAL: Control the graph along the horizontal axis
h. AUTOSET: Press for automatically re-establishing the settings and displaying the input signal

4.7.1.2 Measurement techniques of oscilloscope

As mentioned above, the oscilloscope is the instrument for the measurement of voltage in a function of time which it can be explained from the waveform of the signal on the screen by the x-y mode of operation. The screen is divided into divisions, with the horizontal axis is instead of voltage, whilst the vertical axis replaces time, as can be seen from Figure 4.10.

First of all, the probe of the oscilloscope should be tested in order to establish the most accurate value on the voltage measurement; therefore the user should calibrate or compensate the probe before using the oscilloscope by connecting the probe into the 'probe comp' and ground, then adjusting it until there is a smooth signal (a square wave with a flat top) by pressing the 'auto set' button. However, the oscilloscope probe should be re-compensated before using every time.

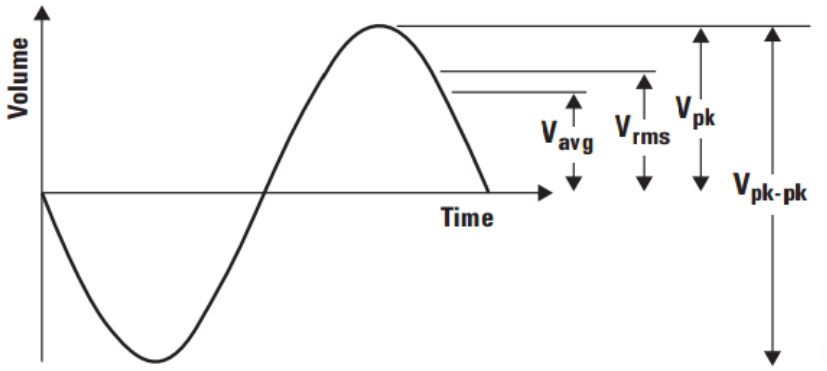

Figure 4.10: Common voltage sine wave parameters

(Agilent Technologies, Inc., 2013.)

From the Figure 4.10, V_{pk-pk} is peak-to peak voltage, V_{pk} is peak voltage, V_{avg} means the average of all one full cycle waveform, and V_{rms} is instead of the rms value of AC voltage which rms abbreviates root-mean-square. The formula of V_{avg} and V_{rms} are presented in equations (4.1) and (4.2), respectively (Knight, 2013). The time period (t) is related to the frequency (f), which is defined as the number of cycles performed per second, as indicated in the formula (4.3).

$$V_{avg} = \frac{V_{pk-pk}}{\pi} = V_{pk}\frac{2}{\pi} = V_{pk} \times 0.637 \quad (4.1)$$

$$V_{rms} = \frac{V_{pk-pk}}{2\sqrt{2}} = \frac{V_{pk}}{\sqrt{2}} = V_{pk} \times 0.707 \quad (4.2)$$

$$t = \frac{1}{f} \quad (4.3)$$

4.7.2 Measurement of the voltage source

For measurement of the voltage source, the voltage source is discharged from the function generator by connecting it to the oscilloscope. The researcher chooses the resistance 1 Ω (R_{sense_0}) and measures the voltage across the resistor (V_{sense_0}), as shown in Figure 4.11.

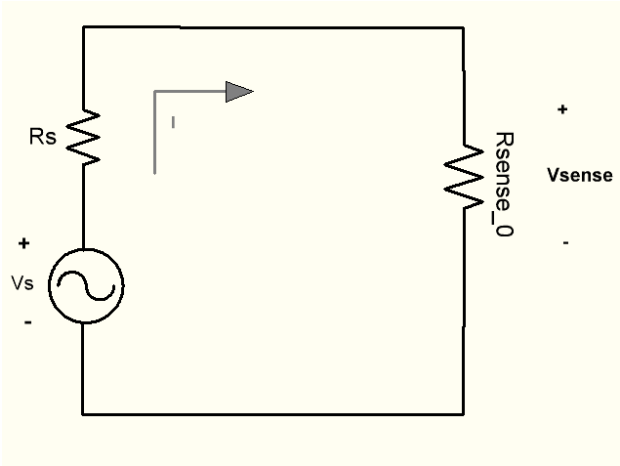

Figure 4.11: the circuit for measurement voltage source

From the Figure 4.11, the formula below can be used for calculating the real voltage source (V_S).

$$V_S = \frac{(R_S + R_{sense\_0})}{R_{sense\_0}} \times V_{sense\_0} \quad (4.4)$$

4.7.3 Measurement of the current in coil 1 and the current in coil 4

Measuring and collecting the current in source coil (I_1) and the current in coil 4 (I_4): to find the current I_1, put 5 Ω shunt resistance (R_0) connected in series with coil 1 and then measure the voltage across R_0. For current I_4, this can be computed by measuring the voltage across the load resistance, as presented in Figure 4.12 and Figure 4.13. Subsequently, the

researcher gently slides the receiver part off from the transmitter every 5mm and collects the data until the light of the LED goes off.

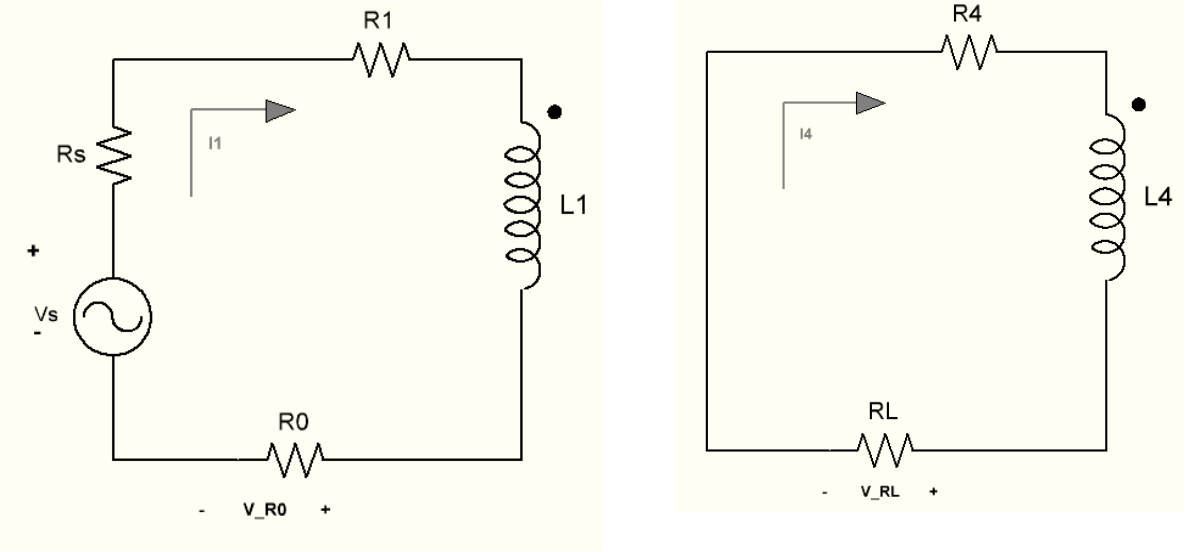

(a) (b)

Figure 4.12: (a) The measure current for coil 1; (b) The measurement current for coil 4

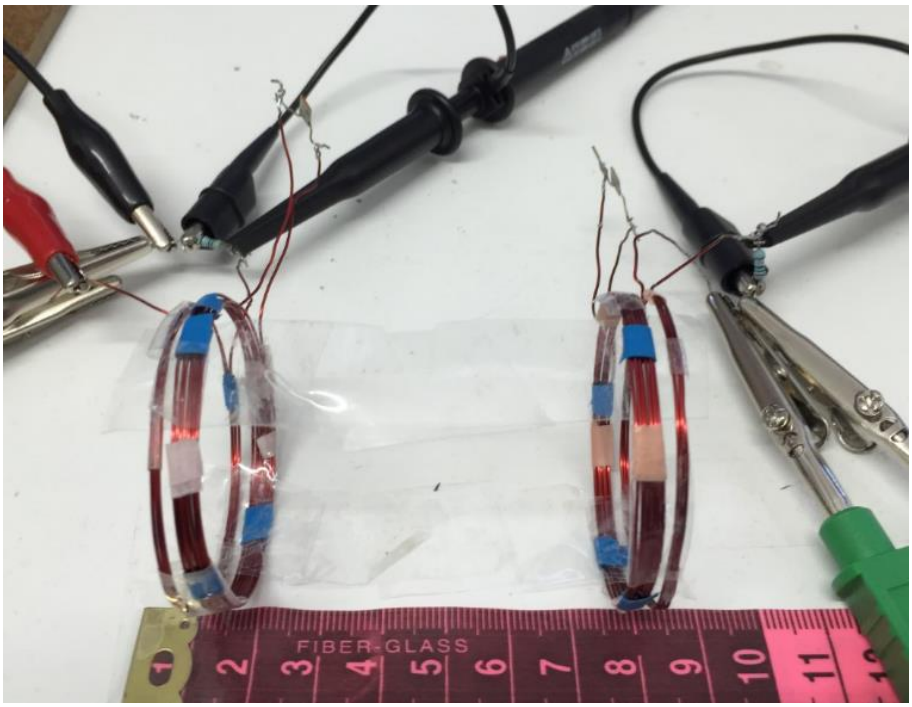

Figure 4.13: The measurement I_1 and I_4 in this experiment

4.7.4 Measuring the mutual inductances

For analysis of the relation power transferred efficiency formula, the mutual inductance M is significant. The coupling coefficient is dependent on the function of the distance. However, for this experiment, the researcher sets the distance between the source coil and transmitter coil, and between the receiver coil and the load coil as fixed at 2 mm; then the researcher folds coil 1 and coil 2, and coil 3 and coil 4 together, respectively. Therefore, the values of M_{12} and M_{34} of this experiment are constant whereas M_{23} depends on the distance that the researcher measures every 5 mm apart from each other. However, the measurement of the mutual inductance of each M can be done only between one pair of coils at one time; hence the other coils are set to be an open circuited.

To measure the mutual inductance M_{12}, put the voltage source into source coil (coil 1) and assume coil 2 is an open circuit where the current in the secondary coil becomes zero, as shown in Figure 4.14. Afterwards, measure the voltage across coil 1 V_{L1} and voltage across coil 2 V_{L2}.

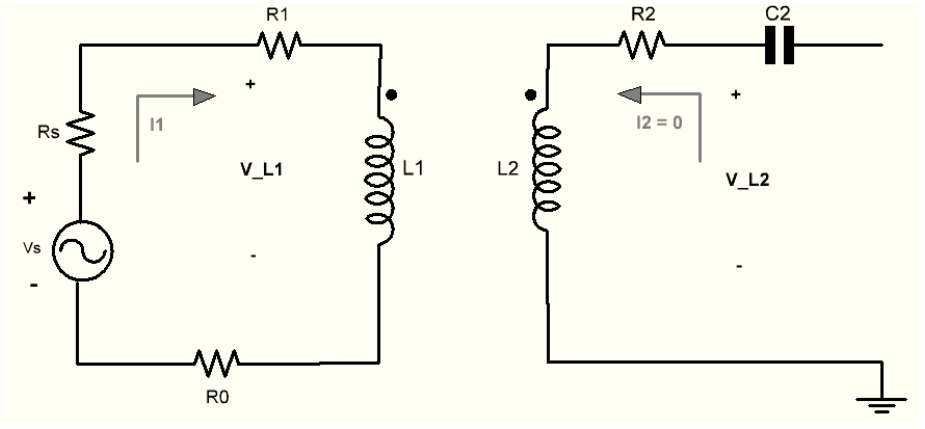

Figure 4.14: Circuit for measurement the mutual inductance M_{12}

From Figure 4.14, the equation can be written as follows:

$$V_{L1} = j\omega L_1 I_1 \quad (4.5)$$

$$V_{L2} = j\omega M_{12} I_1 \quad (4.6)$$

Therefore, from the equations (4.5) and (4.6), M_{12} can be written as follows:

$$M_{12} = \frac{V_{L2}L_1}{V_{L1}} \tag{4.7}$$

For the mutual inductance M_{34}, the method for measurement is similar as M_{12}. The researcher selects to put a source into coil 4 and open circuit in coil 3, as presented in Figure 4.15. Then, the voltage across coil 3 V_{L3} and voltage across coil 4 V_{L4} are measured.

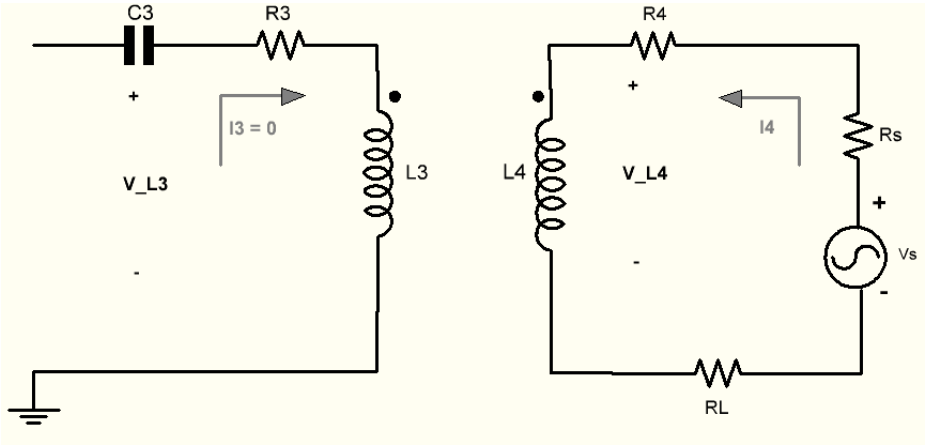

Figure 4.15: Circuit for measurement the mutual inductance M_{34}

From the Figure 4.15, the circuit equation can be written as:

$$V_{L4} = j\omega L_4 I_4 \tag{4.8}$$

$$V_{L3} = j\omega M_{34} I_4 \tag{4.9}$$

Hence, the equation M_{34} of this system is:

$$M_{34} = \frac{V_{L3}L_4}{V_{L4}} \tag{4.10}$$

The process for finding the mutual inductance M_{23} by measurement is by putting a source into coil 2 and open circuit coil 3, similar to the method for measuring M_{12} and M_{34}. For gauging the current in coil 2, the researcher puts the 10 Ω resistance as sense_1 resistance (R_{sense_1}), and measure the voltage of V_{sense_1}. The Figure 4.16 shows the circuit used to establish the values of M_{23} by measurement.

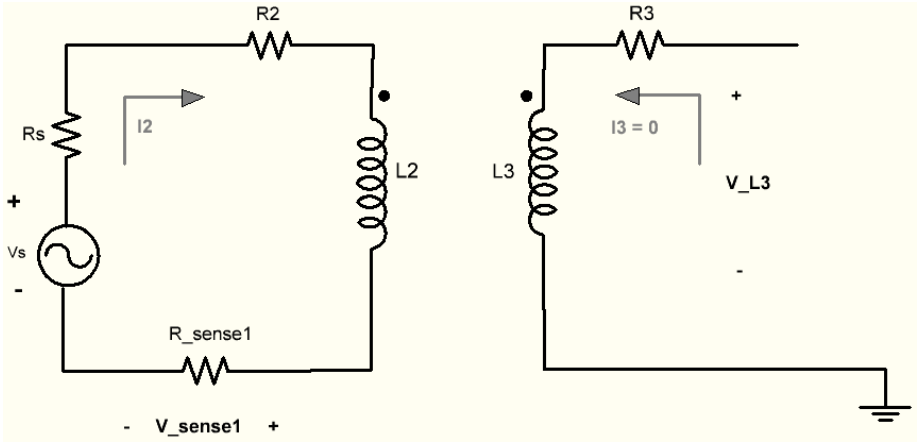

Figure 4.16: Circuit for measurement the mutual inductance M_{23}

As the Figure 4.16, the equation is shown:

$$V_{sense\_1} = R_{sense\_1} I_2 \tag{4.11}$$

$$V_{L3} = j\omega M_{23} I_2 \tag{4.12}$$

Therefore, M_{23} can be calculated by:

$$M_{23} = \frac{V_{L3} R_{sense\_1}}{j\omega V_{sense\_1}} \tag{4.13}$$

However, the author measures M_{23} from 0.5 cm to 6 cm in each 5 mm.

4.7.5 Measuring and finding the relative power transfer efficiency

For measuring the relative power transfer efficiency η, the voltage of coil 1 and coil 4 are measured to find the current I_1 and I_4. The relative power transfer efficiency of this experiment shown as:

$$\eta = \frac{P_{OUT}}{P_{IN}} = \frac{P_L}{P_{IN}} = \frac{\left(V_L^2 / R_L\right)}{V_S I_1 cos\theta} \times 100\% \tag{4.14}$$

Where θ may be measured by oscilloscope or calculated following the equation (4.15).

$$\theta = tan^{-1}\left(\frac{\omega L_1}{R_1}\right) \tag{4.15}$$

Chapter 5 – Results and analysis

5.1 Introduction

This chapter examines and represents the results of the experiment and provides data analysis. All the data from the experiment is given here. Moreover, this section will compare the information from the measurement and the theory calculation.

5.2 The results

The researcher designed the signal source with a sine wave at the frequency of 10.5 MHz. The voltage source can be measured by using an oscilloscope, which the input voltage shows in the Figure 5.1.

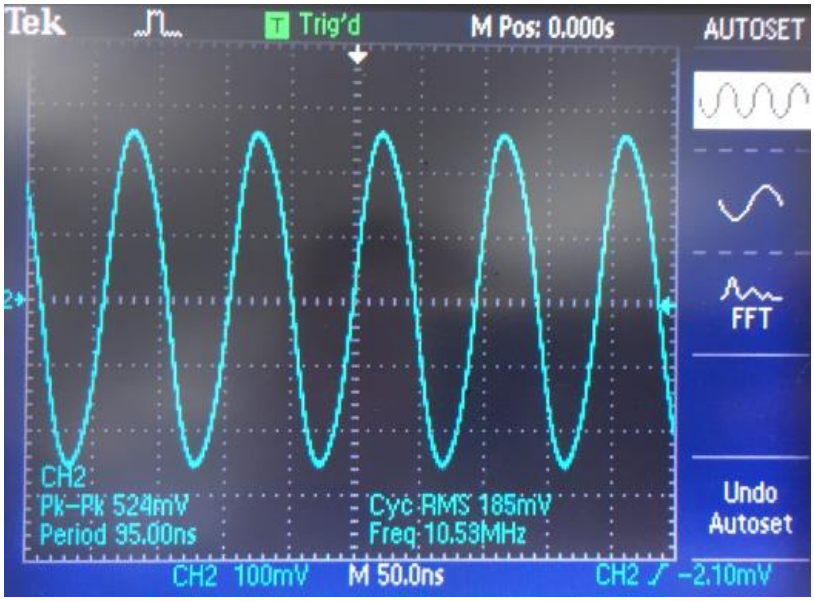

Figure 5.1: The voltage input source

From Figure 5.1, the measured voltage of V_{sense_0} is 524m$V_{pk\text{-}pk}$. Therefore, following the equation (4.4), V_S is 0.524 = 26.5 $V_{pk\text{-}pk}$. Following the equation (4.2), the voltage source (V_S) is 13.25V_{pk} and 9.37 V_{rms}.

All parameters of each coil are summarized in the Table 5.1 by measurement and calculation from the equations (3.9), (3.16), (3.17) and (3.19), which the self-inductance of

each coil (L) in μH, the ohm-resistance of each coil (R) in Ω, the lumped capacitance (C) in pF, and Q-factor with loaded of all coils at 10.5 MHz. The load resistance uses 10 Ω, measurement R_L is 9.7 Ω; and the resistance of 5 Ω (R_0) putting in a source coil for calculating the current in coil 1, while measurement R_0 is 4.6 Ω.

Coil (Antenna)		**L** (μH)	**R** (Ω)	**C** (pF)	**Q-factor** (loaded)
Power coil (Loop coil 1)	Measurement	0.6	0.2	-	0.725
	Calculation	0.81	0.2157	-	0.971
Transmitter coil (Loop coil 2)	Measurement	3.9	0.5	59	5145.928
	Calculation	4.03	0.502	57	5296.275
Receiver coil (Loop coil 3)	Measurement	3.9	0.5	59	5145.928
	Calculation	4.03	0.5068	57	5296.275
Load coil (Loop coil 4)	Measurement	0.6	0.2	-	4.072
	Calculation	0.81	0.2157	-	5.33

Table 5.1: The summary of all parameter values for this experiment

From R, L and C parameters in Table 5.1, the impedances of each coil can be computed by equations (3.5) and (3.7):

$$Z_{11} = R_S + R_1 + R_0 + j\omega L_1 \quad = 54.8 + 39.584j = 67.6 \angle 35.842\ \Omega \qquad (5.1)$$

$$Z_{22} = R_2 + j\omega L_2 + \frac{1}{j\omega C_2} = R_2 = 0.5\ \Omega$$

$$Z_{33} = R_3 + j\omega L_3 + \frac{1}{j\omega C_3} = R_3 = 0.5\ \Omega$$

$$Z_{44} = R_L + R_4 + j\omega L_4 \quad = 9.9 + 39.584j = 40.8 \angle 75.958\ \Omega$$

From the experiment, the researcher found the light of the LED off in the distance at approximately 3.5 to 4 cm away from the transmitter coil to the receiver coil. However, the LED gradually light up until the length about 1.5 cm to 2 cm, the LED light is brightest, and then the brightness gently dimmed until the light disappeared.

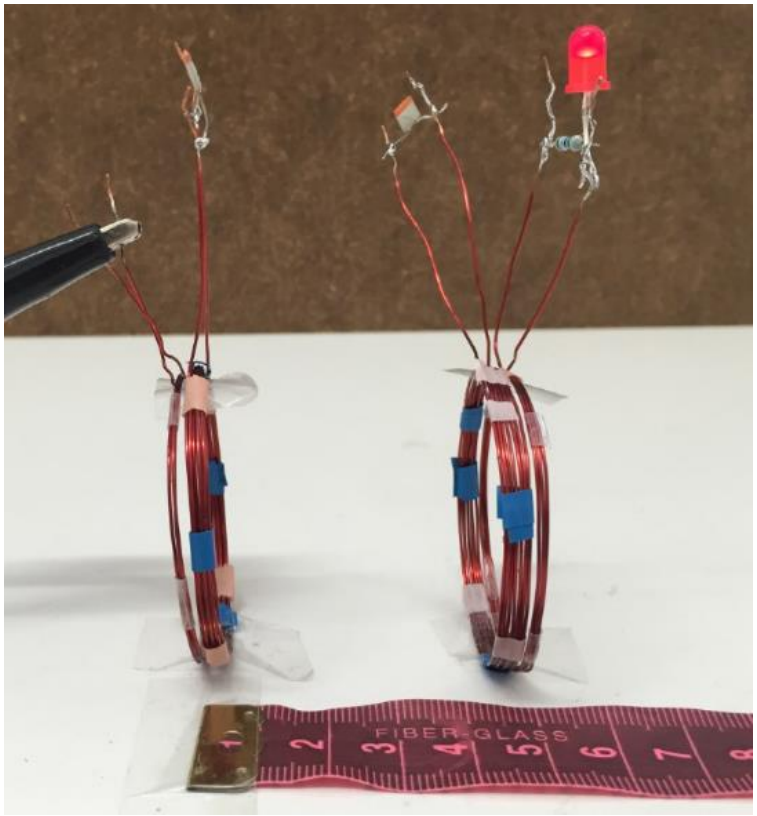

Figure 5.2: The example of the experiment with LED's light at 3.5 cm between the transmitter coil and the receiver coil

Hence, the data is gathered from the distance d_{23} from 0.5 cm to 6 cm at each 5 mm. However, the researcher collected the output voltage across the load coil (V_L) and the voltage across V_0 by using an oscilloscope in order to find the currents in coil 1 and coil 4. The results of voltage V_0 and V_L at each 5 mm are illustrated:

At d_{23} 0.5 cm:

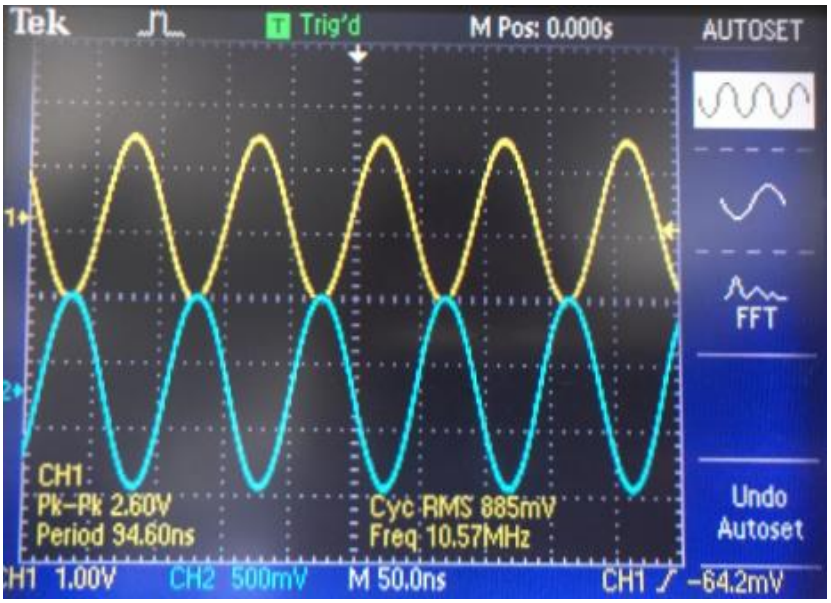

Figure 5.3: The voltage V_0 across R_0 is shown in yellow graph, whereas blue graph presents as the voltage V_L at the distance d_{23} of 0.5 cm

At d_{23} 1 cm:

Figure 5.4: The voltage V_0 across R_0 is shown in yellow graph, whereas blue graph presents as the voltage V_L at the distance d_{23} of 1 cm

At d_{23} 1.5 cm:

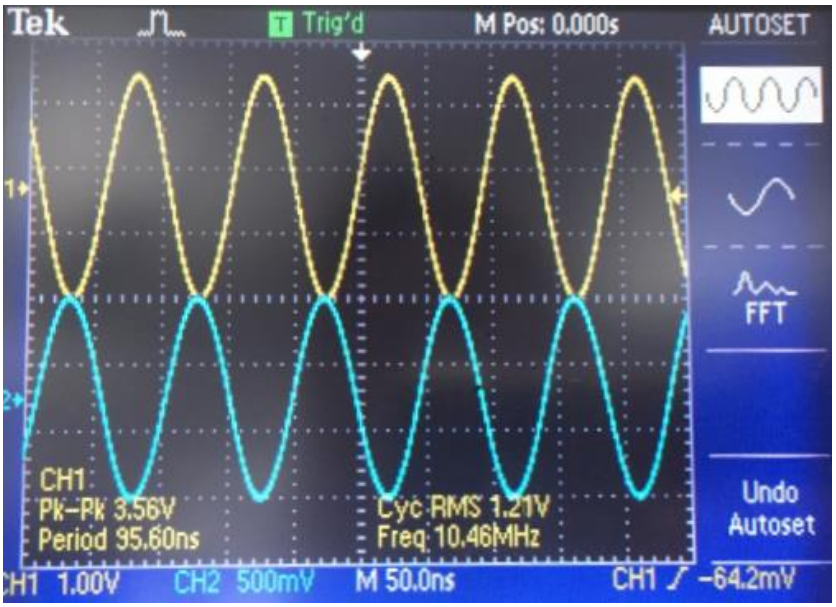

Figure 5.5: The voltage V_0 across R_0 is shown in yellow graph, whereas blue graph presents as the voltage V_L at the distance d_{23} of 1.5 cm

At d_{23} 2 cm:

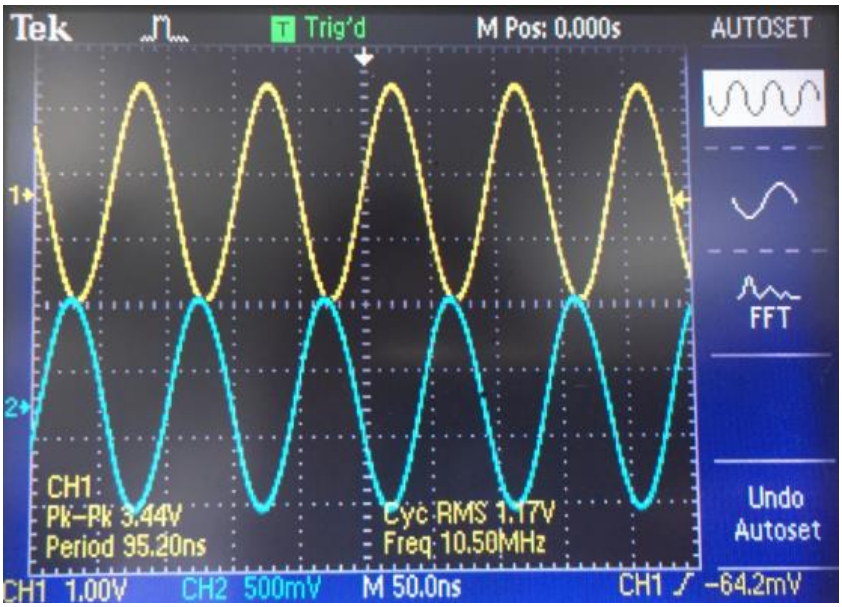

Figure 5.6: The voltage V_0 across R_0 is shown in yellow graph, whereas blue graph presents as the voltage V_L at the distance d_{23} of 2 cm

At d_{23} 2.5 cm:

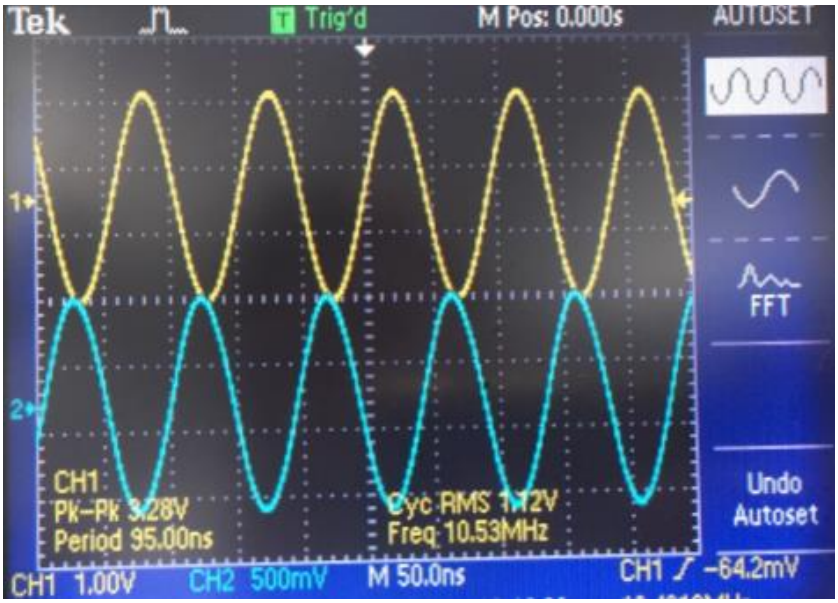

Figure 5.7: The voltage V_0 across R_0 is shown in yellow graph, whereas blue graph presents as the voltage V_L at the distance d_{23} of 2.5 cm

At d_{23} 3 cm:

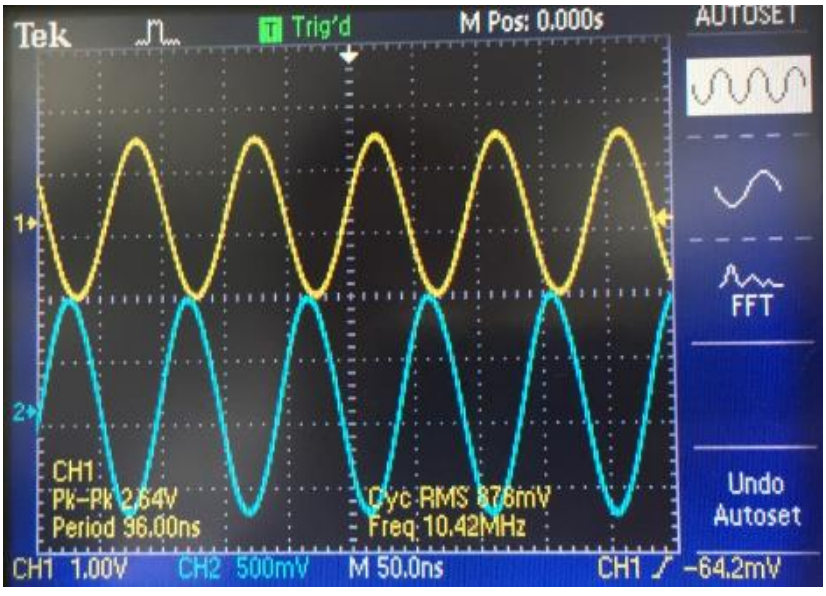

Figure 5.8: The voltage V_0 across R_0 is shown in yellow graph, whereas blue graph presents as the voltage V_L at the distance d_{23} of 3 cm

At d_{23} 3.5 cm:

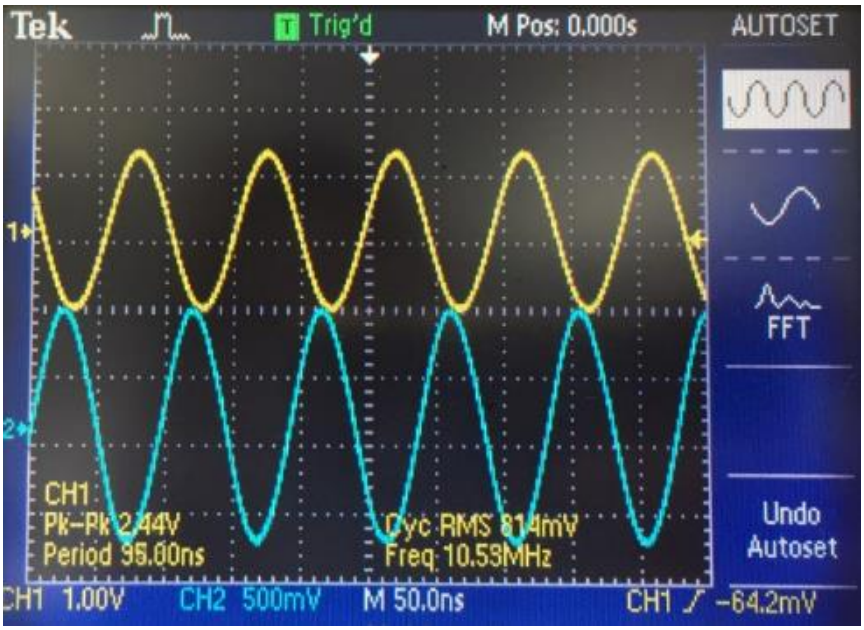

Figure 5.9: The voltage V_0 across R_0 is shown in yellow graph, whereas blue graph presents as the voltage V_L at the distance d_{23} of 3.5 cm

At d_{23} 4 cm:

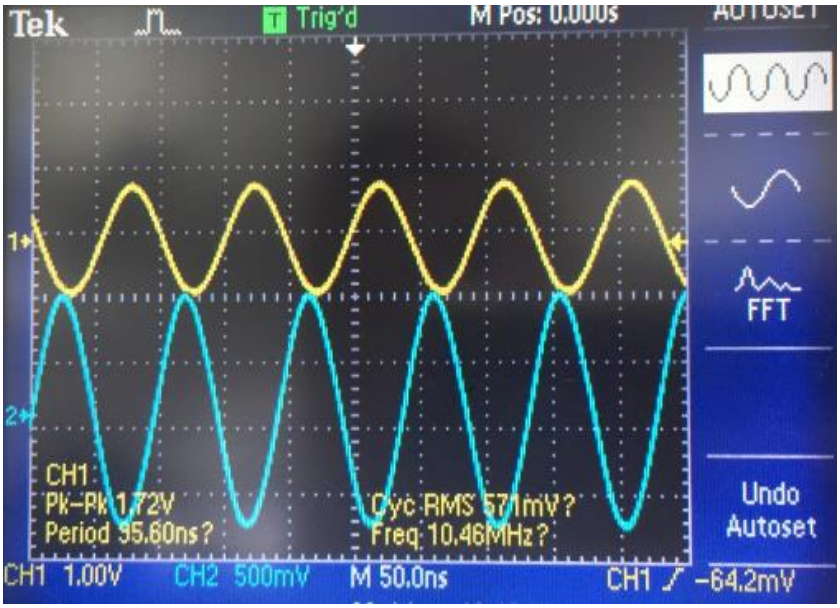

Figure 5.10: The voltage V_0 across R_0 is shown in yellow graph, whereas blue graph presents as the voltage V_L at the distance d_{23} of 4 cm

At d_{23} 4.5 cm:

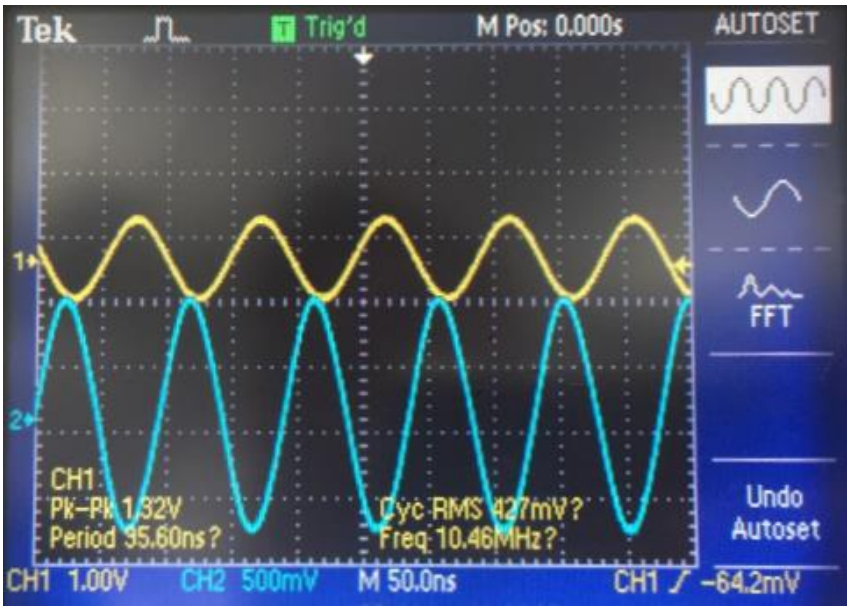

Figure 5.11: The voltage V_0 across R_0 is shown in yellow graph, whereas blue graph presents as the voltage V_L at the distance d_{23} of 4.5 cm

At d_{23} 5 cm:

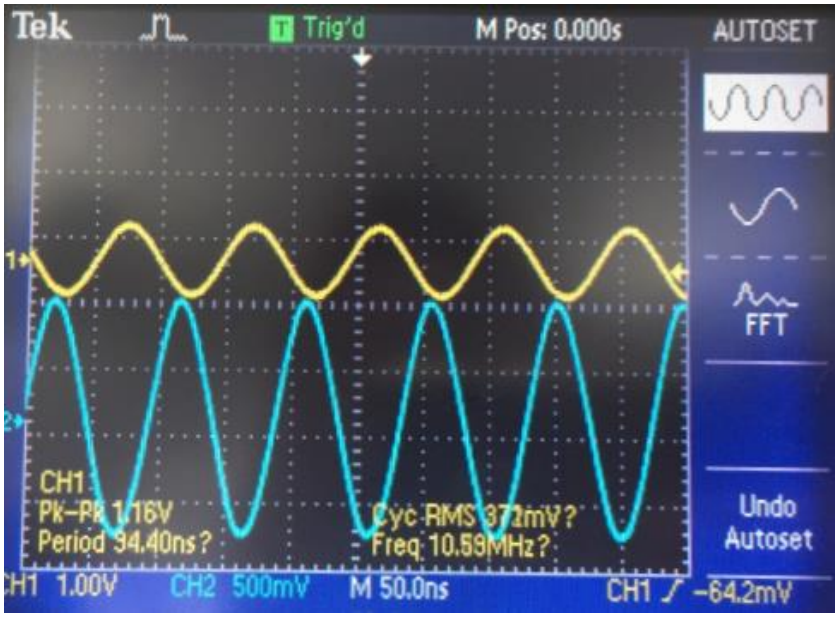

Figure 5.12: The voltage V_0 across R_0 is shown in yellow graph, whereas blue graph presents as the voltage V_L at the distance d_{23} of 5 cm

At d_{23} 5.5 cm:

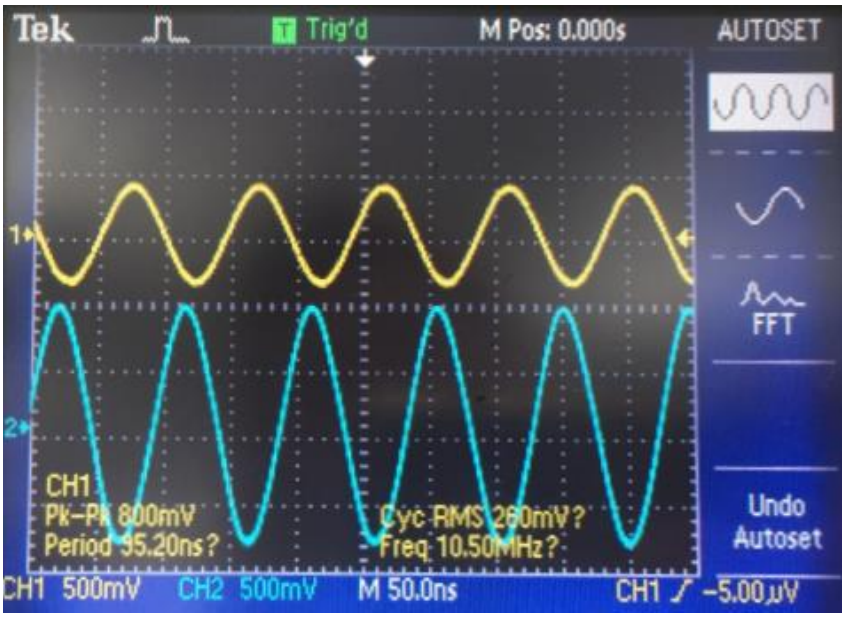

Figure 5.13: The voltage V_0 across R_0 is shown in yellow graph, whereas blue graph presents as the voltage V_L at the distance d_{23} of 5.5 cm

At d_{23} 6 cm:

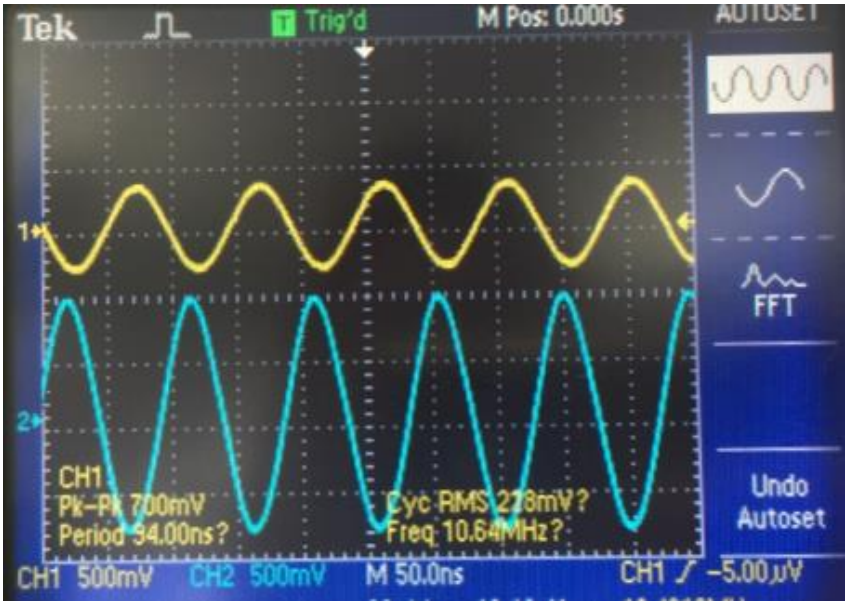

Figure 5.14: The voltage V_0 across R_0 is shown in yellow graph, whereas blue graph presents as the voltage V_L at the distance d_{23} of 6 cm

The data of the voltages through the loads R_L and R_0, collected at every 5 mm as presented from Figure 5.3 to Figure 5.14, are shown in Table 5.2 by V_0 and V_L in voltage peak to peak, and peak voltage.

Distance (d_{23})	**V_0**		**V_L**	
	V_{0pk-pk}	**V_{0pk}**	**V_{Lpk-pk}**	**V_{Lpk}**
0.5 cm	1.5	0.75	2.6	1.3
1.0 cm	1.5	0.74	3.08	1.9
1.5 cm	1.56	0.78	3.56	1.78
2.0 cm	1.6	0.8	3.44	1.72
2.5 cm	1.65	0.825	3.28	1.64
3.0 cm	1.7	0.85	2.64	1.32
3.5 cm	1.7	0.85	2.44	1.22
4.0 cm	1.77	0.885	1.72	0.86
4.5 cm	1.8	0.9	1.32	0.66
5.0 cm	1.8	0.9	1.16	0.58
5.5 cm	1.8	0.9	0.8	0.4
6.0 cm	1.8	0.9	0.7	0.35

Table 5.2: Summary the voltage of load resistance (V_L) and voltage across R_0 (V_0) vary at the distances d_{23} between the transmitter coil and the receiver coil in voltage peak-to-peak (V_{pk-pk}) and in the peak voltage (V_{pk}) by measurement

The current in coil 1 is needed to find the relative power transfer efficiency. As following from the equation V = IR and Figure 4.12(a), the current in coil 1 can be calculated by using Equation (5.2), where R0 is measured by the researcher that is 4.6 Ω, and is illustrated in Table 5.3.

$$I_1 = \frac{V_0}{R_0} = \frac{V_0}{4.6} \tag{5.2}$$

Distance (d_{23})	**$I_{1pk\text{-}pk}$ (A)**	**I_{1pk} (A)**
0.5 cm	0.326	0.163
1.0 cm	0.326	0.163
1.5 cm	0.339	0.17
2.0 cm	0.3478	0.174
2.5 cm	0.359	0.18
3.0 cm	0.37	0.185
3.5 cm	0.37	0.185
4.0 cm	0.385	0.1925
4.5 cm	0.391	0.1955
5.0 cm	0.391	0.1955
5.5 cm	0.391	0.1955
6.0 cm	0.391	0.1955

Table 5.3: The current in coil 1 (I_1) varies at the distances d_{23} between the transmitter coil and the receiver coil by measurement

The relative power transfer efficiency can be calculated by following the equations (4.14) and (4.15) using the data from Tables 5.2 and Table 5.3. However, from the formula (4.15), the angle of current in coil 1 I_1 is 35.842. Therefore, the relative power transfer efficiency (P_L/P_{IN}) from this experiment is represented in Table 5.4.

Distance (d_{23})	**The relative power transfer efficiency η**	**The relative power transfer efficiency η in percent (%)**
0.5 cm	0.09963	9.96
1.0 cm	0.14002	14.00
1.5 cm	0.17939	17.94
2.0 cm	0.16341	16.34
2.5 cm	0.14404	14.4
3.0 cm	0.09063	9.06
3.5 cm	0.07739	7.74
4.0 cm	0.03693	3.69
4.5 cm	0.02143	2.14
5.0 cm	0.01667	1.67
5.5 cm	0.00786	0.79
6.0 cm	0.00607	0.61

Table 5.4: The relative power transfer efficiency at the distances d_{23} between coil 2 and coil 3 by measurement

Findings M_{12}, M_{23} and M_{34} can be measured by following the equations (4.5) to (4.13).

For M_{12}:

Following from Figure 4.14 and the equation (4.7), the results are shown in Figure 5.15.

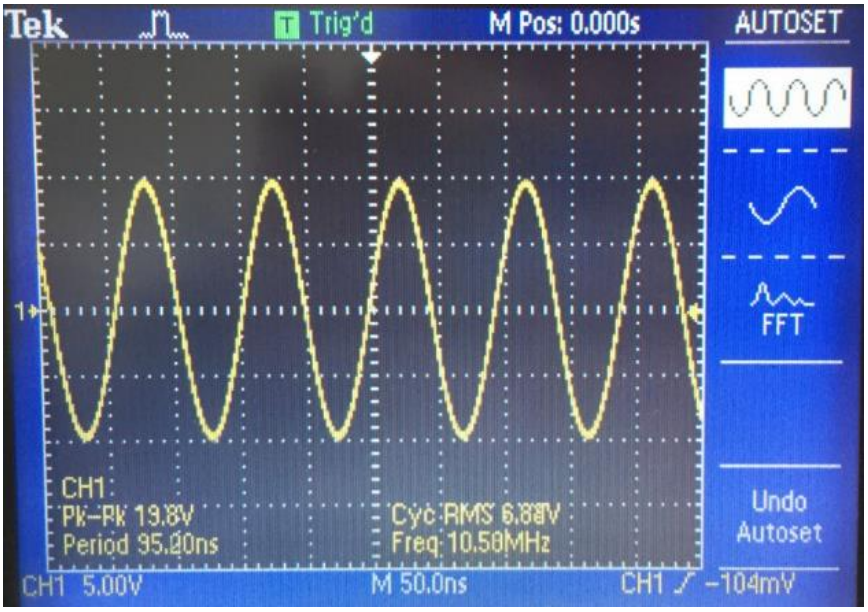

(a)

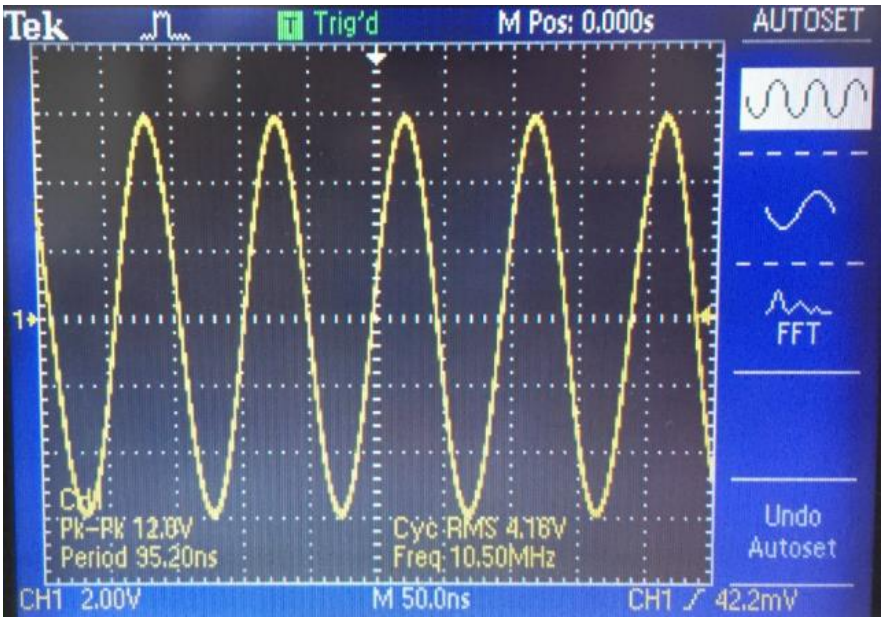

(b)

Figure 5.15: (a) Voltage across loop coil 1 V_{L1}; (b) Voltage across loop coil 2 V_{L2}

From the Figure 5.15 (a) and (b):

$V_{L1} = 19.8V_{pk\text{-}pk}$; $V_{L2} = 12V_{pk\text{-}pk}$

Hence, $M_{12} = 0.3599\ \mu H$

For M_{34}:

Following from Figure 4.15 and the equation (4.10), the results are shown in Figure 5.16.

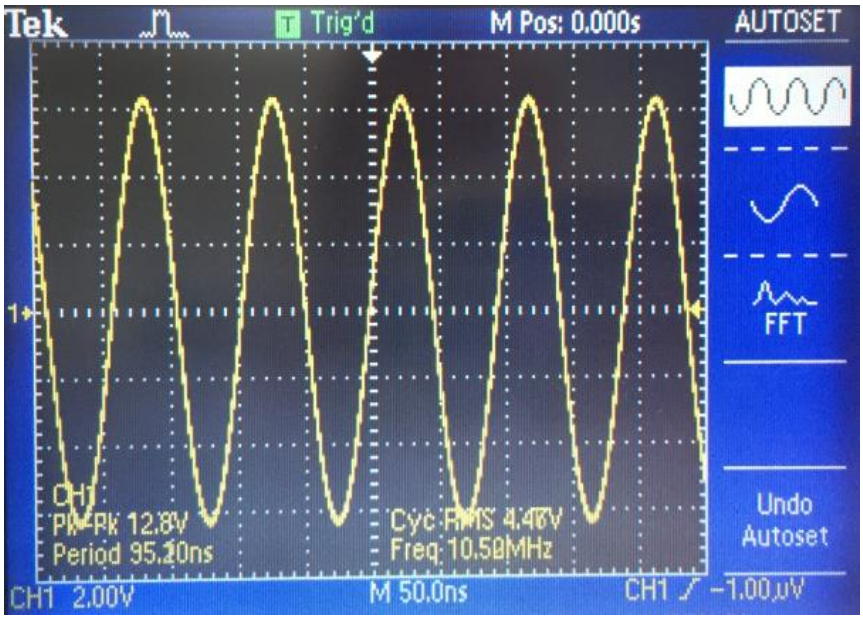

(a)

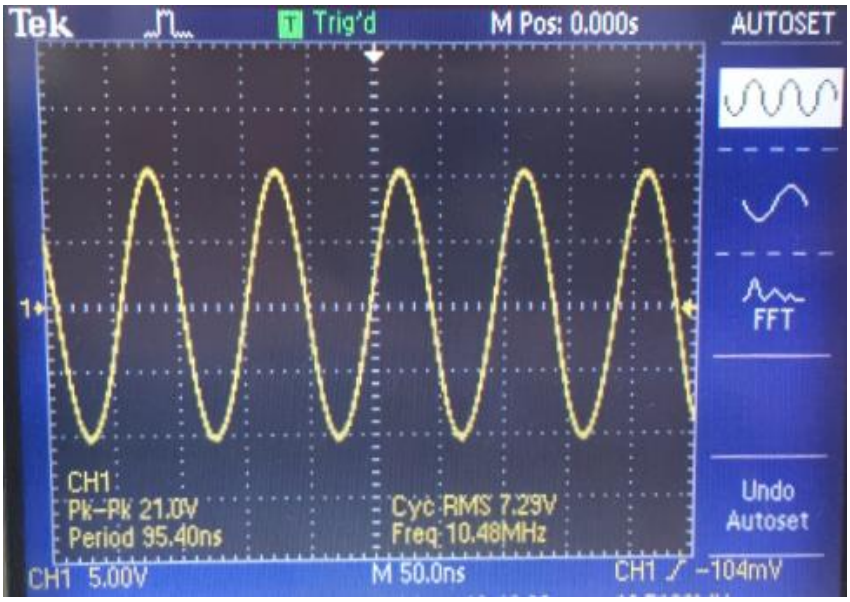

(b)

Figure 5.16: (a) Voltage across loop coil 3 V_{L3}; (b) Voltage across loop coil 4 V_{L4}

From the Figure 5.16 (a) and (b):

$V_{L4} = 21V_{pk\text{-}pk}$; $V_{L3} = 12.8V_{pk\text{-}pk}$

Hence, $M_{12} = 0.37\ \mu H$

For M_{23}:

For findings M_{23} follows Figure 4.16 and the equation (4.13). The researcher collected the data of the mutual inductance M_{23} from 0.5 cm to 6 cm at every 5 mm. The results are shown the table 5.5 and in the Appendix.

Distance (d_{23})	**V_{sense_1} ($V_{pk\text{-}pk}$)**	**V_{L3} ($V_{pk\text{-}pk}$)**
0.5 cm	1.6	3.84
1.0 cm	1.48	2.4
1.5 cm	1.42	1.46
2.0 cm	1.4	1.0
2.5 cm	1.37	0.68
3.0 cm	1.4	0.64
3.5 cm	1.4	0.52
4.0 cm	1.4	0.372
4.5 cm	1.35	0.256
5.0 cm	1.35	0.208
5.5 cm	1.35	0.184
6.0 cm	1.35	0.148

Table 5.5: The voltage across R_{sense_1} (V_{sense_1}) and voltage across inductance in coil 3 V_{L3} vary at the distances d_{23} when coil 3 is an open circuit

Hence, following the equation (4.13) and R_{sense_1} = 10 Ω, the mutual inductance is displayed in Table 5.6.

Distance (d_{23})	**Mutual inductance M_{23} (μH)**
0.5 cm	0.364
1.0 cm	0.246
1.5 cm	0.16
2.0 cm	0.108
2.5 cm	0.0752
3.0 cm	0.07
3.5 cm	0.0563
4.0 cm	0.0403
4.5 cm	0.03
5.0 cm	0.0234
5.5 cm	0.021
6.0 cm	0.0166

Table 5.6: The mutual inductance M_{23} between coil 2 and coil 3 vary at the distances d_{23}

Therefore, the calculation of the relative power transfer efficiency η can be followed the equation (3.14) by using data from above, as shown in Table 5.7.

Distance (d_{23})	**The relative power transfer efficiency η**	**The relative power transfer efficiency η in percent (%)**
0.5 cm	0.05777	5.78
1.0 cm	0.11565	11.57
1.5 cm	0.21968	21.97
2.0 cm	0.31478	31.48
2.5 cm	0.34244	34.24
3.0 cm	0.30231	30.23
3.5 cm	0.25712	25.71
4.0 cm	0.1659	16.59
4.5 cm	0.10204	10.2
5.0 cm	0.06733	6.73
5.5 cm	0.05573	5.57
6.0 cm	0.03547	3.55

Table 5.7: The relative power transfer efficiency at the distances d_{23} between coil 2 and coil 3 by calculation

5.3 Discussion

From the Tables 5.4 and Table 5.7, the relative power transfer efficiency by measurement and calculation can be plotted into the graph with the distance d_{23} from coil 1 to coil 4, as shown in Figure 5.17.

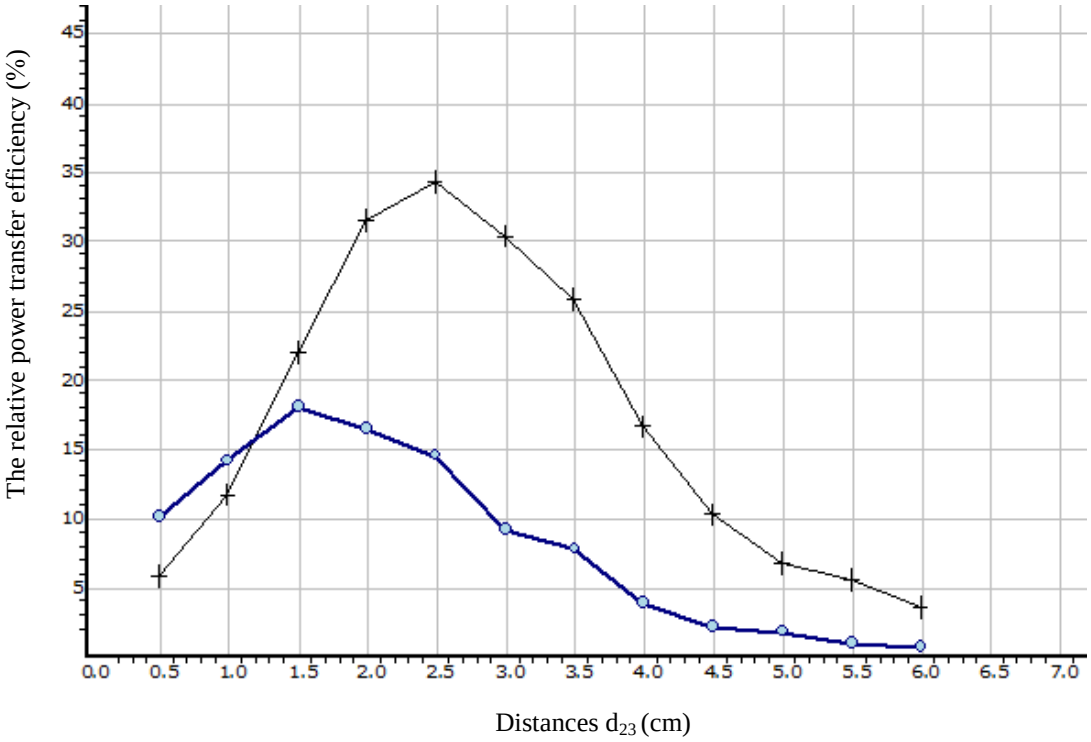

Figure 5.17: The relative power transfer efficiency as a function of the distances d_{23} between coil 2 and coil 3. The circle point (◦) is the relative power transfer efficiency by measurement, whereas the + point represents the efficiency by calculation

In the graph in Figure 5.17, the blue line with the circuit point is the direct experiment result and the black line with the plus dot is the theory model result obtained from the calculation and experimental extracted parameters, i.e. the mutual inductances and intrinsic loss rates. From the graph, it can be seen that the relative power transfer efficiency by measurement and calculation results; they are presented in the same way in both graphs. Starting from 0.5 cm, the efficiency by measurement rises rapidly until there is a maximum relative power transfer at around 1.5 to 2 cm, with approximately 20 percent of the efficiency; whereas by the calculation, the relative power efficiency reaches the maximum point at a distance of 2.5 cm, with an efficiency of about 30 percent. Over the transfer distance of 3 cm, the line of the graph gradually declines to less than 10 percent of the

efficiency by measurement; while the efficiency by calculation, an efficiency of less than 10 percent is reached after a distance of 4.5 cm.

Nevertheless, it can be noticed that the most experimental results of the transmitter efficiency are lower than the values of the efficiency wireless power transfer by calculation. The discrepancy in the results between the theory calculation and the experiment is due to it being unable to reach the optimal operation point, meaning the non-continuous tuning of the coupling loops between coils. Moreover, this is because the researcher neglects the mutual inductance between coil 1 and coil 4 (M_{14}), coil 1 and coil 3 (M_{13}), and coil 2 and coil 4 (M_{24}) for ease to calculate, since the mutual inductance of M_{14}, M_{13} and M_{24} are low. However, these mutual inductances can be put into effect for the results.

In addition, the graph can be compared with the observations of the LED light, as the author mentioned before; the light of the LED is dim at 0.5 cm and then slightly lights up until the light is the brightest at the distances d_{23} of around 2 cm to 2.5 cm, which is the same as the maximum point on this graph. Afterward, the light of the LED gradually dims until at the length of distance d_{23} approximately 4 cm. However, the reason that the researcher has selected to detect the LED light is because this LED requires the voltage of 1.2 to 3.6 V with a current rating of approximately 10 to 30 mA. This resembles the current consumption of sensor node, where the highest consumption is around 30 mA (Crossbow Technology, 2007), as mentioned in Chapter 2. So, if the LED light shines brightest at one point, the optimal operation for charging sensor node is at that point.

Therefore, from the experiment, it can be concluded that the four coils with 4.5 cm diameters can charge the sensor node through the source coil connected to the battery for the charging node which is connected to the load coil. To summary, at the distance of 3.4 cm from the source coil to the load coil, there is optimum transfer energy. However, there can be a transfer of power until approximately 5.4 cm from the source to charge the sensor node.

Chapter 6 – Conclusions, limitations and recommendations

6.1 Conclusions

The purpose of this study is to prolong the network lifespan of the sensor nodes in the wireless sensor network (WSN) system. The researcher focuses on the various types of alternative energy: solar energy, mechanical vibration energy, wind energy and wireless power transmission (WPT) in order to extend the lifespan of the node sensors for as long as possible. In this decade, the WSN has become significant, a key component in areas such as in buildings, utilities, industry, the home, on ships, moving systems automation, aircraft, health, transport, the environment, medical, the military, entertainment, crisis management, security, agriculture and smart spaces, and even in warfare (Jain, 2011; Stankovic, 2006). The WSN is used for collecting and gathering the data from measurements or is used to search for interested information. However, it is necessary to have a battery in the nodes in a WSN that is long life because it is hard to replace the sensor battery because the system sometimes includes more than 100, or even 1000 sensor nodes. Normally, the standard sensor nodes use an AA lithium battery, which has an average lifespan of approximately one year or less (Tan, 2012); this is an ongoing cost and represents a significant budget expenses if the WSN has a large number of sensor nodes. Also, some batteries may use their power faster than others, or may run out unexpectedly.

However, to prolong the lifetime in the WSN, there have many studies on extending the lifespan, such as changing the operating system. Nevertheless, there is still a need to replace the battery. Therefore, the most effective solution would be to use a source of alternative energy for all nodes in the WSN. The main considered factor to select the most suitable energy harvesting is powering the wireless sensor nodes by converting surrounding energy sources as light, vibrations, wind, EM (electromagnetic) radiation and magnetic field (magnetic inductive). This research has used a combination of the published literature and the findings from the experiment of this study. This chapter summarises all the findings and the analysis of this study.

The objectives of the literature review are to combine all the information in order to identify the most appropriate alternative energy for application to the sensor nodes in WSN. The three types of energy harvestings: solar cells or photovoltaic cells (solar energy),

mechanical vibration (vibration or wind; by piezoelectric), and the WPT (EM radiation or magnetic coupling resonant) can be used for WSN.

Nevertheless, the researcher selects the alternative energy source by using the magnetic induction method known as magnetic-coupled resonant WPT technology. This technology uses a magnetic field to transmit the power by a magnetic induction coil. This energy harvesting method is more flexible and is possible in all conditions; it can work under water and also when it is raining, comparing to the solar cell, which has limited capabilities depending on the strength of the light. The WPT model is easy to configure and install with sensor nodes. Moreover, it is worthwhile applying this energy harvesting method because the costs of this technology are low. Hence, the alternative energy by using magnetic WPT has become an attention and drawn a great interest from academics and companies in recent years. The researcher therefore combines the WSN with magnetic WPT energy harvesting, and concludes that this WPT alternative energy has the potential to power the sensor nodes in the wireless sensor system.

The key point of using the magnetic coupled resonant WPT technique for this study is that the power can be sent from the source to the vicinity by wirelessly in a distance. Consequently, this WPT energy harvesting is the most suitable means for charging the sensor nodes, using a robot handling the transmitter energy source to transfer power to the sensor node, with overall control by a person or a computer at a distance. It can help to cut the cost of changing the battery every year.

In this research project, the WPT method is conducted as the experiment to show that the energy can be transmitted at a distance by sifting through the coil. The author designs four coils for transmitting the energy from the source to the sensor nodes, which can be divided into two parts – the transmitter part and the receiver part. The transmitter part includes a source coil (coil 1) and a transmitter coil (coil 2), whereas the receiver part consists of a receiver coil (coil 3) and a load coil (coil 4). The transmitter coil and the receiver coil are connected to the capacitors to tune the same resonant. The source coil and the load coil are adjoined to the signal source and the load, respectively.

It can be seen from the result in Chapter 5 that from coil 1 to coil 4 with the load 10 ohm at the distances of approximately 3.4 cm, the power can be transferred with maximum efficiency. In addition, for this experiment, the power can be transmitted from the source coil to the load coil up to a distance of around 5.4 cm.

In conclusion, focusing on prolonging the lifespan of sensor nodes in WSN by using alternative energy is significant. Energy harvesting by using the magnetic induction technique called magnetic coupled resonant WPT is suitable for applying to all nodes for charging a battery and for extending the lifespan of the WSN.

6.2 Limitations

The limitations of this study involve the experiment methodology. This research relies on the results from the experiment; if this is designed in an alternative form, the results will be different. The data can be altered based on the relationships between the constructs or the coil composition, such as the type of wire for wound coils, the size of the wire, the diameter of the coil, the shape of the coil, the number of turns, etc. In addition, the results might be different if a different source, load or frequencies are used. However, the researcher should study of the effects of the component tolerances, and identify and compare these using the various types of coils, and all the conditions which may change the data and results of the designed experiment.

Furthermore, as from the experiment and the summary of Table 5.1, it can be seen that coil 2 and coil 3 have high Q-factor due to the high frequency as shown in Equation (3.9). High Q-factor means high quality of the coil. However, high Q-factor increases coil temperature. An overheating in coil could be the source of dangers for practical application. Therefore, the researcher should pay attention and research about the effect between them.

6.3 Recommendations and future work

As previously discussed, the magnetic coupled WPT technique has attracted the interest of both the academic and the industrial worlds. Therefore, this energy harvesting methods continues to improve and evolve to be more efficient. The combination of other alternative energy methods, such as using a battery source to WPT technology, causes an improvement in the performance of WPT in order to extend the lifespan for nodes in WSN, for example, by combining solar energy harvesting with the WPT technology by putting the solar panel with drive battery in transmitter part. However, each type of energy harvesting which is combines with the WPT should be suitable with a specific application, or depend on the environment surrounding the WSN.

In addition, the WPT can transfer the energy from one transmission to more than one device (multiple receivers). Hence, further development will explore the characterisation, model and analysis of this method. This improvement technique will be convenient and save time in the charging of the WSN.

Bibliography

Abatti, P. J., Pichorim, S. F. and Miranda, C. M. (2015). Maximum Power Transfer versus Efficiency in Mid-Range Wireless Power Transfer Systems. *Journal of Microwaves, Optoelectronics and Electromagnetic Applications*, 14(1).

Agilent Technologies, Inc. (2013). *Make Better RMS Measurements with Your DMM: Application Note*. [pdf] USA: Agilent Technologies. Available at: http://cp.literature.agilent.com/litweb/pdf/5988-6916EN.pdf [Accessed 20 Nov. 2015].

Agrawal, D. P., Biswas, R., Jain, N., Mukherjee, A., Sekhar, S. and Gupta, A. (2006). Sensor systems: State of the art and future challenges. *Handbook on the theoretical and algorithmic aspects of sensor, ad hoc wireless, and peer-to-peer networks*. Taylor and Francis group, LLC.

Akbari, S. (2014). Energy harvesting for wireless sensor networks review. *Computer science and information systems*, ACSIS, 2, pp. 987-992.

Akimoto, M. and Iizuka, M. (2013). Load Modulation Applied to Magnetic Resonance Wireless Power Transfer Technology and Its Applications. *Regular Articles*, 11(10).

Akyildiz, I.F., Su, W., Sankarasubramaniam, Y. and Cayirci, E. (2002). Wireless sensor networks: a survey. *Elsevier Computer Networks*, 38(4), pp. 393-422.

Alippi, C., Anastasi, G., Francesco, M. D. and Roveri, M. (2009). Energy management in wireless sensor networks with energy-hungry sensors. *IEEE Instrumentation & Measurement Magazine*, 12(2), pp. 16-23.

ApogeeKits Electronic Kits and Tools. (2015). *Solar Modules and Photovoltaic Panels*. [online] Available at: http://www.apogeekits.com/solar_cell_small_sol2.htm [Accessed 5 Jan. 2015].

Bakshi, U. A., Bakshi, A. V. and Bakshi, K. A. (2008). Chapter 3: Signal generator. *Electronic measurements and instrumentation*. Technical Publication Pune.

Balanis, C. A. (2005). *Antenna Theory: Analysis and design*. 3rd ed. New Jeysey: Wiley.

Balouchi, F. and Gohn, B. (2012). *Wireless power mobile devices, consumer electronics, industrial devices, wireless power infrastructure, and wireless charging of electric vehicles: Technology analysis, environmental impact, and market forecasts*. Pike Research LLC.

Beeby, S. P., Tudor, M. J. and White, N. M. (2006). Energy harvesting vibration sources for microsystems applications. *Measurement Science and Technology*, 17.

Beh, T.C., Kato, M., Imura, T. and Hori, Y. (2010). Wireless Power Transfer System via Magnetic Resonant Coupling at Fixed Resonance Frequency-Power Transfer System Based on Impedance Matching. *World Electric Vehicle Journal*, 4, pp. 744-753.

Bhattacharyya, D., Kim, T.H. and Pal, S. (2010). A Comparative Study of Wireless Sensor Networks and Their Routing Protocols. *Sensors 2010*, 10.

Bhuvaneswari, P.T.V., Balakumar, R., Vaidehi, V. and Balamuralidhar, P. (2009). Solar energy harvesting for wireless sensor networks. *First International Conference on Computational Intelligence, Communication Systems and Networks*, 9, pp. 57-61.

Brain, M. (2006). *How lithium-ion batteries work.* [online] Available at: http://electronics.howstuffworks.com/everyday-tech/lithium-ion-battery.htm [Accessed 15 Dec. 2015].

Buchmann, I. (2003). *BU-209: How does a supercapacitor work.* [online] Cadex Electronics Inc. Available at: http://www.BatteryUniversity [Accessed 10 Nov. 2015].

Buettner, M., Greenstein, B., Sample, A., Smith, J. R. and Wetherall, D. (2008). Revisiting Smart Dust with RFID Sensor Networks. *HotNets*, pp. 37-42.

Buettner, M., Prasad, R., Sample, A., Yeager, D., Greenstein, B., Smith, J. R and Wetherall, D. (2008). Demo Abstract: RFID Sensor Networks with the Intel WISP. *SenSys'08*, pp. 393-394.

Burton, L. (2007). *Application of information systems and secondary data*. School of public room.

Callaway, E.H. (2003). *Wireless sensor networks: Architecture and protocols*. CRC Press Company.

Camilo1, T.,Carreto, C., Silva, J.S. and Boavida, F. (2006). An Energy-Efficient Ant-Based Routing Algorithm for Wireless Sensor Networks. *Ant Colony Optimization and Swarm Intelligence*, pp. 49-59.

Cannon, B. L., Hoburge, J. F., Stancil, D. D. and Goldstein, S. C. (2009). Magnetic Resonant Coupling As a Potential Means for Wireless Power Transfer to Multiple Small Receivers. *IEEE Transactions on power electronics*, 24 (7).

Center for technology and aging. (2009). Technologies for Remote Patient Monitoring in Older Adults. *Position Paper*.

Chandrakasan, A., Amirtharajah, R., Cho, S.H., Goodman, J., Konduri, G., Kulik, J., Rabiner, W. and Wang, A. (1999). Design considerations for distributed microsensor systems', *Custom Integrated Circuits, Proceedings of the IEEE*, pp. 279-286.

Chen, J (2007). *Feedback networks: Theory and circuit application*. Singapore: World Scientific.

Cook-Chennault, K. A., Thambi, N. and Sastry, A. M. (2008). Powering MEMS portable devices—a review of non-regenerative and regenerative power supply systems with special emphasis on piezoelectric energy harvesting systems. *Smart Materials and Structures*, 17, pp. 1-33.

Corke, P., Wark, T., Jurdak, R., Hu, W., Valencia, P. and Moore, D. (2010). Environmental Wireless Sensor Networks. *Proceedings of the IEEE*, 98(11), pp. 1903-1917.

Creswell, J. W. (2008). *Research design: Qualitative, quantitative, and mixed methods approaches*. 3rd ed. CA: Sage publications.

Crossbow Technology, Inc. (2004). *MPR-MIB users manual*. Revision A. California: Crossbow Resources.

Dondi, D., Bertacchini, A., Larcher, L., Pavan, P., Brunelli, D. and Benini, L. (2008). A solar energy harvesting circuit for low power applications. In: *IEEE International Conference on Sustainable Energy Technologies.* Singapore: IEEE, pp. 945 – 949.

Driscoll, D. L. (2011). Introduction to primary research: Observations, surveys, and interviews. *Writing spaces: Readings on writing*, 2.

Duong, T. P. and Lee, J.W. (2011). Experimental Results of High-Efficiency Resonant Coupling Wireless Power Transfer Using a Variable Coupling Method. *IEEE Microwave and wireless components letters*, 21(8), pp. 442-444.

Elliott, P. C. (2010). *The Basics of Digital Multimeters: A guide to help you understand the basic Features and Functions of a Digital Multimeter*. Ideal industries, Inc.

EPCglobal. (2005). *EPC radio-frequency identity protocol class-1 generation-2 UHF RFID protocol for communications at 860 MHz-960 MHz version 1.0.9.*

Erturk, A. and Inman, D. J. (2011). *Piezoelectric Energy Harvesting.* UK: John Wiley & Sons.

Fu, L., Cheng, P., Gu, Y., Chen, J. and He, T. (2013). Minimizing Charging Delay in Wireless Rechargeable Sensor Networks. In: *INFOCOM*, Turin: IEEE, pp. 2922 – 2930.

Galán, R. C., Fernández-Berni, G., Carranza-González, L., Cembrano, S. L., Moreno, E R., Rodríguez-Vázquez, Á. and Sierra, S. R. (2010). *Project V-MOTE*. [online] Available at: http://www2.imse-cnm.csic.es/vmote/english_version/deteccion_texturas.php [Accessed 10 Nov 2014].

Gay, D., Levis, P., Behren, R.V., Welsh, M., Brewer, E. and Culler, D. (2003). *ThenesC language: Aholisticapproach to networked embedded systems*. Programming Language Design and Implementation (PLDI).

Gilbert, J.M. and Balouchi, F. (2008). Comparison of energy harvesting systems for wireless sensor networks. *International Journal of Automation and Computing*, 5(4).

Guibas, L. and Zhao, F. (2004). An Information Processing Approach. *Wireless Sensor Networks*. San Francisco, CA.

Gungor, V.C. and Hancke, G.P. (2009). Industrial Wireless Sensor Networks: Challenges, Design Principles, and Technical Approaches', *IEEE Transactions on Industrial Electronics*, vol. 56(10), pp. 4258-4265.

He, S., Chen, J., Jiang, F., Yau, D. K. Y., Xing, G., and Sun, Y. (2013). Energy Provisioning in Wireless Rechargeable Sensor Networks. *IEEE Transactions on Mobile Computing*, 12(10), pp. 1931-1942.

Hill, J. L. (2003). *System Architecture for Wireless Sensor Networks*. University of California, California, Berkeley.

Hirayama, H. (2012). Equivalent Circuit and Calculation of Its Parameters of Magnetic-Coupled-Resonant Wireless Power Transfer. *Wireless Power Transfer - Principles and Engineering Explorations*. InTech.

Hoang, H. and Bien, F. (2012). Maximizing Efficiency of Electromagnetic Resonance Wireless Power Transmission Systems with Adaptive Circuits. *Wireless Power Transfer - Principles and Engineering Explorations*, InTech.

ICNIRP (International commission on non-ionizing radiation protection) (1998). Guidelines for limiting exposure to time-varying electric, magnetic, and electromagnetic fields (Up to 300 GHz)', *Health Physics*, 74(4), pp. 494-522.

IEEE International Committee on Electromagnetic Safety (SCC39) (2006). *C95.1-2005 - IEEE Standard for safety levels with respect to human exposure to radio frequency electromagnetic fields, 3kHz to 300 GHz*.

Imura, T., Okabe, H. and Hori, Y. (2009). Basic experimental study on helical antennas of wireless power transfer for electric vehicles by using magnetic resonant couplings. In: *IEEE Vehicle Power and Propulsion Conference*. Dearborn, IEEE, pp. 936-940.

Intanagonwiwat, C., Govindan, R., Estron, D., Heidemann, J. and Silva, F. (2013). *Directed Diffusion for Wireless Sensor Networking*.

Intel (2004). *Intel Showcases Innovative Wireless Sensor Networks For In-Home Health Care Solutions*. [online] Available at: http://www.intel.com/pressroom/archive/releases/2004/20040316corp.htm [Accessed 7 Oct. 2014].

Jackson, J. D. (1962). *Classical Electrodynamics*. New York: John Wiley & Sons.

Jackson, R. (2010). Wireless Sensor Networks-Applications and Energy Storage Technologies. *Sensor Report*, 3, pp. 30-32.

Jacobsen, R. H., Toftegaard, T. S. and Kjærgaard, J. K. (2012). Chapter 10 - IP Connected low power wireless personal area networks in the future internet. *Technologies and Protocols for the Future of Internet Design: Reinventing the Web*. US: IGI Global.

Jain, N. (2011). Energy Efficient and Cluster Based Routing Protocol for Wireless Sensor Network: A Review. *International Journal of Advance Technology & Engineering Research (IJATER)*, 1(1).

Jawarkar, U., Panchore, P. and Deshmukh, S. (2013). Overview of Wireless Sensor Network and its Applications. *International Journal of Electronics Communication and Computer Engineering*, 4(2), pp. 29-32.

Jonah, O. and Georgakopoulos, S. V. (2012). Optimal helices for wireless power transfer via magnetic resonance. *Wireless and microwave technology conference (WAMICON), IEEE 13th Annual*, pp.1-4.

Karalis, A., Joannopoulos, J. D. and Soljačić, M. (2008). Efficient wireless non-radiative mid-range. *Annals of Physics*, 323, pp. 34–48.

Kawamura, A. and Kim, T. W. (2013). Proposed Equivalent Circuit and Parameter Identification Method for Electro-Magnetic Resonance Based Wireless Power Transfer. *J Electr Eng Technol*, 8, pp.769-777.

Kesler, M. (2103). *Highly resonant wireless power transfer: safe, efficient, and over distance*. WiTricity Coroiration.

Kesler, M. and McCarthy, C. (2013). Highly resonant wireless power transfer in subsea application. *WiTricity White Paper*.

Khan, Z. A. and Sampalli, S. (2012). AZR-LEACH: An Energy Efficient Routing Protocol for Wireless Sensor Networks. *Int'l J. of Communications, Network and System Sciences*, 5(11), pp. 785-795.

Kim, J., Choi, W.S. and Jeong, J. (2013). Loop switching technique for wireless power transfer using magnetic resonance coupling. *Progress In Electromagnetics Research*, 138, pp. 197-209.

Kim, J and Bien, F. (2013). Electric Field Coupling Technique of Wireless Power Transfer for Electric Vehicles. *TENCON Spring Conference, IEEE*, pp. 267-271.

Knaian, A. N. (2000). *A Wireless Sensor Network for Smart Roadbeds and Intelligent Transportation Systems*. Massachusetts Institute of Technology.

Knight, D. W. (2013). *The RMS Average*.

Kochláň, M. and Ševčík, P. (2012). Supercapacitor power unit for an event-driven wireless sensor node. In: *Computer Science and Information Systems*. Wroclaw: the Federated, pp. 791–796.

Krishnamachari, B. (2005). *Networking Wireless Sensors*. UK: Cambridge University.

Kumar A., Mirabbasi, S. and Chiao, M. (2009). Resonance-based wireless power delivery for implantable devices. *Biomedical Circuits and Systems Conference*. Beijing: IEEE, pp. 25-28.

Kumar, S. S. and Kashwan, K. R. (2013). Research Study of Energy Harvesting in Wireless Sensor Networks. *International Journal of Renewable Energy Research*, 3(3).

Kurs, A., Karalis, A., Moffatt, R., Joannopoulos, J. D., Fisher, P. and Soljacic, M. (2007). Wireless Power Transfer via Strongly Coupled Magnetic Resonances. *Science*, 317, pp. 83-86.

Kurs, A., Moffatt, R. and Soljačić, M. (2010). Simultaneous mid-range power transfer to multiple devices', A*pplied physics letters*, 96.

Kürschner, D., Rathge, C. and Jumar, U. (2013). Design Methodology for High Efficient Inductive Power Transfer Systems with High Coil Positioning Flexibility. *IEEE Transactions on Industrial Electronics*, 60(1), pp. 372-381.

Kymissis, J., Kendall, C., Paradiso, J. and Gershenfeld, N. (1998). Parasitic power harvesting in shoes. *Presented at the Second IEEE International Conference on Wearable Computing*.

Lee, D. S., Liu, Y. H. and Lin, C. R. (2012). A wireless sensor enabled by wireless power. *Sensors*, 12.

Lee, V. (2012). *Energy Harvesting for Wireless Sensor Networks.* University of California, Berkeley.

Leland, E. S., Lai, E. M. and Wright, P. K. (2004). A self-powered wireless sensor for indoor environmental monitoring. *WNCG 2004 – Wireless Networking Symposium*.

Levis, P. and Gay, D. (2009). *TinyOS Programming*. Stanford University Campus.

Levis, P., Madden, S., Gay, D., Polastre, J., Szewczyk, R., Woo, A., Brewer, E. and Culler, D. (2004). The emergence of networking abstractions and techniques in TinyOS. *NSDI'04 Proceedings of the 1st conference on Symposium on Networked Systems Design and Implementation*, 1.

Levis, P., Madden, S., Polastre, J., Szewczyk, R., Whitehouse, K., Woo, A., Gay, D., Hill, J., Welsh, M., Brewer, E. and Culler, D. (2004). *TinyOS: An Operating System for Sensor Networks*. Ambient Intelligence.

Li, X., Zhang, H., Peng, F., Li, Y., Yang, T., Wang, B. and Fang D. (2012). A Wireless Magnetic Resonance Energy Transfer System for Micro Implantable Medical Sensors. *Sensors 2012*, 12(8).

Libelium Comunicaciones Distribuidas S. L. (N.D.). *Technical Overview*. [online] Avaliable at: http://www.libelium.com/products/plug-sense/technical-overview/ [Accessed 5 Jan. 2015].

Lin, M., Rowaihy, H., Bolbrock, T., Cao, G. and Porta, T. L. (2008). Data Collection Using RFID and a Mobile Reader. *IEEE Global Telecommunications Conference*. New Orleans, LO: IEEE GLOBECOM, pp. 1-6.

Mainwaring,A., Polastre,J., Szewczyk,R., Culler,D. and Anderson, J. (2002). Wireless Sensor Networks for Habitat Monitoring. *WSNA*, 02.

Mathúna, C. O., Donnell, T. O., Martinez-Catala, R. V., Rohan, J., Flynn, B. O. (2008). Energy scavenging for long-term deployable wireless sensor networks. *Talanta*, 75(3), pp. 613–623.

Matin, M.A. and Islam, M.M. (2012). Overview of Wireless Sensor Network. *Wireless Sensor Networks - Technology and Protocols*. InTech.

Mongia, R. (2007). *RF and Microwave Coupled-Line Circuits*. Norwood, MA: Artech House.

Moschitta, A. and Neri, I. (2014). Power consumption Assessment in Wireless Sensor Networks. *ICT - Energy - Concepts Towards Zero - Power Information and Communication Technology.* InTech.

Nair, A. (2012). Wireless Power Transfer System via Magnetic Resonant Coupling. *Proc. of the Second International Conference on Advances in Computing, Control and Communication (CCN)*.

Nechibvute, A., Chawanda, A. and Luhanga, P. (2012). Piezoelectric Energy Harvesting Devices: An Alternative Energy Source for Wireless Sensors. *Smart Materials Research*, 2012.

Oliveira, L. M. L. and Rodrigues, J. J. P. C. (2011). Wireless Sensor Networks: a Survey on Environmental Monitoring. *Journal of Communications*, 6(2).

Ostaffe, H. (2009). *Sensors Mag RF Energy Harvesting Enables Wireless Sensor Networks*. [online] Available at: http://www.sensorsmag.com/sensors-mag/rf-energy-harvesting-enables-wireless-sensor-networks-6175 [Accessed 5 Apr. 2015].

RamRakhyani, A. K., Mirabbasi, S. and Chiao, M. (2011). Design and Optimization of Resonance-Based Efficient Wireless Power Delivery Systems for Biomedical Implants. *IEEE Transactions on Biomedical Circuits and Systems*, 5(1), pp. 48-63.

Ramsden, E. and Dix, C. (2003). Low-pass filtering for vibration sensors. *Sensor technology and design*.

Reve, S. V. and Choudhri, S. (2012). Management of Car Parking System Using Wireless Sensor Network. *International Journal of Emerging Technology and Advanced Engineering*, 2(7), pp. 262-268.

Roundy, S., Wright, P. K. and Rabaey, J. (2003). A study of low level vibrations as a power source for wireless sensor nodes. *Computer Communications*, 26 (11), pp. 1131–1144.

Russell, A. (1906). The Magnetic Field and Inductance Coefficients of Circular, Cylindrical and Helical Currents. *Proceedings of the Royal Academy of Science*, 20, pp. 476-506.

Sah, A. K. and Pant, D. R. (2014). Analysis and optimization of wireless power transfer link. *International conference on technology and innovation management and IOE graduate conference*, pp. 82-93.

Sample, A. P., Yeager, D. J., Powledge, P. S., Mamishev, A. V. and Smith, J. (2008). Design of an RFID-Based Battery-Free Programmable Sensing Platform. *IEEE Transactions on Instrumentation and Measurement*, 57(11), pp. 2608-2615.

Sample, A.P., Meyer, D.A., and Smith, J.R. (2011). Analysis, Experimental Results, and Range Adaptation of Magnetically Coupled Resonators for Wireless Power Transfer. *IEEE Transactions on Industrial Electronics*, 58(2), pp. 544-554.

Sanghoon, C., Kim, Y. H., Kang, S. Y., Lee, M. L., Lee, J. M. and Zyung, T. (2011). Circuit-Model-Based Analysis of a Wireless Energy-Transfer System via Coupled Magnetic Resonances. *IEEE Transactions on Industrial Electronics*, 58(7).

Shi, Y., Xie, L., Hou, Y. T. and Sherali, H. D. (2011). On renewable sensor networks with wireless energy transfer. In: *INFOCOM*. Shanghai: IEEE, pp. 1350-1358.

Shih, E., Cho, S.H., Ickes, N., Min, R., Sinha, A., Wang, A. and Chandrakasan, A. (2001). Physical Layer Driven Protocol and Algorithm Design for Energy-Efficient Wireless Sensor Networks. *MobiCom'01*, pp. 272–286.

Silva, A., Liu, M. and Moghaddam, M. (2012). Power-Management Techniques for Wireless Sensor Networks and Similar Low-Power Communication Devices Based on Nonrechargeable Batteries. *Journal of Computer Networks and Communications*, 2012.

Smith, J. R., Sample, A., Buettner, M., Reina, J. and Parks, A. (2011). *WISP (Wireless Identification and Sensing Platform)*. [online] Sensor Systems Laboratory. Available at: http://sensor.cs.washington.edu/WISP.html [Accessed 19 Feb. 2015].

Sodano, H. A., Inman, D. J. and Park, G. (2005). Generation and Storage of Electricity from Power Harvesting Devices. *Journal of Intelligent Material Systems and Structures*, 16(1), pp. 67–75.

SparkFun Electronics. (2014). *sparkfun*. [online] Available at: https://www.sparkfun.com [Accessed 24 Dec 2014].

Stankovic, J. A. (2006). *Wireless Sensor Networks*. University of Virginia.

Starner, T. (1996). Human-powered wearable computing. *IBM Systems journal*, 35(3&4), pp. 618-629.

Tan, Y. K. (2012). The prospect of energy-harvesting technologies for healthcare wireless sensor networks. *Healthcare Sensor Networks: Challenges Toward Practical Implementation*. CRC Press.

Taufik, T., Thornton, J. and Dolan, D. (2012). Piezoelectric Converter for Wind Energy Harvesting. In: *Ninth International Conference on Information Technology - New Generations*. Las Vegas, NV: IEEE, pp. 222-224.

Tektronix, Inc. (2009). *Oscilloscope Fundamentals*.

Tektronix, Inc. (N.D.). *Lithium-Ion Battery Maintenance Guidelines.* USA.

Tesla, N. (1914). *Tesla patent 1,119,732 apparatus for transmitting electrical energy*. United States Patent office.

The Solar Foundation and SEIA (the solar energy industries association) (2014). *Brighter Future: A Study on Solar in U.S. Schools Report.*

Tomicek, D., Tham, Y.H., Seah, W. K.G. and Rayudu, R. K. (2013). *Vibration-powered wireless sensor for structural monitoring during earthquakes*, The 6th International Conference on Structural Health Monitoring of Intelligent Infrastructure. Hong Kong.

Vasanthi, V., Nagarajan, P., Bharathi, B. and Hemalatha, M. (2010). A Perspective Analysis of routing protocols in wireless sensor network. *International Journal on Computer Science and Engineering (IJCSE)*, 2(8).

Voigt, T., Ritter, H. and Schiller, J. (2003). Utilizing solar power in wireless sensor networks. T*he 28th Annual IEEE International Conference on Local Computer Networks*, 3, pp. 416-422.

Want, R. (2006). An introduction to RFID technology. *IEEE Pervasive Computing*, 5(1), pp. 25-33.

Wei, X., Wang, Z. and Dai, H. (2014). A Critical Review of Wireless Power Transfer via Strongly Coupled Magnetic Resonances. *Energies 2014*, 7(7), pp. 4316-4341.

Weinstein, R. (2005). RFID: a technical overview and its application to the enterprise. *IT Professional*, 7(3), pp. 27-33.

Wheeler, H. A. (1928). Simple Inductance Formulas for Radio Coils. *Proceedings of the Institute of Radio Engineers,* 16 (10), pp. 1398-1400.

White, N. M. and Turner, J. D. (1997). Thick-film sensors: past, present and future. *Measurement Science and Technology*, 8, pp. 1–20.

Wilson, J. B. and Natale, S. M. (2001). Quantitative and qualitative research: An analysis. *International journal of value-based management*, 14, pp. 1–10.

Xie, L., Shi, Y., Hou, Y. T. and Lou, W. (2013). Wireless power transfer and applications to sensor networks. *IEEE Wireless Communications*, 20(4), pp. 140-145.

Xie, L., Shi, Y., Hou, Y. T. and Sherali, H. D. (2012a). Making Sensor Networks Immortal: An Energy-Renewal Approach with Wireless Power Transfer. *IEEE/ACM Transactions on networking*, 20(6), pp. 1748-1761.

Xie, L., Shi, Y., Hou, Y. T., Lou, W., Sherali, H. D. and Midkiff, S. F. (2012b). On renewable sensor networks with wireless energy transfer: The multi-node case. In: *9th Annual IEEE Communications Society Conference on Sensor, Mesh and Ad Hoc Communications and Networks (SECON)*. Seoul: IEEE, pp. 10-18.

Yao, Y., Zhange, H. and Geng, Z. (2011). Wireless charger prototype based on strong coupled magnetic resonance. *International Conference on Electronic & Mechanical Engineering and Information Technology*, 5, pp. 2252-2254.

Zahid Kausar, A.S.M., Reza, A. W., Saleh, M. U. and Ramiah, H. (2014). Energizing wireless sensor networks by energy harvesting systems: Scopes, challenges and approaches', *Renewable and sustainable energy reviews*, 38, pp. 973-989.

Zhang, R. (21014). *Wireless powered communication: Opportunities and challenges*. ECE Department, National University of Singapore, ICC 2014.

APPENDIX

Mutual inductance between transmitter coil and receiver coil M_{23} has difference values, depending on a distance between coils. The researcher collected the data every 5 mm from 0.5 mm to 6 mm. From the Figure 4.16, the results are shown in Figure 1 to Figure 12, and M_{23} can be calculated following from the equation (4.13).

At d_{23} 0.5 cm:

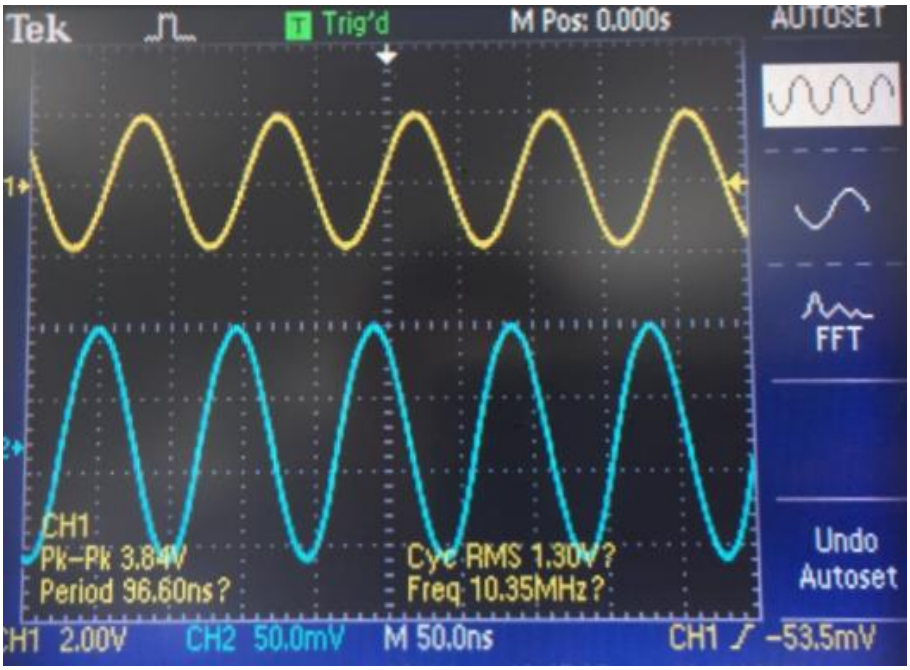

Figure 1: The voltage V_{sense_1} across R_{sense_1} is shown in blue graph, whereas yellow graph presents as the voltage across coil 3 V_{L3} at the distance d_{23} of 0.5 cm

From the Figure 1 and following the equation (4.13), with R_{sense_1} = 10 Ω:

$V_{sense\_1} = 1.6V_{pk\text{-}pk}$; $V_{L3} = 3.84V_{pk\text{-}pk}$

Hence, $M_{12} = 0.364\ \mu H$

At d_{23} 1.0 cm:

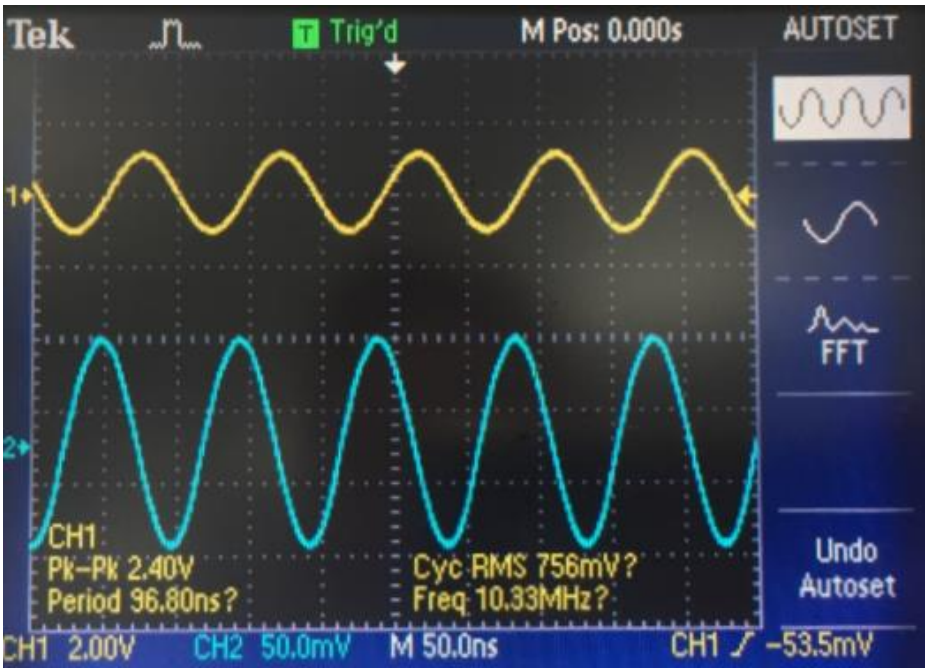

Figure 2: The voltage V_{sense_1} across R_{sense_1} is shown in blue graph, whereas yellow graph presents as the voltage across coil 3 V_{L3} at the distance d_{23} of 1.0 cm

From the Figure 2 and following the equation (4.13), with R_{sense_1} = 10 Ω:

$V_{sense\_1} = 1.48V_{pk\text{-}pk}$; $V_{L3} = 2.4V_{pk\text{-}pk}$

Hence, $M_{12} = 0.246\ \mu H$

At d_{23} 1.5 cm:

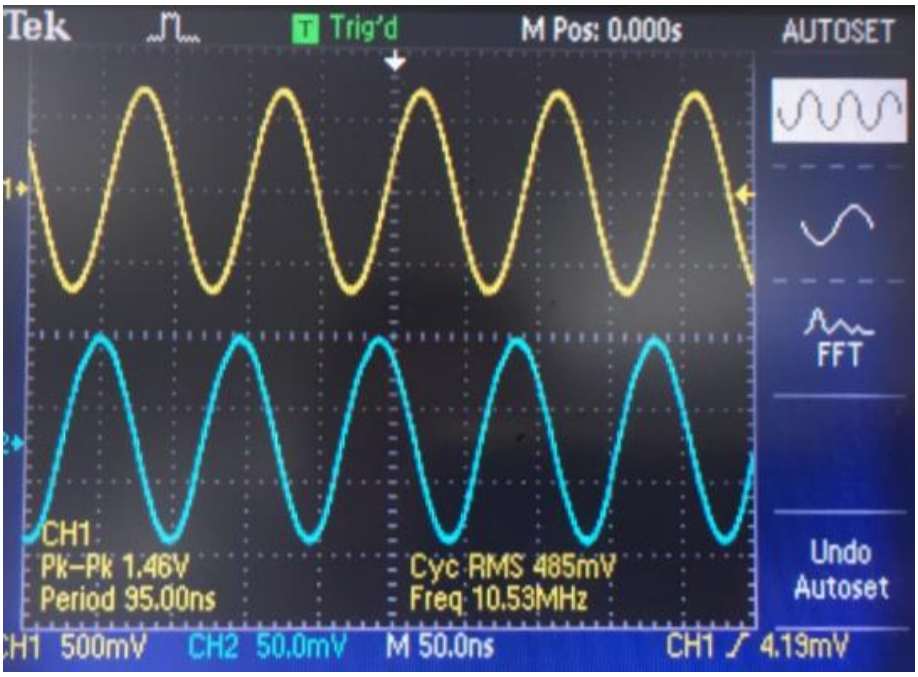

Figure 3: The voltage V_{sense_1} across R_{sense_1} is shown in blue graph, whereas yellow graph presents as the voltage across coil 3 V_{L3} at the distance d_{23} of 1.5 cm

From the Figure 3 and following the equation (4.13), with R_{sense_1} = 10 Ω:

$V_{sense\_1} = 1.42V_{pk\text{-}pk}$; $V_{L3} = 1.46V_{pk\text{-}pk}$

Hence, $M_{12} = 0.16\ \mu H$

At d_{23} 2.0 cm:

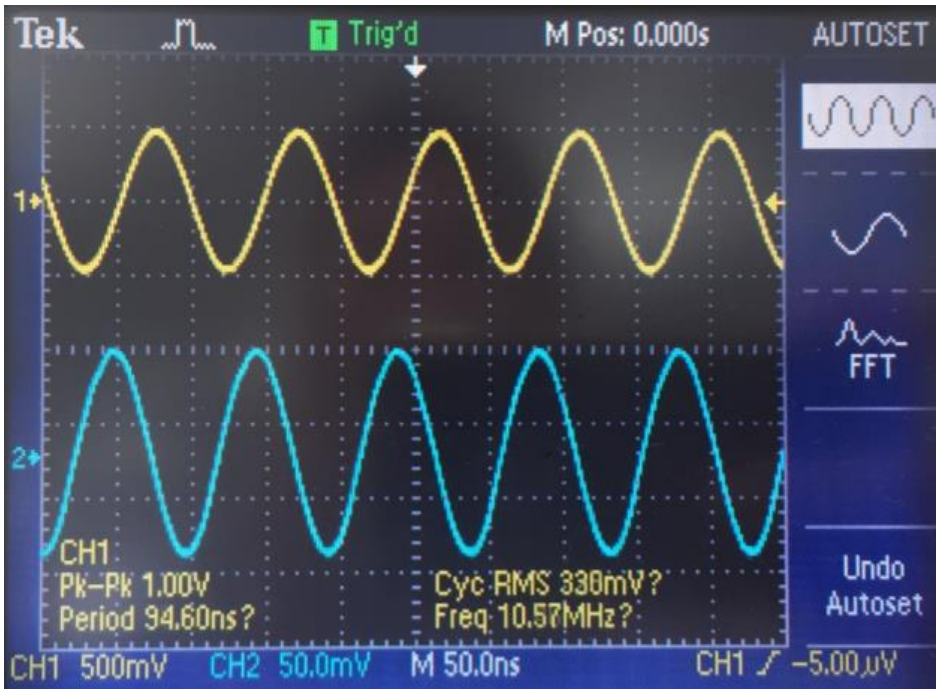

Figure 4: The voltage V_{sense_1} across R_{sense_1} is shown in blue graph, whereas yellow graph presents as the voltage across coil 3 V_{L3} at the distance d_{23} of 2.0 cm

From the Figure 4 and following the equation (4.13), with R_{sense_1} = 10 Ω:

$V_{sense\_1} = 1.4V_{pk\text{-}pk}$; $V_{L3} = 1.00V_{pk\text{-}pk}$

Hence, $M_{12} = 0.108\ \mu H$

At d_{23} 2.5 cm:

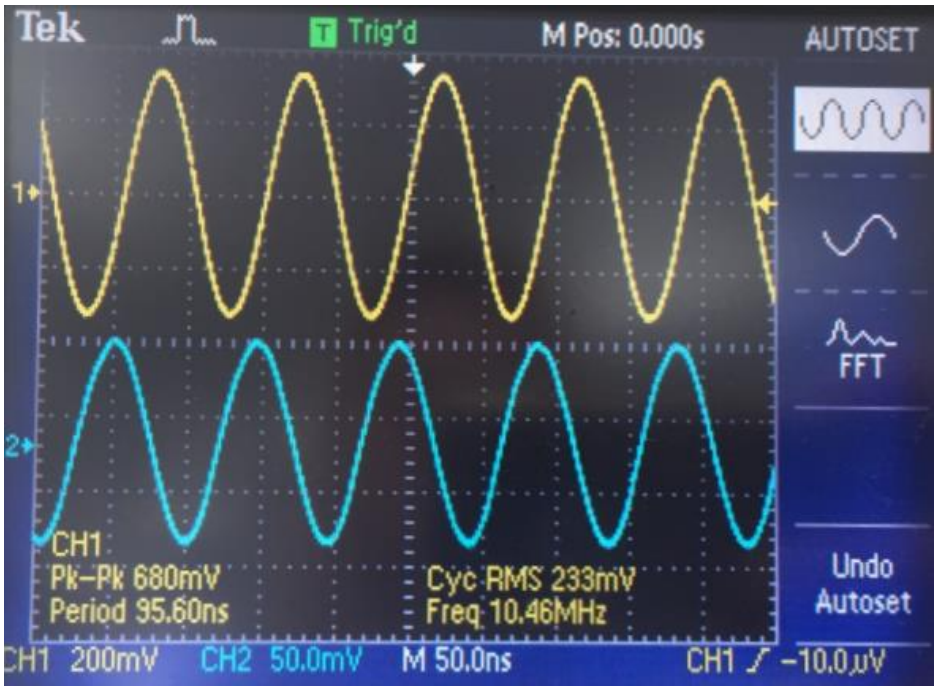

Figure 5: The voltage V_{sense_1} across R_{sense_1} is shown in blue graph, whereas yellow graph presents as the voltage across coil 3 V_{L3} at the distance d_{23} of 2.5 cm

From the Figure 5 and following the equation (4.13), with R_{sense_1} = 10 Ω:

$V_{sense\_1} = 1.37V_{pk\text{-}pk}$; $V_{L3} = 0.68V_{pk\text{-}pk}$

Hence, $M_{12} = 0.0752\ \mu H$

At d_{23} 3.0 cm:

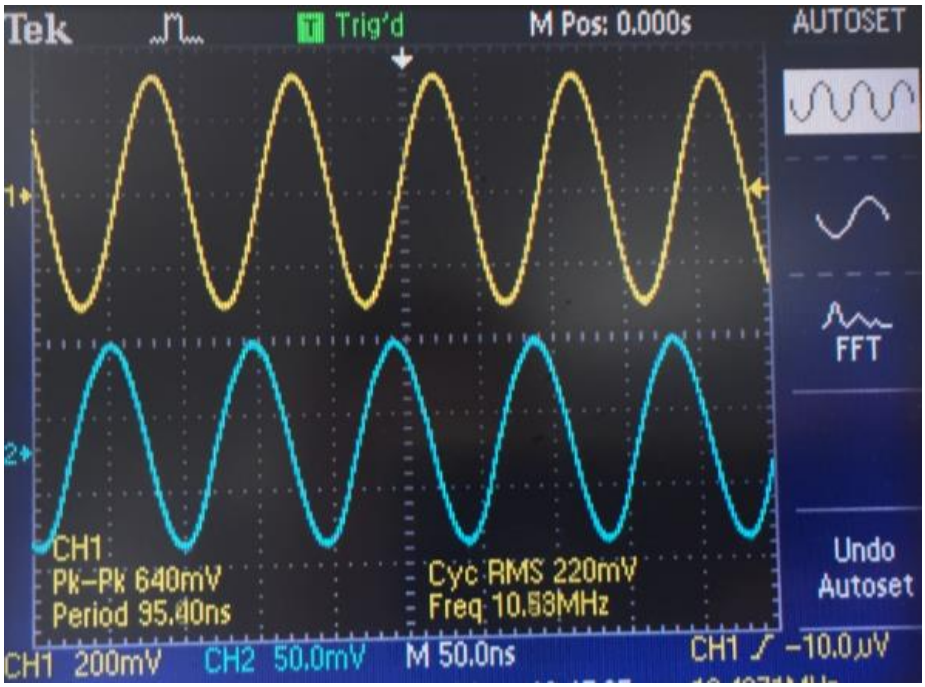

Figure 6: The voltage V_{sense_1} across R_{sense_1} is shown in blue graph, whereas yellow graph presents as the voltage across coil 3 V_{L3} at the distance d_{23} of 3.0 cm

From the Figure 6 and following the equation (4.13), with R_{sense_1} = 10 Ω:

$V_{sense\_1} = 1.4V_{pk\text{-}pk}$; $V_{L3} = 0.64V_{pk\text{-}pk}$

Hence, $M_{12} = 0.0752\ \mu H$

At d_{23} 3.5 cm:

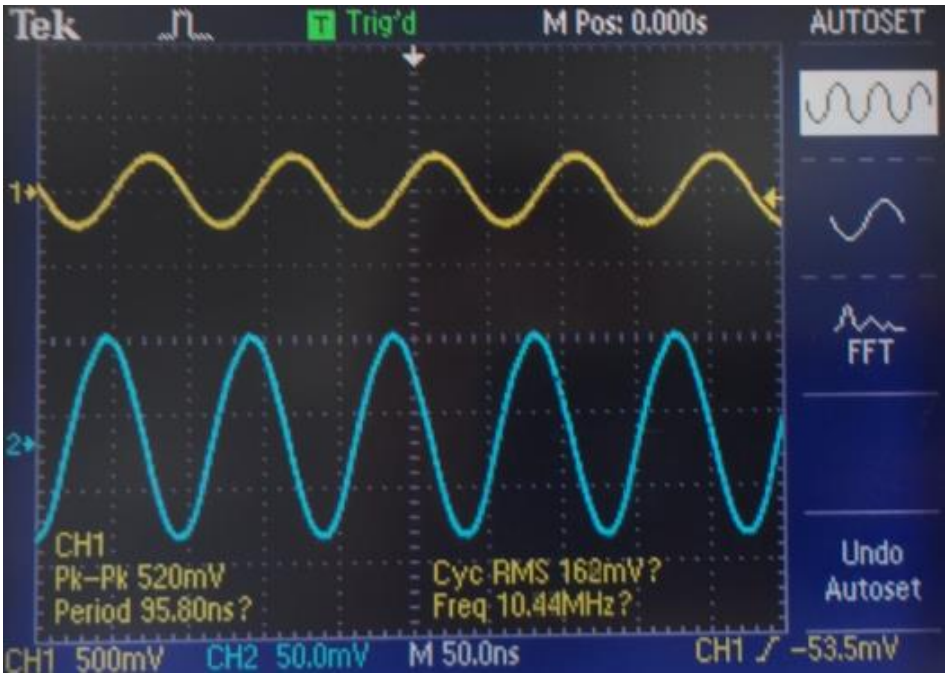

Figure 7: The voltage V_{sense_1} across R_{sense_1} is shown in blue graph, whereas yellow graph presents as the voltage across coil 3 V_{L3} at the distance d_{23} of 3.5 cm

From the Figure 7 and following the equation (4.13), with R_{sense_1} = 10 Ω:

$V_{sense\_1} = 1.4V_{pk\text{-}pk}$; $V_{L3} = 0.52V_{pk\text{-}pk}$

Hence, $M_{12} = 0.0563\ \mu H$

At d_{23} 4.0 cm:

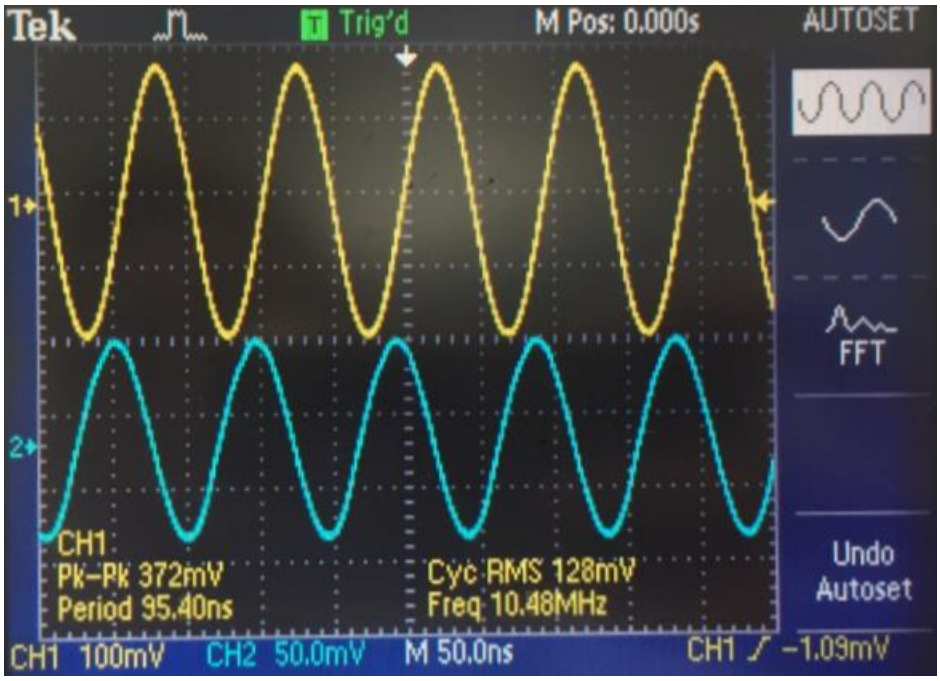

Figure 8: The voltage V_{sense_1} across R_{sense_1} is shown in blue graph, whereas yellow graph presents as the voltage across coil 3 V_{L3} at the distance d_{23} of 4.0 cm

From the Figure 8 and following the equation (4.13), with R_{sense_1} = 10 Ω:

$V_{sense\_1} = 1.4V_{pk\text{-}pk}$; $V_{L3} = 0.372V_{pk\text{-}pk}$

Hence, $M_{12} = 0.0403\ \mu H$

At d_{23} 4.5 cm:

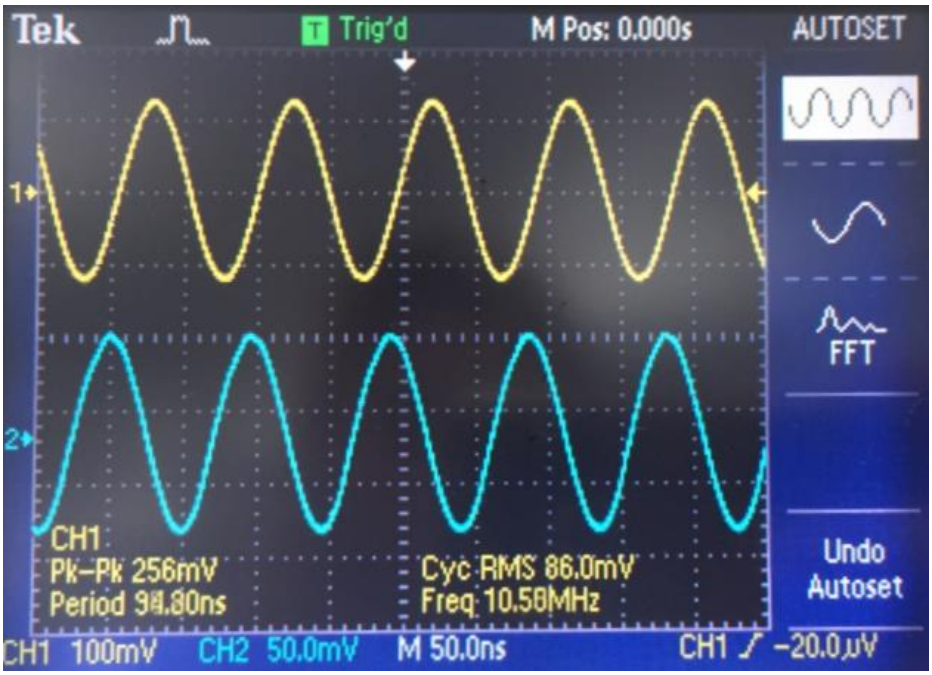

Figure 9: The voltage V_{sense_1} across R_{sense_1} is shown in blue graph, whereas yellow graph presents as the voltage across coil 3 V_{L3} at the distance d_{23} of 4.5 cm

From the Figure 9 and following the equation (4.13), with R_{sense_1} = 10 Ω:

$V_{sense\_1} = 1.35V_{pk\text{-}pk}$; $V_{L3} = 0.256V_{pk\text{-}pk}$

Hence, $M_{12} = 0.03\ \mu H$

At d_{23} 5.0 cm:

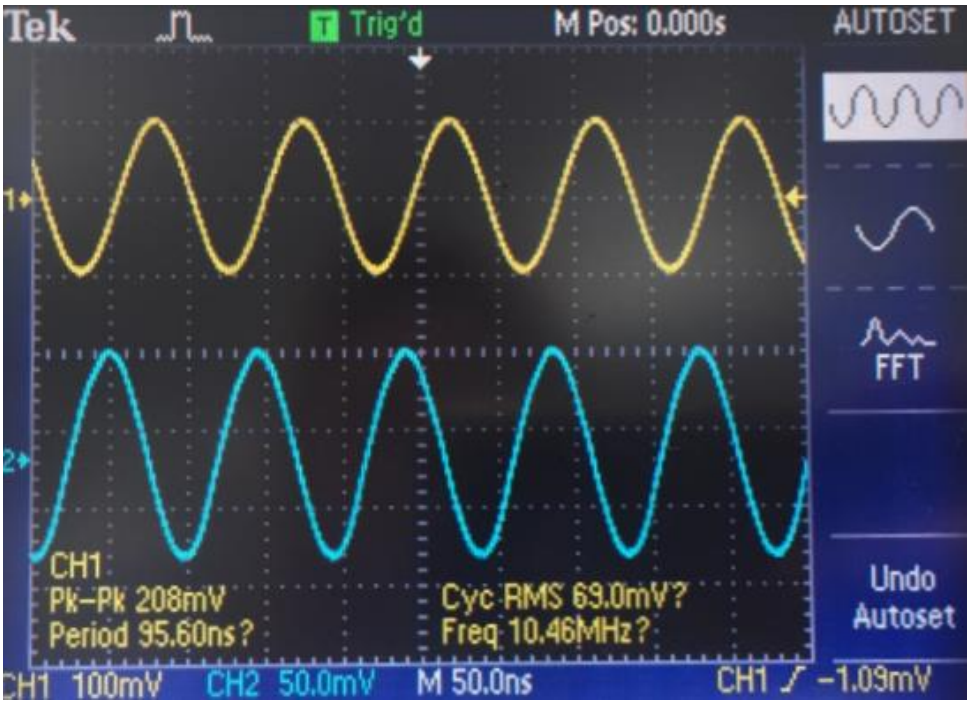

Figure 10: The voltage V_{sense_1} across R_{sense_1} is shown in blue graph, whereas yellow graph presents as the voltage across coil 3 V_{L3} at the distance d_{23} of 5.0 cm

From the Figure 10 and following the equation (4.13), with R_{sense_1} = 10 Ω:

$V_{sense\_1} = 1.35V_{pk\text{-}pk}$; $V_{L3} = 0.208V_{pk\text{-}pk}$

Hence, $M_{12} = 0.0234\ \mu H$

At d_{23} 5.5 cm:

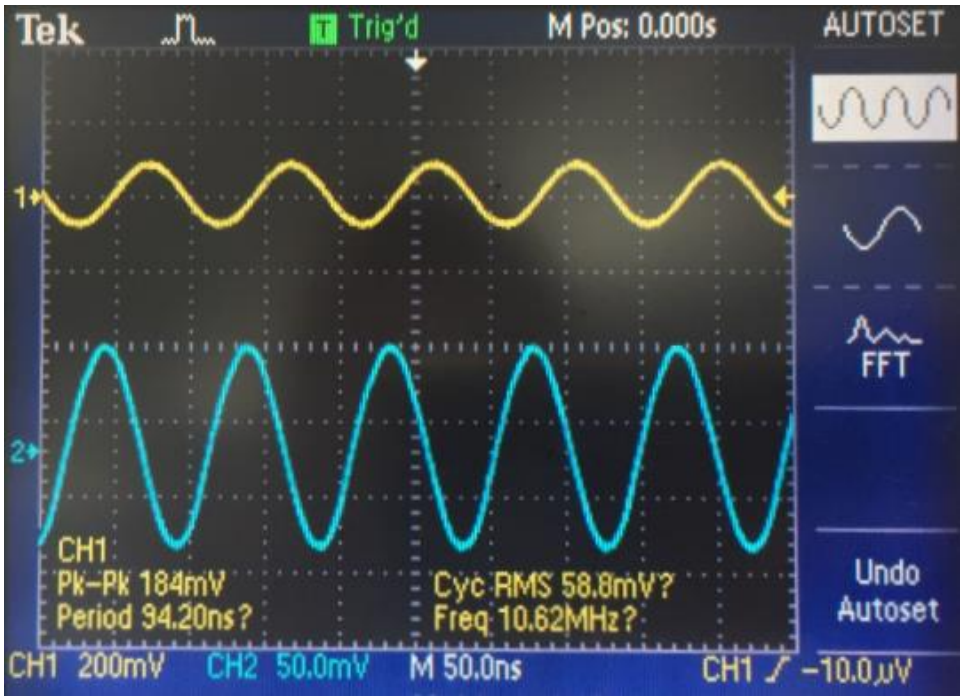

Figure 11: The voltage V_{sense_1} across R_{sense_1} is shown in blue graph, whereas yellow graph presents as the voltage across coil 3 V_{L3} at the distance d_{23} of 5.5 cm

From the Figure 11 and following the equation (4.13), with R_{sense_1} = 10 Ω:

$V_{sense\_1} = 1.35V_{pk\text{-}pk}$; $V_{L3} = 0.184V_{pk\text{-}pk}$

Hence, $M_{12} = 0.021\ \mu H$

At d_{23} 6.0 cm:

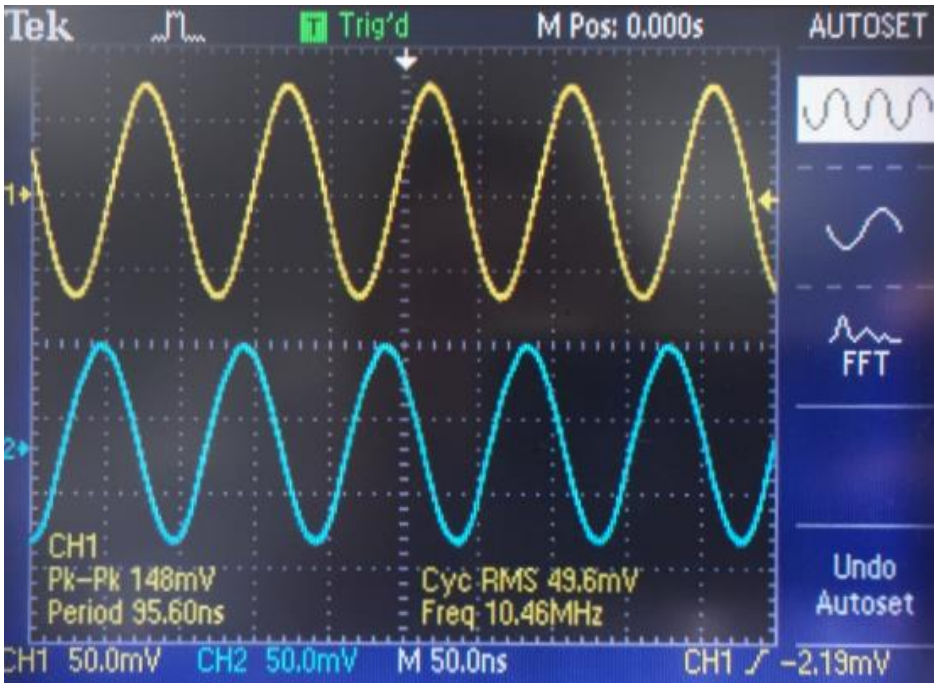

Figure 12: The voltage V_{sense_1} across R_{sense_1} is shown in blue graph, whereas yellow graph presents as the voltage across coil 3 V_{L3} at the distance d_{23} of 6.0 cm

From the Figure 12 and following the equation (4.13), with R_{sense_1} = 10 Ω:

$V_{sense\_1} = 1.35V_{pk\text{-}pk}$; $V_{L3} = 0.148V_{pk\text{-}pk}$

Hence, $M_{12} = 0.0166\ \mu H$